

ALMA MATER STUDIORUM – Università di Bologna

FACOLTÀ DI CHIMICA INDUSTRIALE

Dipartimento di Chimica Industriale e dei Materiali

NEW CATALYSTS FOR ACRYLONITRILE SYNTHESIS

Tesi di dottorato di ricerca in
CHIMICA INDUSTRIALE (Settore CHIM/04)

Presentata da

Dr. **Alessandro CASTELLI**

Relatore

Prof. **Fabrizio CAVANI**

Correlatore

Dr. **Guido PETRINI**

Coordinatore

Prof. **Fabrizio CAVANI**

ciclo XXIII

Anno 2010

| | | |
|----------|--|-----------|
| 1 | INTRODUCTION..... | 1 |
| 1.1 | <i>Acrylonitrile.....</i> | 2 |
| 1.1.1 | History, use and market | 2 |
| 1.1.2 | Properties | 3 |
| 1.1.3 | Processes for the synthesis of ACN ⁷ | 4 |
| 1.1.4 | Propene ammoxidation and Sohio Process ⁸⁻¹⁰ | 5 |
| 1.2 | <i>Propane Vs Propene.....</i> | 7 |
| 1.3 | <i>Ammoxidation.....</i> | 9 |
| 1.3.1 | Ammoxidation of Hydrocarbons ¹¹ | 9 |
| 1.3.2 | Ammoxidation of propene ^{8,10} | 10 |
| 1.3.3 | Catalysts for propene ammoxidation ⁸⁻¹⁰ | 11 |
| 1.3.4 | Ammoxidation of propane | 13 |
| 1.3.5 | Catalysts for propane ammoxidation ⁸ | 15 |
| 1.4 | <i>Rutile-type structure</i> | 18 |
| 1.4.1 | Rutile Structure | 18 |
| 1.4.2 | Rutile structure properties..... | 20 |
| 1.4.3 | Heterogeneous ammoxidation catalyst design..... | 24 |
| 2 | EXPERIMENTAL | 27 |
| 2.1 | <i>Catalysts</i> | 27 |
| 2.1.1 | Catalysts preparations | 27 |
| 2.1.2 | Rutile Phase | 29 |
| 2.1.3 | Antimony oxides phases ²¹⁻²³ | 30 |
| 2.1.4 | Rutile – antimony oxide phase cooperation..... | 32 |
| 2.1.5 | Synthesis | 33 |
| 2.1.6 | Catalysts characterization | 35 |
| 2.2 | <i>Catalytic tests</i> | 37 |
| 2.2.1 | Plant..... | 37 |
| 2.2.2 | Analysis | 39 |
| 2.2.3 | Thermic system..... | 42 |
| 2.2.4 | Calculation sheet..... | 42 |

| | | |
|----------|--|-----------|
| 3 | RESULTS AND DISCUSSION..... | 45 |
| 3.1 | <i>Ga/Sb and Cr/Sb mixed oxides.....</i> | 45 |
| 3.1.1 | Characterization | 45 |
| 3.2 | <i>Catalytic results</i> | 65 |
| 3.2.1 | Cr1Sbxcpw - Propene ammoxidation..... | 65 |
| 3.2.2 | Cr1Sbxcpw - Propane ammoxidation..... | 69 |
| 3.2.3 | Ga1Sbxcp – Propene ammoxidation | 72 |
| 3.2.4 | Ga1Sbxcp – Propane ammoxidation | 74 |
| 3.2.5 | Cr1Sbxasl – propene ammoxidation | 76 |
| 3.2.6 | Cr1Sb2xosl – propene ammoxidation | 78 |
| 3.3 | <i>Catalysts comparation</i> | 80 |
| 3.4 | <i>Starting materials</i> | 86 |
| 4 | CONCLUSIONS..... | 87 |
| 5 | BIBLIOGRAPHY | 91 |
| 6 | ACKNOWLEDGEMENTS..... | 93 |

1 INTRODUCTION

Everyone, in some way, gets in contact with acrylonitrile (ACN) every day.

Annual worldwide production of ACN outstrips 6,2 million tons (in 2008), with an European capacity of 1,25 million tons, for such manufacture of polymers and copolymers as synthetic fibres, plastics and elastomer.

ACN is nowadays produced by sohio process, which in the late '50s superseded the old acetylene-hydrocyanic acid route, by means of gas phase ammoxidation of propylene; then new processes based on ammoxidation of a cheaper starting resource propane have been developed, so that has been reached an industrial scale. Today more than 95% of the world acrylonitrile is produced with Sohio process.

Propane ammoxidation:



Propene ammoxidation:



Ammoxidation (also known as ammonoxidation, oxyamination or oxidative ammonolysis) describes the nitriles production by means of alkanes and alkenes oxidation in presence of ammonia.

Two main systems are active in gas ammoxidation of propane and propene to acrylonitrile: (i) Multy Metal Molybdate containing Bi, Fe, Ni, Co, Mo and additives like Cr, Mg, Rb, K, Cs, P, B, Ce, Sb and Mn; (ii) Rutile-type antimonate containing Sb, Sn, Nb, Fe, V, Cr, U, Ga.

Studies on the rutile-type structure and relative catalytic properties are not extensive, so it is interesting to get information about the new systems based on rutile-type antimonate which is able to operate as a catalyst or as a promoter in complex molybdenum-based system.

1.1 Acrylonitrile

1.1.1 History, use and market

After its discovery by hand of C. Moureau via dehydrogenation with phosphorous pentoxide of acrylamide (or ethylene cyanohydrin), ACN offered no application but its use as a copolymer in synthetic rubber shortly before the Second World War in Germany (Buna-N) and U.S. (GR-A, NBRNitrile rubber) mainly because of its high resistance to fuel and other apolar substances. Then this expensive and multistep process has been overtaken by a new one discovered and developed by Sohio with a considerable costs reduction; after its war-time application, this process fulfilled the needs of fibre factory, main field of market supply from '50s to date, along with a minor use in resins, thermoplastics, elastomer and intermediate in productions of nylon and acrylamide.

Fibres manufacture uses ACN as a copolymer (with vinyl acetate or methyl acrylate) in two different ways, acrylic (>85% w/w) and Modacrylic (50 - 85% w/w), to produce textile; acrylic fibres are useful as a precursor in production of carbon fibres, which is a suitable material for high technology use (army, aerospace, automotive).

Resins containing ACN are relevant in different and wide fields of application: SAN (styrene-ACN) is a copolymer known for its glass replacement ability due to its mechanical properties and transparency; ABS (SAN in polibutadyene matrix) is a strategic material in Electronics and in automotive applications because of its high rigidity and endurance¹².

Nylon 6,6 is a well known polyamide which is used mainly in textile production, above all collant and clothing³. ACN is a raw material for production of adiponitrile, which reacts with esamethylendyamine to form the amide.

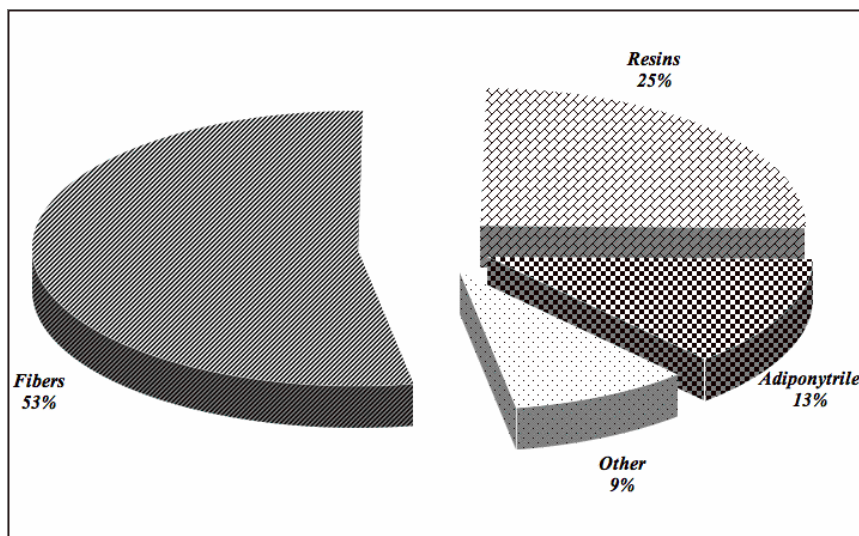


Fig. 1.1 ACN Worldwide employment

Annual worldwide production of ACN has grown from 118 thousand tons in 1960 to more than 5,2 million tons in 2005 (Fig.1.1 shows the ACN world use, in terms of production.), with higher growth rate in developing Countries (South America and China)⁴ while its demand in western Countries is still around the same as in 2005.

1.1.2 Properties

Acrylonitrile (also known as 2-propenenitrile, propenenitrile, vinyl cyanide, cyanoethene, ACN) is a chemical compound with formula $\text{CH}_2=\text{CH}-\text{CN}$ registered with the CAS number 107-13-1⁵⁶. It consists of a vinyl group linked to a nitrile and it looks like a clear colourless or slightly yellow liquid with a pungent odour; in tab 1.1 the chemical-physical data for acrylonitrile⁵ are reported.

| | |
|--------------------------|---------------|
| Melting point | -83°C |
| Boiling point | 77°C |
| Solubility (water) | 70g/Kg |
| Specific gravity | 0.81 |
| Vapour pressure | 11KPa at 20°C |
| Flesh point | 0°C |
| Explosion limits | 3-17% |
| Autoignition temperature | 480°C |

Tab. 1.1 Chemical-Physical data of ACN

ACN is a dangerous reactant which requires a high level of attention when manipulated or disposed: R45 (may cause cancer, carcin class 2), R11 (highly flammable), R23/24/25 (toxic by inhalation, in contact with skin and if swallowed), R37/38 (irritating to respiratory system and skin), R41 (risk of serious eyes damage), R43 (may cause sensitisation by skin contact), R51/53 (toxic to aquatic organisms, may cause long-term adverse effects in the aquatic environment)⁵.

The conjugated system composed by vinylc and cyano group results in double bond activation from polar nitrile group; it gives to ACN high reactivity which brings spontaneous exothermic polymerization (induced by light or bases), which is why this nitrile has to be stored and packed with inhibitors of polymerization (4-methoxyphenol)⁵. The double bond in ACN can undergo different reactions: Diels-Alder, Hydrogenation, Cyanoethylation, hydrodimerization, hydroformilation. The nitrile in ACN can undergo hydrolysis to acrylamide (partial hydrolysis) and to acrylic acid; ACN and primary alcohol react in presence of acids to acrylic esters⁷.

1.1.3 Processes for the synthesis of ACN⁷

Before the discovery of the Sohio process (which will be thoroughly illustrated later) there were many ways to produce ACN:

- Ethylene Cyanohydrin process has first produced acrylonitrile in Germany and in America on industrial scale. Ethylene oxides react with aqueous hydrocyanic acid at 60°C to yield ethylen cyanhydrin; ACN is produced by its dehydration in liquid phase at 200°C.



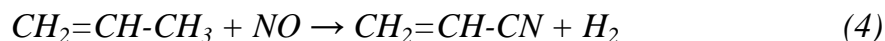
- Catalytic addition of hydrocyanic acid to Acetylene was the major route of ACN supply before the beginning of ammoxidation processes (in the 70s); commercially it was performed at 80°C in dilute hydrochloric acid in presence of cuprous chloride.



- Addition of hydrocyanic acid to acetaldehyde, did not reach industrial scale



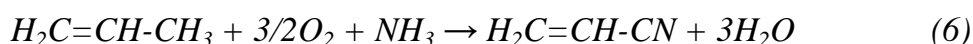
- Nitrosation of propene, never achieved commercial status



- Dehydrogenation of propionitrile, has never been commercially developed

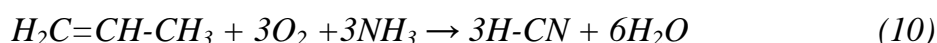


- Ammoxidation of propene (SOHIO process) displaced the processes (2) practised by Du Pont, American Cyanamid and (3) performed by Union Carbide, American Cyanamid and BASF.



1.1.4 Propene ammoxidation and Sohio Process⁸⁻¹⁰

Performing the main reaction (6), during ammoxidation of propene other products are produced as described by reaction (7)(8)(9)(10)(11)(12)



Although the high number of undesired reactions, even favourable in oxidant atmosphere at high temperature, the continuous development of the catalytic system leads to a rise in ACN selectivity from 50% up to 80%.

The SOHIO process uses a fluid bed reactor (necessary to remove efficiently the heat of reaction) where in a single pass is possible to reach a conversion of propene over 95% with a selectivity in ACN near 80%. Ammonia and olefin are fed highly pure (>90% for propene and 99,5% for ammonia) and preheated (150-200°C) to the reactor separately to avoid homogeneous reactions; ammonia to propene molar ratio is

between 1.05 and 1.2 and oxygen to propene molar ratio is between 1,9 and 2,1. Reactor works at a temperature between 420 and 450°C with a residence time of 3-8s with a superficial linear gas velocity between 0,2 and 0,5 m/s. The system operates at around atmospheric pressure because ACN from propene formation is a first order reaction, while undesirable products are of higher order; low pressure is in favour of the target molecules, but overpressure is necessary to maintain fluidized condition.

In a reactor 10m large and 7/8m high, catalyst average load is 75tons with a particle size lower than 40µm in diameter.

The outcoming flow (Tab.1.2) oversteps a cyclone to lose finer solid particles and to reach a refrigerated water absorber (5°C) in which N₂, CO_x and unreacted propene exit and reach incineration. Ammonia is neutralized with sulphuric acid and it is separated as solid while nitriles remain dissolved. After tricky distillation and settling it is possible to separate water and organic phases; water solution is concentrated (97%) and refluxed, while the organic one, rich in ACN and HCN and containing also traces of acetone, acetaldehyde, propionaldehyde and acrolein, carries on to purification step in which the liquid flow undergoes a double distillation and vacuum ultra purification so that ACN reaches more than 94% purity grade.

| Product | Amount |
|------------------|---------------|
| Acrylonitrile | 5.2 |
| Hydrocyanic acid | 1.8 |
| Acetonitrile | 0.7 |
| Carbon monoxide | 1.0 |
| Carbon oxide | 1.6 |
| High Nitriles | - |
| Heavy compounds | 1.0 |
| Propane | 0.8 |
| Propene | 0.5 |
| Water | 26.3 |
| Ammonia | 0.2 |
| Oxygen | 2.2 |
| Nitrogen | 59.7 |

Tab. 1.2 Typical fluid bed reactor effluent composition (loaded with Sohio 41 catalyst)

1.2 Propane Vs Propene

Only in the last decade came along the right conditions to take into account propane technology for ACN production. The development of new catalysts, correlated with new technologies of process along with the increase of propylene feedstock (up to 300 \$/tons more expensive than saturated molecula), made alkane ammoxidation competitive on the market, especially if we consider that the price of olefin engraves on full cost in the amount of 67%. The need to substitute old plant along with the easily way to revamp the old ones made the challenge appealing.

In January 2007 Asahi Kasei Corporation started with a production based on propane technology and originated with the modification of an existing 70000ton/y ACN plant.

Some considerations are useful to understand this topic:

- Propane ammoxidation is a reaction composed of two theoretical steps:
 - An endothermic process in which propane is dehydrogenated to propene
 - An exothermic process in which propene is ammoxidated to ACN

Esothermicity of ammoxidation is greater than endothermicity of dehydrogenation; the overall process is an exothermic auto-sustained reaction. To start from propene means splitting this reaction in two steps in which it is necessary to supply heat for propene production (i.e. in cracking technology, the actual main route of alkene yield) and to drain heat for ACN production, with a consequent energetic inefficiency.

- To Split a reaction in many steps means that we have the opportunity to tune “easily” and thoroughly a catalyst so obtaining the better results which is possible to reach (right temperature, pressure, reactor, catalyst, precursors, contact time). Being able to condensate many stages and eventually to reach the single step means to strike a balance. In the first case high full costs reflect high production (high gain); in the latter one low production means high transformation efficiency and lower plant costs.

- An effective process for propane conversion to ACN has been developed over 30 years ago. It works at a higher temperature than the propene process and it needs the use of gas-phase precursors (causing problems in materials resistance and the increase of purification/recycling apparatus and costs). A strategic choice in ammoxidation to develop a successful replacing process is the conversion of an existing plant as long as the reactor conditions are the same.
- As far as the economical factor is concerned, many things have to be taken into consideration: the reaction conditions, productivity and process costs. Propane works at a temperature 100-150°C higher than propene (due to an increase of homogeneous phase reactions), at a contact time 4-6 times longer, at lower conversion and selectivity, with a fixed investment 10-15% more expensive and with a feedstock 5-6 times cheaper. These parameters have some aftermaths such as higher ammonia consumption (due to the higher contact time, which leads to a higher oxidation to nitrogen) and more difficulties in reaction management (higher temperature and low ACN selectivity lead to higher deep oxidation products, which have strong effects on reaction heat and system temperature).
- Choosing the starting materials it is not the final goal: different technological solutions have been developed to increase propane productivity and to enlarge the gain gap between alkane and alkene technologies.

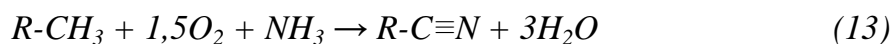
The actual situation lies on the borderline defined with these two different processes, so that a little improvement in catalysts and processes or market changes may lead to prefer one feedstock or the other.

1.3 Ammoxidation

1.3.1 Ammoxidation of Hydrocarbons¹¹

Ammoxidation is an oxidative process in which an Oxygen, Ammonia and Hydrocarbon mixture is selectively converted to nitrile and water; deep oxidation and unwanted nitriles are parallel and consecutive reaction products.

It is possible to feed every kind of hydrocarbon, even though alkanes, alkenes and aromatics are the main carbon source converted. It is possible to feed pure oxygen, but most commonly air is used.



The reaction is characterized by high exothermicity (ΔH° propene ammoxidation = -515KJ/mol) and increasing amount of moles (0,5) which makes the ammoxidation favourite at every temperature. The exothermic character of this class of reactions is increasing due to secondary products, such as carbon dioxide, which proceeds with higher energy release.

The ammoxidation reaction involves three consecutive steps:

- Hydrocarbon oxidation to form the intermediates on the active site; this is the tricky step due to the hydrocarbon thermodynamic tendency to be over-oxidated to degradation and/or combustion products
- Nitrogen insertion; the activated ammonia on the catalytic site in presence of oxygen can overcome combustion to produce N_2 as main nitrogen-waste product whereas the insertion of oxygen rather than nitrogen gives aldehyde in place of nitrile
- Oxidative dehydrogenation of the N-bonded species

The oxidative activation of the substrate is the main step, so it is crucial to design a system which is able to dehydrogenate with high efficiency and high selectivity in order to avoid over oxidation. This is why a catalyst for ammoxidation is usually also effective as a catalyst for dehydrogenation, but not the other way around.

1.3.2 Ammoxidation of propene^{8,10}

Analyzing the alkene ammoxidation in literature almost every paper ascribes to propene.

The accepted general mechanism refers to the catalytic cycle (Fig.1.2) composed of three main steps:

- α -H abstraction (operated by Bi^{3+} , Sb^{3+} , Te^{4+})
- Olefin chemisorption and N/O insertion (over Mo^{6+} , Sb^{5+})
- Lattice reoxidation (on redox couple $\text{Fe}^{2+}/\text{Fe}^{3+}$, $\text{Ce}^{3+}/\text{Ce}^{4+}$)

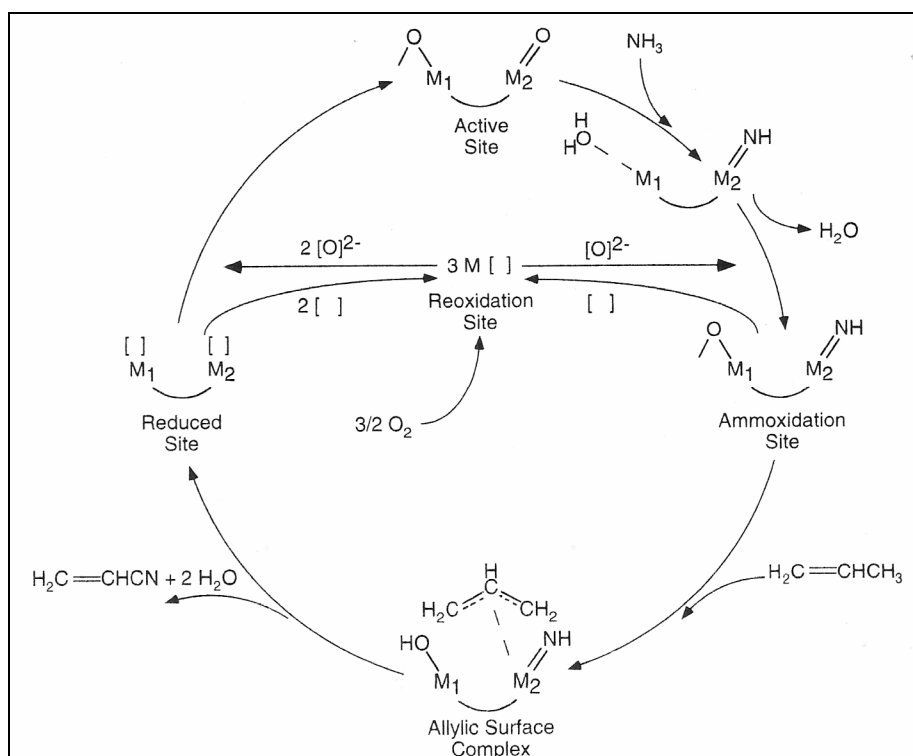


Fig. 1.2 Alkene ammoxidation Cycle

The cycle starts from the active site composed by two contiguous metal atoms in a solid system: the first (M_1) bonded to bridge oxygen and the second (M_2) bonded with oxygen by means of double bond. The site interacts with ammonia and forms an imino group (M_2) after the expulsion of a molecule of water. Propene co-ordinates on M_2 while Oxygen on M_1 breaks the bridge bonding with the allylic hydrogen (α -H) to form allylic complex (coordinated by way of π bond on M_2); it is possible to catch a

radical hydrogen if the O-abstractor has a partial radical character too, conveyed by some electron density present on the metal (M_1). Insertion of nitrogen is now possible and after a final oxidation ACN can leave the catalytic site along with a couple of water molecules. The reduced catalytic sites send vacancies to the reoxidation site, which is able to dissociate bimolecular oxygen in lattice oxygen (O^{2-}), which moves toward the O-deficient metal and so neutralizes the vacancy.

The mechanism described above is possible in a solid system which is able to accommodate different metal cations arranged in complex bifunctional catalytic sites and in which oxygen, electron and anion vacancies are free to move in the lattice.

Multifunctionality which is needed in propene as well as in propane ammoxidation, can be achieved in two ways:

- Phase cooperation (antimonate): two different catalytic sites related to two different phases operate very close to each other, so that the molecules undergo the first reaction, desorb from the active site and then reach the second reaction to complete the transformation. Sometimes the phase boundary is not sharp-cut, but it is connected by a midway phase which settles the mismatch by means of nonstoichiometry.
- Element cooperation (multi metal molybdate): the sites which are able to transform the hydrocarbon lie in the same phases so that the molecule does not need to desorb from a site to complete the ammoxidation, but it just needs to move from an element to another on the same lattice.

1.3.3 Catalysts for propene ammoxidation⁸⁻¹⁰

There are two classes of solid systems which are able to match with the properties listed above and actually used to perform propane ammoxidation:

- Multi metal molybdate (MMM) constituted of Mo Bi Fe Ni Co and additivated with Cr, Mg, Rb, K, Cs, P, B, Ce, Sb and Mn, dispersed in silica (50%w/w) for fluid bed reactor application. The active site, as described in par. 1.2.2, is composed of Bi (M_1) and Mo (M_2) and can be described with Be_2MoO_6 (Fig.1.3). Bi-O-Mo bridging oxygen, which belongs more to Bi

than to Mo, is active in α -H abstraction and Mo=O is responsible for NH-to-O substitution and NH insertion. The two electron pairs associated with two Bi atoms in Bi-O-Bi group or redox couple made by Fe, Ce, U and Cu are responsible for the O₂ dissociation.

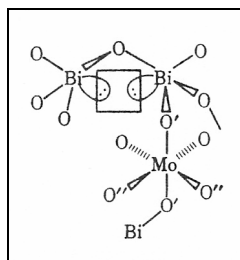


Fig. 1.3 Bi-Mo Catalytic Site of Bi₂MoO₆: O' represents the Bi-oxygen active in α -H abstraction and O'' represents the oxygen substituted by nitrogen. Two lone pairs between Bi are the hypothetic site which is able to dissociate bimolecular oxygen for the solid state re-oxidation mechanism.

- Antimonate with rutile-type structure. The catalytic site is made of four metal antimonate cations: two bonded Sb⁵⁺ in the centre with two external Sb³⁺, as shown in Fig.1.4. Sb⁵⁺ activates and inserts ammonia as well as coordinating the olefin; the oxygen associated with the trivalent antimony is responsible for the α -H abstraction. In addition to antimony, at least one of the redox couple made by Fe, Ce, Cr and U is present to replenish the oxygen vacancy which had been created during the ammoxidation cycle.

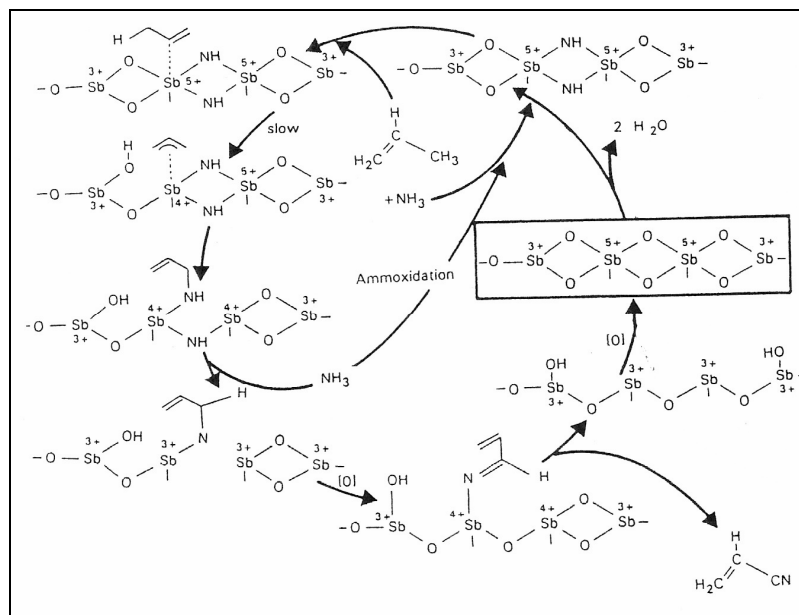


Fig. 1.4 Antimony based catalytic site for propene ammoxidation. Starting from the oxidated site (in the square), the cycle represented in Fig. 1.2 is accurate: after the N-activation, propene is co-ordinated on Sb^{5+} and transformed in allylic intermediate by means of H-abstraction made by Sb^{3+} ; N-insertion is then operated by Sb^{5+} and after partial oxidation, ACN is desorbed and the catalytic site is re-oxidated.

1.3.4 Ammoxidation of propane

As already seen above, the activation of hydrocarbon is the crucial step in the ammoxidation process, especially the one in which alkane is converted due to the well known paraffin inertia.

The propene coordination, previously analyzed, starts with olefin allocation on the catalytic site thanks to the electron surplus due to the double bond which is not present in propane.

The key step in propane ammoxidation is the C-H bond dissociation, to form activated complex which is subjected to further H abstraction and propene formation. The activation proceeds via carbocation or carbanion formation by means of homolitical or eterolitical dissociation. Carbocation is more stable in central position (tertiary>secondary>primary) while, on the contrary, carbanion is more stable in ppherical position (primary>secondary>tertiary). Propene is composed of 2 primary and 1 secondary carbons while isobutene is composed by 3 primary and 1

tertiary carbons, so that the reactivity of these probe molecules is associated with the carbon character. It seems reasonable to claim that to compare the conversion rate of propane and isobutene reflects the stability of the associated carbocation ($\text{CH}_3\text{-C}^+(\text{CH}_3)\text{-CH}_3$ is more stable than $\text{CH}_3\text{-CH}^+\text{-CH}_3$) and carbanion ($\text{CH}_3\text{-CH}_2\text{-CH}_2^-$ is more stable than $\text{CH}_3\text{-CH}(\text{CH}_3)\text{-CH}_2^-$). Conversion data are in favour of propane hence the mechanism seems to occur via carbanion formation¹².

In a two stage configuration of propane ammoxidation, hypothetically conducted in two different reactors, the reaction sequence is the following:



It is reasonable to imagine that the same mechanism occurred in a single stage configuration, in which the transformation happened consecutively on two catalytic sites, without an effective desorption mechanism after alkene formation¹³:



Another possible way of propane activation, proposed by Centi and co-workers¹⁴, was investigated by IR studies on probe molecules adsorbed on Vanadium antimonate. Propane can undergo H^- abstraction on Lewis acid site (represented by coordinatively unsaturated vanadium) and subsequent nucleophilic oxygen attack. The obtained intermediate undergoes secondary H-abstraction and oxidation to form the propionate species. Oxidative dehydrogenation yields acrylate, which is the succeeding step in ACN formation. In this mechanism the key step of H^- abstraction can be disturbed by ammonia adsorption on Lewis sites.

Catalysts active in propene ammoxidation are not able to convert effectively propane given their inability to abstract methylen hydrogen of paraffin in place of allylic one in olefin, mainly because of the higher C-H bond energy (89kcal/mol Vs 77 kcal/mol).

It is indeed necessary to implement the catalytic system with an oxidative enhancer (halogen promoter or strong oxidant such as Vanadium) or to develop new catalysts¹³.

1.3.5 Catalysts for propane ammoxidation⁸

As in propylene ammoxidation, molybdate and rutile-type antimonate are effective in transformation of propane in acrylonitrile. Nowadays, the most active system is represented by Mo/V/Nb/Te/O, which is able to reach yield in ACN up to 62%. It has been developed by Mitsubishi Kasei and it is composed of two phases called M1 and M2 whose preparation is very difficult and relevant, along with the composition, the synthesis, the activation, the modality of doping and the nucleation/growth of the phases⁸.

Other catalysts have been developed by different Companies who claim very different reaction condition: propane rich and propane lean conditions, such as maximum conversion and low conversion with recycle, remain mostly unknown.

- Mo/V/Te/Nb/O: in the propane ammoxidation catalyst the metal cations are arranged in more than one phase, mutually consistent in structure. Each phase is pure obtainable and tunable preparations are developed to reach desired solid system composition. M1 phase ($\text{Mo}_{7.8}\text{V}_{1.2}\text{NbTe}_{0.94}\text{O}_{28.9}$ orthorhombic, in Fig1.5) is able to transform independently propane to acrylonitrile with good performance but co-catalyst M2 phase ($\text{Mo}_{4.67}\text{V}_{1.33}\text{Te}_{1.82}\text{O}_{19.82}$ pseudo-hexagonal) is required to promote the unconverted-desorbed propene to ACN; catalyst is composed of 60% M1 phases and 40% M2 phases with traces of other phases. The general metals role is listed after:
 - V is necessary to obtain the required crystalline structure, forming VO_6 lattice network; it is the metal responsible for the alkane dehydrogenation; the lack of vanadium in M2 make the co-catalyst unable in alkane activation.
 - Mo, like V, forms MoO_6 lattice network; catalytically it provides to allylic co-ordination and nitrogen insertion.
 - Te is located in the hexagonal ring and promotes the α -H abstraction in propene conversion to ACN.

- Nb occupies the same position of Vanadium and improves the selectivity in ACN.

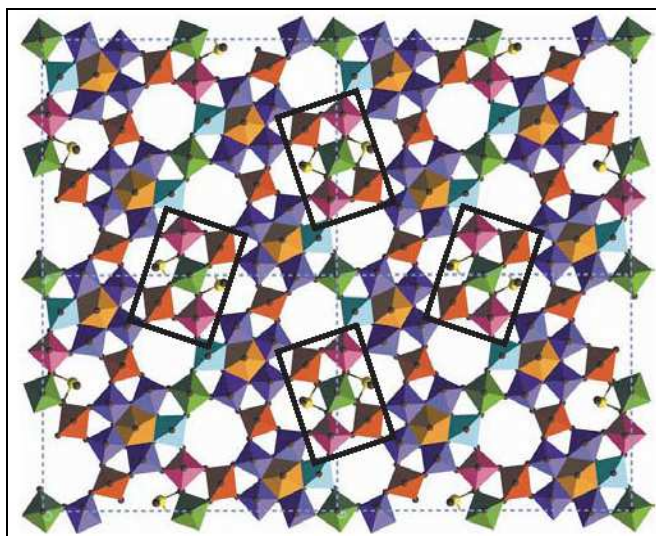


Fig. 1.5 M1 ammoxidation catalyst phase: O atoms are shown as brown spheres in the middle of each coloured four sided. In rectangular boxes are shown four active sites; looking at the upper one: the side lone sphere is Te^{4+} , around central site composed by the $\text{V}^{4+}_{0.8}/\text{Mo}^{5+}_{0.2}$ couple. Two opposite pitched sites are made by $\text{V}^{5+}_{0.5}/\text{Mo}^{6+}_{0.5}$ (bonded out of the square with Mo^{6+}) while the other two ones are made by $\text{Mo}^{6+}_{0.5}/\text{Mo}^{5+}_{0.5}$ (bonded out of the square with Mo^{6+} and Mo^{5+}). The pentacoordinated site, made by four Mo^{6+} external site and one Mo^{5+} , is occupied by Nb^{5+} and finally the site opposite to Te^{4+} bond site and between 4 Mo^{6+} sites is composed by $\text{V}^{4+}_{0.8}/\text{Mo}^{5+}_{0.2}$

- Bimetallic antimonate catalysts are solid systems typified by nonstoichiometry, composed by Sb^{5+} and a metal in 3+ oxidation state (Cr^{3+}) or a couple of the same metal in different oxidation state ($\text{V}^{4+}/\text{V}^{5+}$, $\text{Fe}^{2+}/\text{Fe}^{3+}$), in which the electro-neutrality is maintained by cation vacancies creation. V antimonate is one of the more investigated systems: a catalyst with a molar ratio equal to 1 gives a solid system in which cation-deficient structure is achieved with 0.04 cationic position unoccupied per O^{2-} anion and electro neutrality is maintained by means of different V oxidation state ($\text{V}_{0.92}\text{Sb}_{0.92}\text{O}_4$ is indeed $\text{V}^{3+}_{0.28}\text{V}^{4+}_{0.64}\text{Sb}_{0.92}\text{O}_4$). Preparation methods engrave on V(III) to V(IV) ratio so that it is possible to obtain system with V/Sb molar ratio equal to one in the $\text{V}^{3+}_x\text{V}^{4+}_y\text{Sb}_z\text{O}_4$ range $x=1$ $y=0$ $z=1$ / $x=0$

$y=0.89$ $z=0.89$ (that is $V^{3+}_1Sb_1O_4$ to $V^{4+}_{0.89}Sb_{0.89}O_4$). However it is possible to obtain catalyst with V/Sb ratio different from 1:

- To keep unitary the coefficient of antimony, excess of Vanadium can be inserted in the structure with a mechanism related to an hypothetical insertion of V^{3+} atoms in the cation vacancies made on a quasi- $V^{4+}_{0.89}Sb_{0.89}O_4$ high defective compound (the higher the V^{4+}/V^{3+} ratio, the higher the cation vacancy amount) so that each V inserted is 3+ and, to maintain electro neutrality, three V^{4+} atoms reduce to V^{3+} : this way, starting from a mainly V^{4+} formula, a mainly V^{3+} formula is reached. In the same way, in iron antimonate, the cation is placed in specific position and iron is reduced to evolve the rutile structure of $FeSbO_4$ (FeIII) in tri-rutile superstructure $FeSb_2O_6$ (FeII).
- It is possible to increase the Sb to V ratio, but α or β Sb_2O_4 are formed in crystalline or amorphous forms

1.4 Rutile-type structure

1.4.1 Rutile Structure

Rutile refers to a structure composed by metal fluoride (Me^{2+}) or metal oxide (d-incomplete transition and XIV group Me) in a tetragonal cell in which metal is bonded with six oxygen in octahedral coordination (Fig.1.7) and oxygen is in planar coordination with three metals (Fig.1.6).

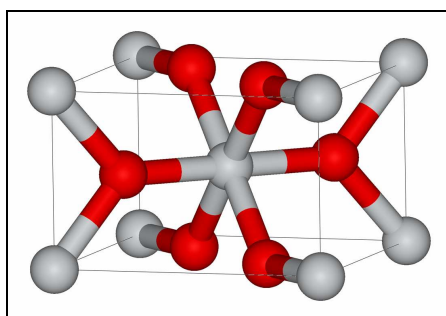


Fig. 1.6 Rutile unit cell: in the centre and in the edge there are octahedric metals and on the other position the oxygens are placed in planar coordination

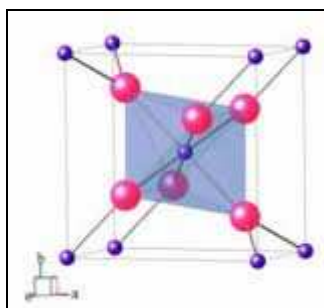


Fig. 1.7 Octahedric coordination of centred metals in rutile structure. Compared to Fig 1.6, the structure here is 90° rotated in the sheet plane and 90° perpendicularly.

It is possible to show another structural view considering a hexagonal coordination instead of tetragonal, as shown in Fig.1.8

Metal ions and oxygen hybridization cause distortion in the rutile structure:

- Highly charged vicinal ions repel each other and destabilize the structure inducing distortion.

- Oxygen bonded to 3 metal atoms reaches pure sp^2 hybridization (from a quasi- sp^2 one) so that a triangular planar configuration is achieved.

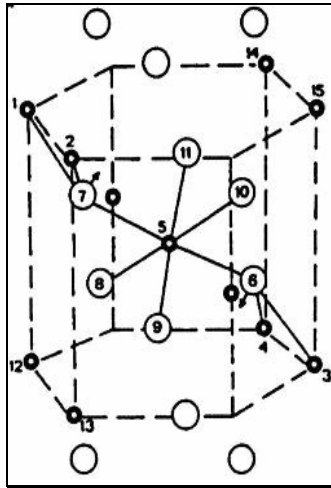


Fig. 1.8 HCP rutile lattice. Full circles in metal cation and empty circles represent oxygen ions.

Octahedra are linked by vertex (c axis) and by edge (a and b axes, 90° rotated) to form infinite chain in c directions, as shown in Fig.1.8 and Fig.1.9. Considering all the octahedral site formed by oxygen (not shown in Fig. 1.9, but existing early in the empty spaces), half of the whole cavity is occupied by metal atoms (Fig.1.10).

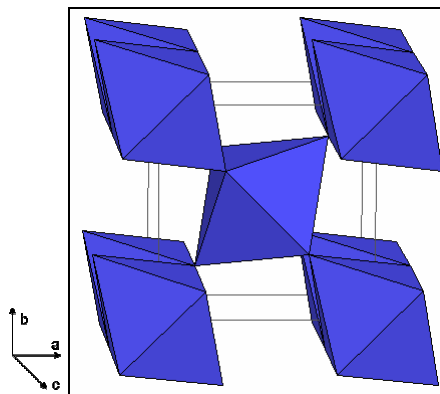


Fig. 1.9 Octahedra connection by edge (a and b directions) and vertex (c axe)

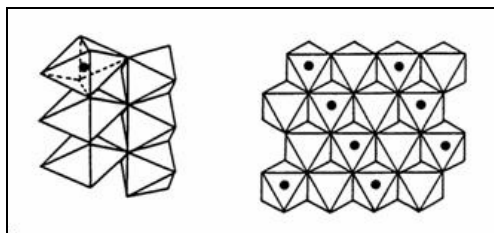


Fig. 1.10 Octahedra edge-linked rotation and half-filled site arrangement.

Rutile systems can be classified as:

- Oxide (TiO_2 , SnO_2)
- Rutile-type (FeSbO_4 , VSbO_4 , CrSbO_4 , AlSbO_4 , GaSbO_4 , CrNbO_4 , FeNbO_4 , RhVO_4) and trirutile (NiSb_2O_6)
- Solid solution ($\text{V}_x\text{Ti}_{1-x}\text{O}_4$, $\text{V}_x\text{Sn}_{1-x}\text{O}_4$)
- Non stoichiometric solid solution (typical in Sb-rutile with the formation of Sn oxides)

Trirutile structure ($\text{Me}_1\text{Me}_2\text{O}_6$) mentioned above is a superstructure in which Me_1 and Me_2 are alternatively accommodated in an ultra ordered network (Fig.1.11).

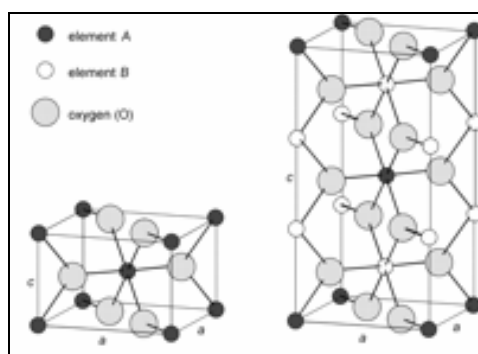


Fig. 1.11 Rutile and tri-rutile structure

1.4.2 Rutile structure properties

- Cationic Radius (Pauling) of cations (Me^{4+}) which are able to get rutile structure are plotted versus the related number of d electrons (Fig.1.12); it is therefore clear that the existence range is $0.52 < r_c < 0.78 \text{ \AA}$. The cationic/anionic radius ratio ($0.37 < r_c/r_a < 0.56$ considering the previous data

and the oxygen radius in III coordination, 1.36 angstrom) is usually useful to predict the coordination geometry: 0.414 as minimum radius ratio in octahedric and 0.732 for cubic. The data are thus coherent but it is important to remember that this theory is applicable only for full ionic compound. This is a constraining factor for the rutile structure, in which covalent partial character is crucial in energetic stabilization. Moreover, the ionic model is unsuitable because of the prediction of four short and two long bonds, which is just the opposite of the real configuration. The loss in ionic character is mainly due to the cationic charge made by the oxygen.

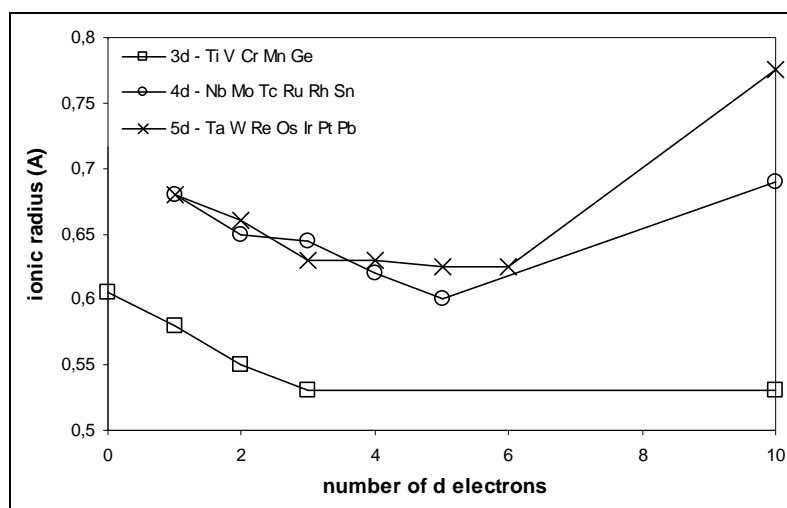


Fig. 1.12 Ionic radiuses (angstrom) versus number of d electron¹⁵. All data refer to charge 4+ and coordination VI.

- Electro-negativity, according to radius data, supports the pure ionic bond character mismatch: the electro-negativity difference between O^{2-} and Me^{4+} describes the character so that values lower than 1,7 define the bond as covalent while values upper than 1,7 define the bond as ionic. As it is well known, it is wrong to consider “pure” a character only on that grounds but it is widely accepted to consider medium a character which is near the borderline value and pure a character clearly far from the borderline. As shown in Fig.1.13, rutile structure lies on the entire range of electro-negativity.

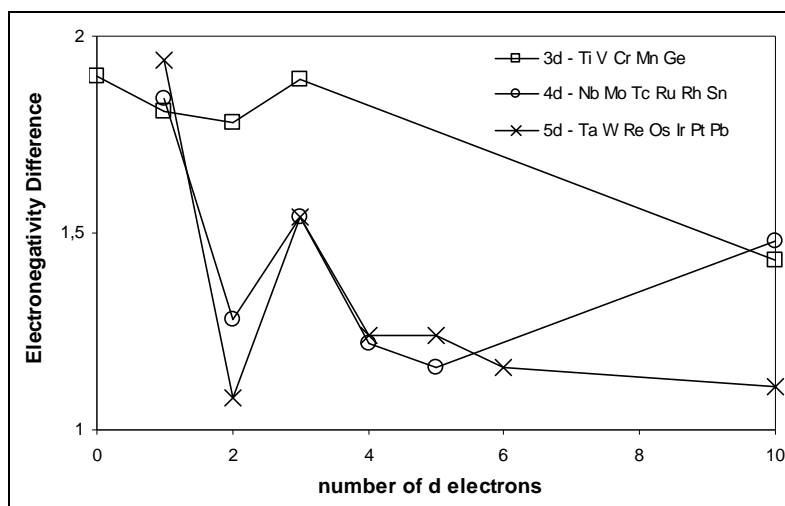


Fig. 1.13 Difference in electronegativity between metal and oxygen versus the number of d electron

- Cell Volume: Rutile structure is able to accommodate cations with very different size, condition which underline the elasticity of the lattice. As already said above, in some cases metal-metal interaction can occur and so the distortion of the cell happens: two ions accommodate on the same plane on “c” direction and attract one another (Fig.1.14). Cation interaction causes a lattice contraction along “c” parameters and a consequent “a” parameter stretching; these events modify the cell geometry but the volume remains the same. Vegard’s law is still valid in every rutile composition range (cell volume increases linearly with the ionic radius of the cation, as shown in Fig. 1.15).

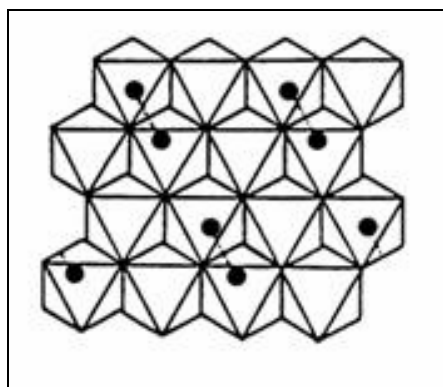


Fig. 1.14 Metal-Metal coupling in vicinals octahedric site in “c” plane direction

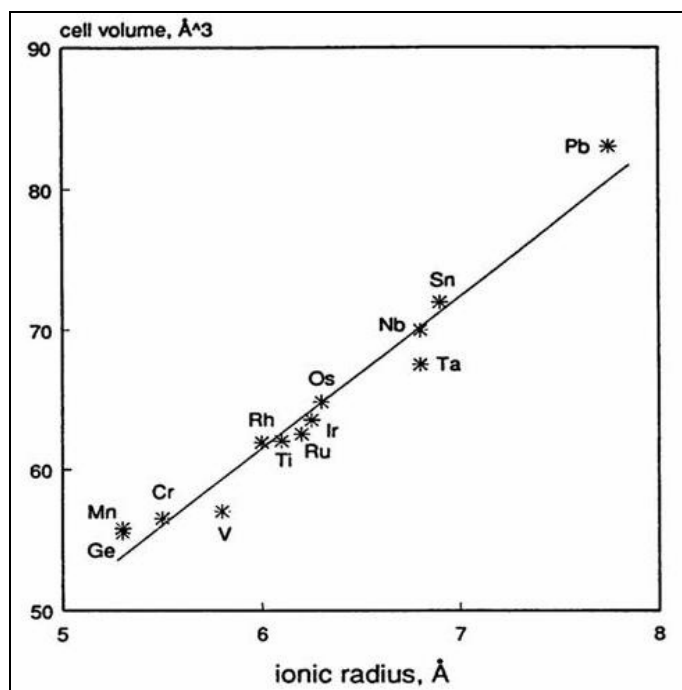


Fig. 1.15 The cell volume value (cubic Angstrom) versus the ionic radius (Angstrom) shows linearity, as stated in Vegard's law.

- Rutile-type structure solid solution can be theoretically formed as interstitial or substitutional:
 - Interstitial solid solution is formed by the insertion of a cation in an empty cavity. Many processes can compensate the positive excess of charge, such as cation vacancy formation, anion interstitial insertion or redox process on original lattice cation.
 - Substitutional solid solution is formed by a substitution of an original cation with another one. To maintain a lattice stability the substitute and the expelled metal have usually to be similar in radius and charge; however it is possible a larger cation insertion, which creates a lattice distortion, but the insertion of a differently charged cation is only possible if accompanied with redox reaction or vacancies creation, so that to maintain electro neutrality.

As far as the half octahedric empty sites are concerned, rutile-type interstitial solid solution has never been prepared, mainly because of the high instability created by the

positive ions inclusion. On the contrary, substitutional rutile can be easily synthesized provided that the general concept of similarity between the metal ions is observed in order to reach homogeneous solid solution; this means that similar cations may be un-soluble and very different metal may be miscible. It is impossible to make previsions and usually only a small range of composition may be obtained.

This structure gives a wide range of possible modifications which lead to different redox, electric and surface properties.

1.4.3 Heterogeneous ammoxidation catalyst design

The efficiency of a catalyst can be described with many parameters such as conversion, productivity and yield, but the power of a solid system in which a transformation of a molecule into another occurs, is mainly described with selectivity. Seven basic principles describe the features that a compound must have in order to drive efficiently a heterogeneous catalytic reaction.

- Lattice oxygen: catalytic mechanism can be shortly defined with the word “coordination”. In gas phase oxidation, the gaseous oxygen is able to attack a molecule without hanging location preferences, so O₂ is intrinsically unselective. The power of catalysis is due to the coordination activated on the reactants by the lattice. Reciprocal positions and the distance between the coordination site and the oxygen site allow the oxygen to attack the substrate only in specific position. Oxygen is present as O²⁻ and it is exposed to gaseous phase to get in contact with the reductant; the vacation left by the reacted oxygen moves toward re-oxidation site and oxygen is replenished with bulk O²⁻.
- Metal-oxygen bond: the strength which keeps the oxygen bonded to the catalysts is a key factor. A weak bond means that the oxygen is very reactive and available to different substrate sites, while, on the other hand, a hard bond highlights a low reactivity or even unreactivity. It is very important to tune the oxygen-lattice bond strength in order to obtain a mild condition

between the two extreme situations “selective/unreactive” and “reactive/unselective”.

- Redox properties: in order to define a reaction as “catalytic”, the reactive mechanism has to be repeated more than once on the catalytic site. The lack of Oxygen, occurred during the reaction on the catalytic surface, is replenished by bulk oxygen while the vacancy moves toward the reoxidation site, in which molecular oxygen is adsorbed from the gas phase, then it is cleaved and introduced in the solid system as O^{2-} . The vacancy is thus neutralized and the redox catalytic cycle is now complete.
- Multifunctionality: the whole mechanism of substrate transformation is made up in different steps: adsorption, activation, N-insertion and, oxidation. Different metals are involved in such reactions in different catalytic sites, so that multifunctionality is often synonymous of multimetallicity. Different metals are different elements with different atomic number (i.e. Bismuth molybdate composed by Bi^{3+} and Mo^{6+}) or the same element with different oxidation state (i.e. antimonate catalyst made of Sb^{3+} and Sb^{5+})
- Site isolation: it is necessary to achieve selectivity, which can be obtained with spatial separation among the surface sites, usually the oxygen ones. The number of vicinal oxygens reflects the reaction stoichiometry achieved in the catalytic mechanism: less oxygen than necessary leads to a hydrocarbon activation without complete transformation; higher amount of vicinal oxygen can push the activated substrate to over-oxidation.
- Cooperation of phases: as already seen before, multifunctionality is reached with the aim of placing different catalytic sites in one single phase or in more than one. The mechanism of substrate transformation starts from adsorption and activation; if the multifunctionality occurs in different phases, the intermediate has to move on the surface from a site to another, in adsorbed (or quasi-adsorbed) conditions. To reach effective cooperation the site has to be near and, consequently, the phases must be intimately linked; it means

that different phases must form a coherent interface, which is usually reached only in similar structures or by means of intermediate lattice.

2 EXPERIMENTAL

2.1 Catalysts

Rutile-type antimonates are catalysts which are active in ammoxidation of hydrocarbons. In order to increase the substrate activation properties of the catalyst, a secondary element (such as vanadium or others active in dehydrogenation) is often added to form a binary system. These elements are able to increase the conversion rate of olefins or to allow the activation of the paraffins.

2.1.1 Catalysts preparations

Many preparations are claimed to be active in the synthesis of such systems and the choice depends on many important factors, like the final product features and the scale applications (lab scale or industrial scale). Generally speaking, the main steps are the following:

- Raw material selection: antimony and the second component can be used in different oxidation state and associated to different anions; preparation claimed to be active in rutile synthesis starts from Carbon oxides (Sb_2O_3 , Sb_2O_5 , V_2O_4 , V_2O_5 , Cr_2O_3 ,...) or from soluble salt (SbCl_3 , SbCl_5 , $\text{Cr}(\text{NO}_3)_3$, $\text{VO}(\text{acac})_2$, SnCl_4 , NH_4VO_3 ...).
- Component mixing: there are basically two ways, a dry one (oxide mixing) and wet one (water solution). The aim of this step is to reach a homogenous intimate-contact mixture.
- Precursor preparation consists of evaporation of the solvent and/or redox reactions.
- Thermic treatment involves phase changes and reactions necessary to obtain rutile structure.

The dry way of catalyst preparation consists of oxide mixture made by graining or milling and subsequent heat treatment; typical preparation made by solid reaction is the formation of vanadium antimonate rutile. It is desirable to obtain a catalyst in this

way because of the easy operation, the absence of liquid reflux and the economic factor; the container and the balls have to be made by materials selected in order to avoid corrosion or element migrations. On the other hand it is difficult to control reaction parameters such as real temperature produced by the reaction itself, pressure impressed on grains by the spheres in the mill, influence of speed induced by the mill. As claimed by Berry et al., the operation described above on Sb_2O_3 and V_2O_5 is easily conducted, but very condition sensitive: the preparation consists of equimolar mixing and a very slow heating rate composed by (i) heating to 600°C in 12 hours, (ii) still 600°C for 12h, (iii) temperature increasing to 750°C in 6 hours and (iiii) isothermal treatment at 750°C for 24h. This reaction, performed in oxygen-free nitrogen, leads to a monophasic vanadium-rich rutile phase ($\text{V}_{1.05}\text{Sb}_{0.95}\text{O}_4$) and sublimation of antimony(III) oxide; no reagents residue are observed. The same reaction made in commercial nitrogen results in a rutile antimony-deficient phase and a $\alpha\text{-Sb}_2\text{O}_4$ phase formed by oxidation of antimony by molecular oxygen; in presence of oxygen, vanadium oxide is subjected to a redox reaction, due to the antimony which reduces V_2O_5 to form the tetroxide. Oxygen excess in the gas phase leads to an initial antimony oxidation to $\alpha\text{-Sb}_2\text{O}_4$ which is unable to react with vanadium. In all preparation methods an excess of antimony leads to the formation of surplus antimony oxide phase while an excess of vanadium results in presence of V_2O_5 as unreacted reagent.¹⁶ Solid state reaction of Chromium and antimony trioxides are described by Filipek et al. to obtain rutile phase in long-time thermic condition (from 500°C to 1000°C in almost 12 days)¹⁷.

The wet way consists of a suspension of Sb_2O_3 in water in which NH_4VO_3 is dissolved. After solvent evaporation the precursor is dried and calcined at 900K . Starting from equimolar V and Sb, rutile phase and traces of $\alpha\text{-Sb}_2\text{O}_4$ are obtained; an excess of antimony leads to an increasing amount of antimony tetroxide¹⁸. Similar preparations are described by Cavani and co-workers starting from Antimony(III) oxide and Vanadium pentoxide pre-treated with hydrogen peroxide to obtain monoperoxovanadium cation ($\text{VO}(\text{O}_2)^+$); also in this case rutile phase is obtained¹⁹.

Another wet way consists of the dissolution of the soluble salt containing the metal to be incorporated into the structure (VCl_3 , SnCl_4 , SbCl_3 , SbCl_5 , $\text{Cr}(\text{NO}_3)_3$, $\text{Fe}(\text{NO}_3)_3$ and so on), in absolute ethanol and the subsequent drip in water buffered at pH 7. Separation, dryness and calcinations complete the synthesis.

2.1.2 Rutile Phase

As already said before, rutile phase occurs during the precursor calcination. Centi and co-workers claim that in vanadium antimony rutile phase, the cation redox reaction takes place in the 350-500°C range²⁰. Cavani et al., studying the solid state reactions between different antimony oxides and vanadium pentoxide, observed the absence of rutile formation at 400°C calcination temperature, traces of SbVO_4 at 500°C (using Sb_2O_3) and complete transformation to rutile phase at 600°C (using Sb_2O_3). At the latter temperature, rutile formation in Sb_2O_4 synthesis is detected in small amount.¹⁹ To obtain rutile phase with good confidence, temperature has to keep in the range of 700-800 °C. Temperatures above 800°C break the rutile lattice to form Carbon oxides more stable.

It is necessary to stress the relevance of the time needed for the rutile formation: intimate contact reached in wet way synthesis corresponds to an easy diffusion of a cation to another phase to give redox reaction. Solid state reactions are related to a spatial separation between the cations placed in different (although intimately mixed and grained) physically separated grains, so that the mutual diffusion needs a great deal of time and sometimes a higher temperature. Actually, in solid state reactions, the higher temperature holds on the order of days (24 hours or more) while in coprecipitation temperature holds on the order of hours (usually 3 hours).

Rutile phases are detectable and usually studied by means of X-ray spectroscopy and Raman spectroscopy:

- In X-ray spectroscopy the antimonate chromium and vanadium rutile lattice cell shows four main lines around 28, 35, 54 and 68 2θ and minor line around 39, 41, 57, 61 and 64 2θ . As observed before, rutile structure owns a very flexible lattice, which is able to accommodate vacancies and excess of

cations by means of non-stoichiometry. This variation results in lines-shift: an expansion of the cell induces a shift of the lines to lower angles and the extent of the movement is different from line to line. Different cations incorporated in the rutile lattice may induce a variation in the crystallinity and in the crystal size; this effect is recognised in XRD spectroscopy observing the lines shape. Scherrer formula relates the crystal size to the peak width at half height:

$$B(2\theta) = K\lambda/L\cos\theta$$

- Raman spectroscopy is a very useful technique, as it is easy and fast. Unluckily the spectra collected are often of low quality, so sometimes they are difficult to be interpreted. It has often been noticed that an improvement in the crystals quality leads to a better peaks resolution. Three bands at about 760, 670, 540 cm^{-1} are typical of the rutile structure and a broad band placed in the 800 – 900 cm^{-1} range is usually assigned to defects in the Sb-O-Sb chain.

2.1.3 Antimony oxides phases²¹⁻²³

Antimony is a silvery lustrous grey metalloid, present in oxidation states III and V, found in nature mainly as the sulphide mineral stibnite (Sb_2S_3). Oxides formed by antimony, included often in oxidation catalysts preparation, are difficult to be studied because of the different existing stoichiometry and different polymorph. The active phase in catalysis is the most stable oxide Sb_2O_4 , but oxide described with the formula Sb_2O_3 , Sb_2O_5 and Sb_6O_{13} may also be obtained.

- Sb_2O_3 may be found in two different allotropes, both stable at room temperature: (i) cubic colourless senarmonite consists of dimeric units highly volatile which is able to sublime above 775K; (ii) orthorhombic valentinite has a layered structure formed by chains hold together by weak Sb-O interactions. There is no evidence of differences in catalysts preparation between the two polymorphs. Volatility of senarmonite leads to use aqueous media in the oxidation reactions. Preparation of antimony trioxide is possible

by oxidation of Sb (or Sb_2S_3) in air or by hydrogenation of higher oxides. In Raman spectroscopy, senarmonite shows a main peak around 261 cm^{-1} and secondary remarkable peaks at 197 and 84 cm^{-1} ; Valentinite shows peaks at 140 , 294 , 223 and 502 cm^{-1} .

- Sb_2O_5 is the other full antimony oxidation state oxide and there is no evidence for the existence of the anhydrous powder. It is possible to synthesize the pentoxide starting from lower oxides in drastic conditions. Preparation of pure Sb_2O_5 starting from $\text{Sb}_2\text{O}_5 \cdot n\text{H}_2\text{O}$, is often claimed to be possible; the heat necessary for the water evaporation is enough for the partial dehydration coupled with the oxygen loss, with the consequent formation of Sb_6O_{13} . Only two Raman bands have been recognized in pentoxide at 502 and 620 cm^{-1} .
- Sb_2O_4 is the main mixed valency oxide, made of equimolar proportion of Sb(III) and Sb(V) and it should be responsible for the catalytic activity in oxidation. It is prepared via Sb_2O_3 oxidation (at temperature above 870K) or via decomposition of higher oxide (upper than to 1000K). “ α ” orthorhombic (also known as cervantite) and “ β ” monoclinic allotropes are available, but the first one is the most common and it is prepared by Sb (or Sb_2O_3) oxidation at 873K or higher oxide decomposition at 1223K . Lower reduction temperature leads to β allotropes formation, also achievable from α one at 1233K in sealed tubes. Cervantite is observed by means of Raman spectroscopy through bands at 200 , 62 , 43 , 140 and 403 cm^{-1} ; β form shows band at 212 , 79 and 405 cm^{-1} .
- Sb_6O_{13} is the mixed oxide made by Sb(V) and Sb(III) in 2:1 ratio. It is made by Sb_2O_5 decomposition at 973K or by Hydrogen peroxide oxidation and it shows a Raman band on 470 cm^{-1} . This oxide has a structure between Sb_2O_4 and Sb_2O_5 . The formation of Sb_2O_4 is a thermal evolution of Sb_2O_5 , as described by the following steps:
 - $\text{Sb}_2\text{O}_5 - \text{Sb}_6\text{O}_{13}$ non-stoichiometric amorphous (723K).

- Sb_6O_{13} non-stoichiometric amorphous - Sb_6O_{13} non-stoichiometric crystalline (977K)
- Sb_6O_{13} non-stoichiometric crystalline - Sb_6O_{13} (977 – 1026K)
- $\text{Sb}_6\text{O}_{13} - \alpha\text{-Sb}_2\text{O}_4$ (>1026K)

2.1.4 Rutile – antimony oxide phase cooperation

Once analysed the great properties of rutile as lattice host structure, his synthesis and the phase characteristics of the antimony oxide, some consideration are needed in order to understand the behaviour of the antimonate catalysts.

It is widely accepted that an excess of antimony in rutile catalysts is needed to form an antimony tetroxide phase, which is able to enhance ACN selectivity. This effect has been discussed by Andersson and co-workers: SbVO_4 is unselective in propane ammoxidation to acrylonitrile while cervantite is not active in alkane conversion; as shown in Fig.2.1, the increase of Sb to V ratio up to 1, leads to a clear decrease in propane conversion and in propene selectivity with a clear increase in ACN selectivity.

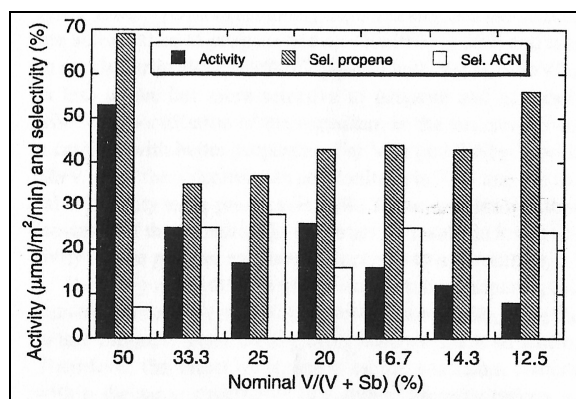


Fig. 2.1 Catalytic properties of rutile with increasing of nominal Antimony amount. Moving from 50 to 33.3 (from $\text{Sb}/\text{V} = 1/1$ to $\text{Sb}/\text{V} = 2/1$), the increase in ACN selectivity is drastic; higher Sb quantity influences significantly the selectivity and affects negatively the activity.

In order to understand the behaviour of the phases inside the catalyst, has been made a comparison of the following solid systems:

- pure SbVO_4 (a)

- mixture of SbVO_4 and $\alpha\text{-Sb}_2\text{O}_4$ after co-calcination at 800°C , (b)
- SbVO_4 after co-calcination with $\alpha\text{-Sb}_2\text{O}_4$ and sub-sequent sieve separation (c)
- $\alpha\text{-Sb}_2\text{O}_4$ after co-calcination with SbVO_4 and sub-sequent sieve separation (d)

This study (Fig. 2.2) points out the effective activity and selectivity in ACN of (b) compared to (a), according to the phase cooperation theory mentioned above. The increase in selectivity of (c) in comparison to (a) is remarkable, which is understandable if an antimony cation migration has been considered; the mechanism of migration, on vanadium cations, is crucial to explain the activity loss and the selectivity improvement on the usually unselective antimony tetroxide (d).

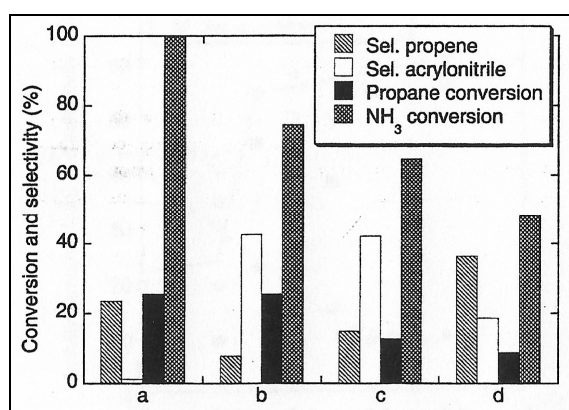


Fig. 2.2 Comparison of the solid systems described above: (a) pure SbVO_4 , (b) mixture of SbVO_4 and $\alpha\text{-Sb}_2\text{O}_4$ after co-calcination at 800°C , (c) SbVO_4 after co-calcination with $\alpha\text{-Sb}_2\text{O}_4$ and sub-sequent sieve separation, (d) $\alpha\text{-Sb}_2\text{O}_4$ after co-calcination with SbVO_4 and subsequent sieve separation.

2.1.5 Synthesis

Chromium antimonate has been synthesized with two different preparation methods:

- Co-precipitation, developed for preparation of SnO_2 based systems by Rhodia²⁴: different weights of starting material (different soluble salt have been tested) have been calculated to obtain 10g of the desired Sb/Cr ratio.

SbCl_5 (or i.e. SbCl_3) and the other cation ($\text{Cr}(\text{NO}_3)_3$, $\text{Ga}(\text{NO}_3)_3$) are dissolved in absolute ethanol (usually 100mL of solvent are used); the first gives a pale yellow solution which becomes transparent and Cr^{3+} salt gives an intense blue mixture. Vigorous stirring has been kept for 15 minutes, at room temperature, to guarantee sufficient homogeneity of the solution. The mixture is then dropped in 100mL of water solution buffered with ammonium acetate (10%w/w) and kept at pH 7 ± 0.2 by means of ammonia aqueous solution (10% w/w). After its separation from the supernatant, the solid has been washed 3 times with distilled water. The precursor is then dried at 120°C for 12 hours and calcined in air at 700°C for 3 hours. A crucial step of this preparation is the managing and accurately weighting the antimony chloride for its very tendency to hydrolyze, also with air moisture, to give gaseous hydrochloric acid and a white solid.

- Slurry, in 100mL of the water solution of $\text{Cr}(\text{NO}_3)_3$, or $\text{Ga}(\text{NO}_3)_3$, antimony trioxide is kept in suspension by stirring at room temperature. After 15 minutes mixing, the solution is dried in rotavapor at 70°C and low pressure, then it is calcined in air. Varying time and temperature of the heat treatment allows obtaining different solid systems.
- High-energy milling is an easy technique already available to prepare vanadium antimonate: the oxides of the cation (Sb_2O_3 or Sb_2O_5 and Cr_2O_3) are weighed and premixed in ethanol to ensure good homogeneity of the sample. After the liquid removal (3 hours at 120°C), the solid mixture is milled for the time needed to complete the solid-state reaction. The milled powder is then calcined for 3 hours at 700°C . In our case carborum tungstenate balls and container were used to avoid contamination or corrosion. Raman analyses of these samples did not point out considerable rutile bands and for this reason no test in ammoxidation has been performed. Further investigations are needed to understand the solid state reaction mechanism in rutile synthesis.

2.1.6 Catalysts characterization

The catalysts prepared with the methods described above are characterized with Raman spectroscopy, EDX probe, XRD spectroscopy, XPS, BET and AAS analysis.

- Raman Spectroscopy analyses are performed on a Renishaw 1000, with confocal microscope confocal Leika DMLM (zoom 5X, 20X e 50X) coupled with a CCD camera. Excitement is made by green Argon at 514nm. The instrument works in reflectivity within an area of $1 \mu\text{m}^2$ (considering a 50X zoom) and 2 μm deep, so Raman spectroscopy is considered a technique for superficial investigation. Raman analysis is fast, in the order of minutes, very punctual and non invasive (usually non destructive, but sometimes bonds rupture occurs due to the high energy of the light source).
- EDX probe INCA Oxford mod 350 SEM Zeiss. Evo 50: the sample is analyzed in powder or tablets form. During the analysis it is possible to collect SEM images of the catalyst.
- XRD diffraction analysis are conducted on an automatic powder diffractometer Phillips X' Pert 9/29 with Bragg Brentano geometry, using Cu $K\alpha$ ($\lambda = 1,5416 \text{ \AA}$) radiation and 1,5kw power. Analysis are performed in the range of $5^\circ - 90^\circ$ (2θ) with $0,02^\circ$ (2θ) steps of 40 seconds each. Inorganic phase searching is based on Hanawalt on PDF-2 (Powder Diffraction File, ICDD) data. Quantitative analysis and structural data are calculated by means of GSAS software (Generalized System Analysis System). Scherrer formula is used for particle size estimation.
- XPS analysis are conducted in ultra high vacuum at 2×10^{-9} Torr, 200kV in "Survey" modality (surface atomic concentrations) and "Multi" modality (signals shape). The analysis works within an area of about $0,5\text{mm}^2$ and 10nm depth.
- BET measurements are made on a Carlo Erba Sorpty 1750 instrument, using nitrogen as adsorption gas. The method of analysis consists of an initial evacuation of adsorbed substances in vacuum conditions at around 200°C

and nitrogen pulses at ca 77K (by means of liquid nitrogen). The pressure is measured during the pulse and gives indication of the monolayer formation; the number of pulses indicates the amount of nitrogen adsorbed as well as the area covered by the molecules.

- ICP-AAS: the sample is dissolved in TFM and hydrochloric acid by means of a Milestone Ethos1 microwave (power around 1500W and at 220°C). Analysis are performed on an ICP PERKIN ELMER “OPTIMA 4300ΔV”.

2.2 Catalytic tests

2.2.1 Plant

In Fig.2.3 it is shown the plant employed in gas phase ammoxidation of propane and propene.

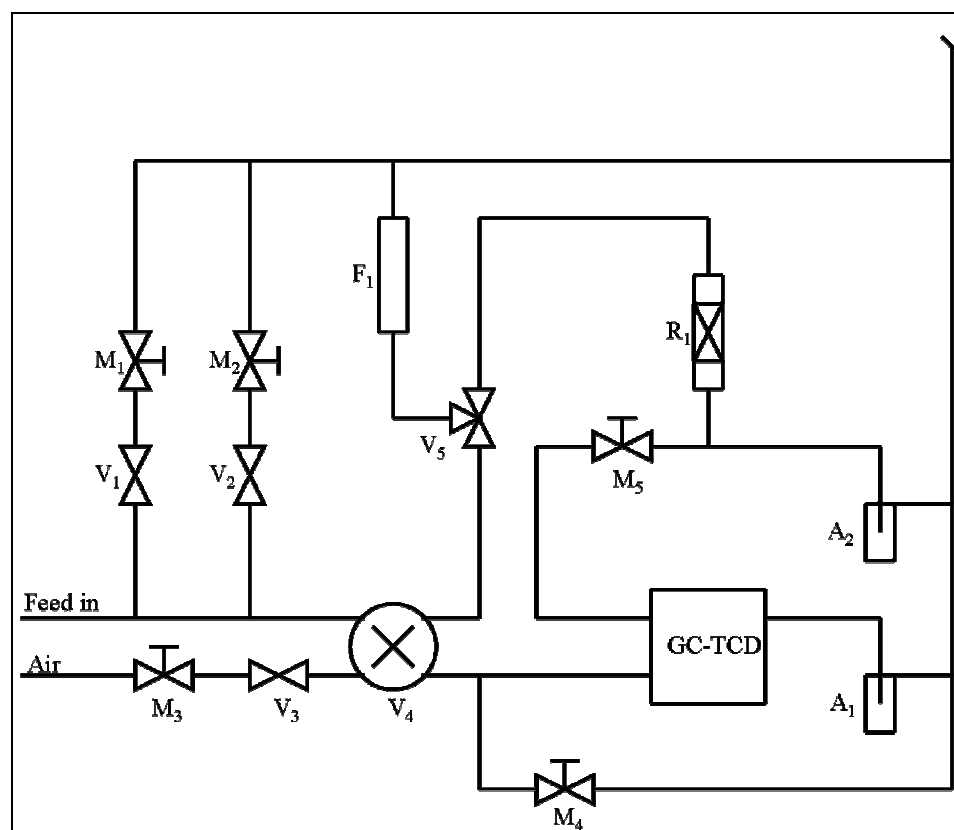


Fig. 2.3 Schematic representation of the gas phase ammoxidation plant

Gas flows are measured by means of Mass Flow Meter (MFM) and are mixed joining together the exit pipes. MFMs are reliable in a fixed range, so the values set around the lower borderline lead to instability of the flow. V1+M1 and V2+M2 are two separated lines useful to spill out part of the reaction stream in order to decrease the total flow. That way it is possible to reach a lower flow than the MFM range or to change the stream (therefore the contact time) during the reaction. The feed line and an air line enter in a 4-way valve (V4) from which two lines come out: one headed to the reactor and the other to the gaschromatograph (GC). In one position of the valve the reaction feed goes to the analysis system while air passes through the reactor; in the

other position the reactant reaches the reactor and the air goes to the (GC). In the first case it is possible to maintain the reactor hot and the catalyst in air environment while the feed undergoes analysis. This is crucial because an oxide kept at high temperature in oxygen-free atmosphere may undergo to irreversible surface modifications and therefore lose the lattice oxygen. In the second case the feed runs to the reactor while air cleans the analysis system lines. V4 is important for the reaction safety because, if some problems occur and a security arrange is necessary, an easy and immediate valve switching quenches the reactor and puts the plant in safe conditions.

Following the analysis line, M4 is useful to waste part of the flow (like M1 and M2): little pressure is necessary to allow the flow feed the GC, but overpressure is unwanted. To handle the pressure of the GC, M4 is adjusted.

The reactor line crosses V5, a three way valve which is able to direct the flow to a soap flow meter (F1) for the flow measurement. That way the reactor has not been crossed by reaction feed, or by other gases so it is fully isolated. This is a way to interrupt the reaction (like in the case already seen with V4), but in this situation the catalyst has not been crossed by air so that it may undergo reduction and surface modification.

The flow that passes through the reactor is subjected to friction loss, which is nearly absent in the soap flow meter. The measured and the real flows are different; we claim that the over pressure induced by the friction loss is negligible so that measured and real flows may be considered equals; it is not possible to measure the stream in the outflow because of the condensation of some products due to the lower temperature and the crossing of the soap.

The flow passes through the reactor and it is parted: a portion reaches the GC, dosed by M5, and the other goes to vent.

Each flow coming out bubbles in a water basic absorber so that products and acids are stopped by condensation or neutralization. Only gases such as carbon oxides, nitrogen, helium, unreacted oxygen and negligible amount of hydrocarbon are released to atmosphere.

2.2.2 Analysis

The plant is integrated with an on-line GC AGILENT 7890 A and an at-line GC able to separate propane and propene

The analysis of the flows is carried on with 3 columns:

- Col 1 leads to a chromatogram like the one shown in Fig.2.4, in which the first peak is formed by O₂, N₂ and CO while the others are related to CO₂ (1.3'), NH₃ (3.8'), Propane/Propene (5.7'), H₂O (12.9'), HCN (15.1'), Acrolein (19.3'), AcCN (20.5') and ACN (22.1').

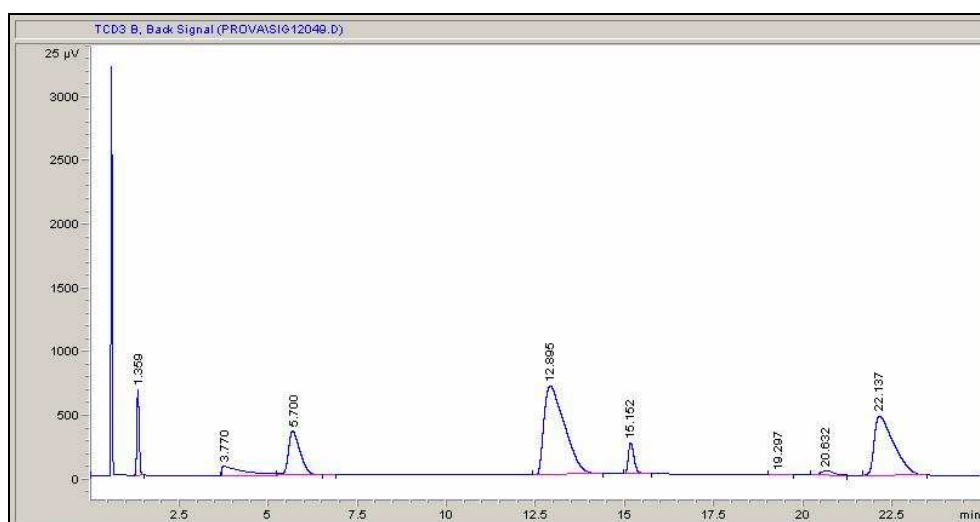


Fig. 2.4 Gas-Chromatogram obtained with the column 1; peaks are resolved except for the ammonia one(3.7s), which shows a long tail on which propene peak is formed.

- Col 2 is a pre-separation column, in which O₂, N₂ and CO pass un-held at the same time.
- Col 3 makes the separation of the previously un-separated peaks eluted in Col 2 (Fig.2.5): O₂ (2.4'), N₂ (3.2') and CO (6.6').

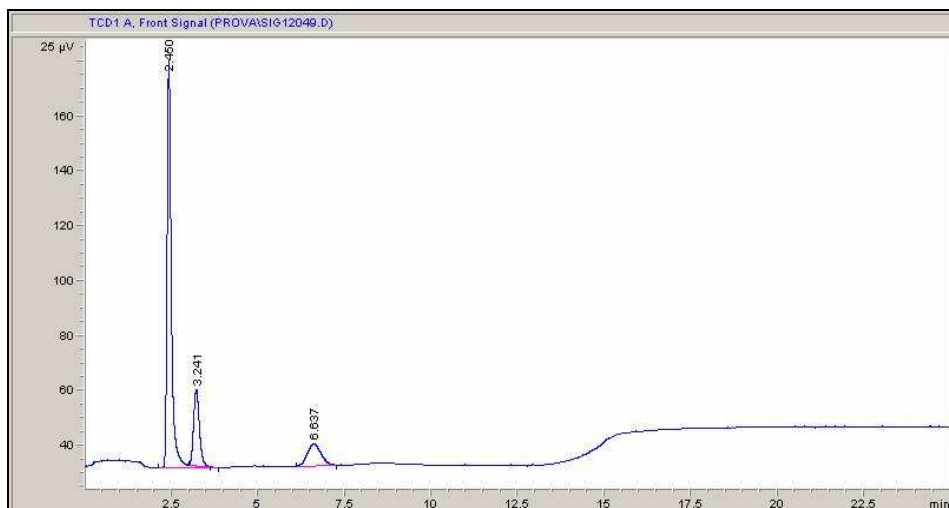


Fig. 2.5 Gas-Chromatogram obtained on Column 3: Nitrogen (3.2') comes out as oxygen shoulder.

The sample insertion in the GC occurs by means of pneumatic valves handled with the instrument software. Three valves are required, as shown in Fig. 2.6.

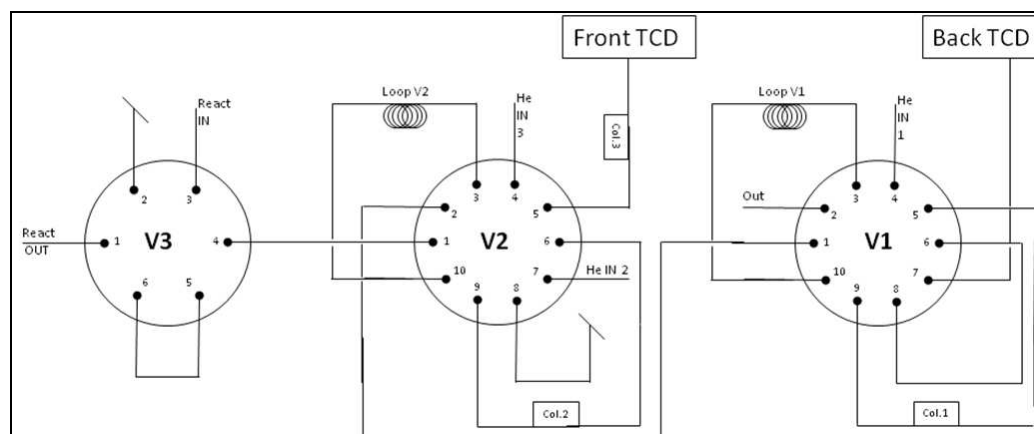


Fig. 2.6 The sampling valves needed to feed the columns.

V3 is the first-six-way-valve in which the flow coming from the line before the reactor (react in) and the flow coming out of the reactor (react out) are selected to be sent to the other valves or to be joined to the vent line.

V2 is a ten-way-valve in which the flow selected in V3 and two separated flows of Helium enter and then may be connected to a loop (loop V2), to the vent line or to the column 2. The last one is then directed to the vent line, to the other valve or to the column 3. In the “off” position, the flow coming from V3 crosses the loop and reaches V1; at the same time an He feed washes the column 2 counter-current and goes to vent

while the other He feed passes through column 3/TCD. In the “on” position the flow coming from V3 is joined to the V1 line directly and a helium line crosses the loop and reaches the column 2, the column 3 and eventually the detector. The other He line goes to vent. This system is useful because in column 3 it is possible to separate oxygen, nitrogen and carbon monoxide, but at the same time the column filler can not get in contact with ammonia. In fact, the gas feed injected by loop V2 is pre-separated in column 2, in which O₂, N₂ and CO exit all together not restrained (retention time is indeed dead column time) and go to column 3; after these substances retention time, the valve switches so that gases not eluted have been washed away by an helium flow. This way Oxygen, nitrogen and carbon monoxide in the column 3 have been separated and reach the detector TCD front.

In V1 the flow coming from the second valve and helium are fed; a loop and the column 1 line may be joined with the inner line. Gases coming out from column 1 and the loop may be connected to the back detector or to the vent line. In the “off” position the feed crosses the loop while the column and TCD have been crossed by Helium. In the “on” position the loop V3 is washed by helium and the content goes to back detector after having been separated in column 3.

The normal position of valves 1 and 2 is “off”, which means that loop is loading and helium is cleaning the columns and the detectors. When analysis starts, the valves automatically turn in “on” position and the sample reaches the columns. After ca. 3 minutes valve 2 repositions itself on “off” position, as well as valve 1 at the end of the analysis after 25 minutes.

In ammoxidation of propene, no other device is required.

In propane ammoxidation, however, along with unreacted alkane, propene is present in reacted flow. In the analysis system described above, propane and propene are not separated, so they have been revealed at the same elution time (same peak). The quantification of propane and that of propene are operated on another instrument equipped with a Flame Conductivity Detector (FID) by means of sample injection with syringe, drawn by a septa inserted in the line coming out of the reactor and directed to vent. The response factors of propane and propene are the same both in TCD and in

FID detector, so that it is possible to analyze the flow in the FID GC and to use the data collected as ratio amount with the parameter calculated on the other GC.

GC is calibrated every 3 month by means of syringe injection using: pure oxygen, pure nitrogen, carbon oxide 4% and monoxide 4% in helium, pure propane, pure propene, water in acetone, hydrocyanic acid by argentometric titration, acrolein in water, acetonitrile and acrylonitrile in water. Calibrations of loops are made using oxygen and carbon oxides.

2.2.3 Thermic system

In order to avoid condensation of products such as water, AcCN and ACN, all the pipelines and the apparatus crossed by the flow coming out of the reactor are maintained at least at 150°C by means of heating ceramics resistance belt, resistance tape and resistance oven. The power supply along with temperature signal from thermocouple are handled and displayed with regulators and programmers.

2.2.4 Calculation sheet

Data are elaborated automatically by means of a Microsoft Excel programmed calculation sheet.

- First data inserted refer to date, sample ID, sample characteristics, sample volume and weight.
- The flow data are written as follows: MFM setting, flow, feed area, flow measure. The program automatically calculates the retention time and the feed composition. It is possible to calculate the amount of feed wasted in order to change the retention time and to recalculate the flux to the reactor.
- The peaks areas are inserted and parameters of reaction such as conversion, yield, selectivity, carbon balance are calculated. The results are corrected on the flux changing due to the reaction stoichiometry.
- In propane ammoxidation, the results given by FID are inserted and an ano/ene ratio is calculated; this ratio, which is applied to the hydrocarbon

area revealed on TCD, allows calculating the amount of propane unreacted and, of course, of propene produced.

- If the carbon balance falls within 95% and 105%, data are considered as reliable and are normalized on balance and selectivity, i.e. sum of selectivities has to give 1 then every selectivity is divided for the sum of selectivities. If the carbon balance is out of range, data are rejected and the test is remade.
- Data collected are plotted in graphs which are useful to represent the catalytic performance and to compare different catalysts.

3 RESULTS AND DISCUSSION

3.1 Ga/Sb and Cr/Sb mixed oxides

3.1.1 *Characterization*

We chose Ga and Cr as the main component of single-metal antimonates because at variance with V in V/Sb/O systems, the most stable valence state for both metal ions is 3+. With rutile V/Sb/O, the presence of a valence state higher than 3+ in the mixed oxide is the main reason for the generation of cationic defects, and of low-coordination O ions, that are recognized to play an important role in the activation of the alkane. On the other hand, in V/Sb/O systems the structure cannot accommodate antimony amount higher than the equiatomic ratio, 1/1; indeed, the various non-stoichiometric V/Sb series reported in the literature contain either a 1/1 atomic ratio between the two components, or an excess of V atoms. Any excess antimony is finally spread over the surface of the rutile V/Sb/O in the form of an amorphous antimony oxide, which also plays an important role for the ammoxidation of the intermediately formed propene into acrylonitrile.

Different is the case for rutile Cr/Sb mixed oxide; in fact, non-stoichiometry is not so much due to the presence of Cr with oxidation state higher than 3+, but to the incorporation of excess Sb, in the form of either Sb^{3+} or Sb^{5+} . In other words, the excess Sb, necessary to favour the transformation of the olefin intermediately formed to acrylonitrile, is not present as a separate phase, but indeed is incorporated inside the rutile framework. Due to the similar features of Cr^{3+} and Ga^{3+} cations (no oxidation state higher than 3+ stable at high temperature, similar ionic radius), we were wondering whether the same structural behaviour experimentally observed with Cr/Sb/O might be expected also in the case of Ga/Sb rutile mixed oxides.

| Me/Sb at. ratios preparation | Code | Me/Sb at. ratios analysis | S.S.A. m²/g | Preparation procedure |
|---|----------------|--|-----------------------------------|---|
| Ga/Sb 1/1 | Ga1Sb1 cp | 1/1.17 ^b | 113 | Co-precipitation |
| Ga/Sb 1/2 | Ga1Sb2 cp | 1/1.61 ^b | 91 | Co-precipitation |
| Ga/Sb 1/3 | Ga1Sb3 cp | 1/4.12 ^b | 50 | Co-precipitation |
| Cr/Sb 1/1 | Cr1Sb1 cp | 1/0.8 ^b | 37 | Co-precipitation |
| Cr/Sb 1/2 | Cr1Sb2 cp | 1/1.6 ^b | 67 | Co-precipitation |
| Cr/Sb 1/3 | Cr1Sb3 cp | 1/2.8 ^b | 54 | Co-precipitation |
| V/Sb 1/1 | V1Sb1 cp | Nd | 26 | Co-precipitation |
| V/Sb 1/2 | V1Sb2 cp | Nd | | Co-precipitation |
| V/Sb 1/3 | V1Sb2 cp | Nd | 7 | Co-precipitation |
| Cr/Sb 1/1 | Cr1Sb1 cpw | 1/1.15 ^b | 23 | Co-prec.+ NH ₄ Cl wash |
| Cr/Sb 1/1.5 | Cr1Sb1.5 cpw | 1/1.42 ^a | | Co-prec.+ NH ₄ Cl wash |
| | | 1/1.56 ^b | 22 | |
| Cr/Sb 1/2 | Cr1Sb2 cpw | 1/1.92 ^a | | Co-prec.+ NH ₄ Cl wash |
| | | 1/2.10 ^b | 27 | |
| Cr/Sb 1/2.5 | Cr1Sb2.5 cpw | 1/2.70 ^b | 23 | Co-prec.+ NH ₄ Cl wash |
| Cr/Sb 1/3 | Cr1Sb3 cpw | 1/3.50 ^b | 34 | Co-prec.+ NH ₄ Cl wash |
| Cr/Sb 2/1 | Cr2Sb1 asl | Nd | 53 | Slurry aq. Sb acetate |
| Cr/Sb1.5/1 | Cr1.5Sb1 asl | Nd | 47 | Slurry aq. Sb acetate |
| Cr/Sb 1/1 | Cr1Sb1 asl | Nd | 50 | Slurry aq. Sb acetate |
| Cr/Sb 1/1.5 | Cr1Sb1.5 asl | Nd | 37 | Slurry aq. Sb acetate |
| Cr/Sb 1/2 | Cr1Sb2 asl | Nd | 29 | Slurry aq. Sb acetate |
| Cr/Sb 1/2.5 | Cr1Sb2.5 asl | Nd | 22 | Slurry aq. Sb acetate |
| Cr/Sb 1/3 | Cr1Sb3 asl | Nd | 17 | Slurry aq. Sb acetate |
| CrSb 1/2 | Cr1Sb2a osl | Nd | 29.0 | Slurry aq. Sb ₂ O ₃ |
| CrSb 1/2 | Cr1Sb2b osl | Nd | 41.0 | Slurry aq. Sb ₂ O ₃ |
| CrSb 1/2 | Cr1Sb2d osl | Nd | 45.6 | Slurry aq. Sb ₂ O ₃ |
| CrSb 1/2 | Cr1Sb2f osl | Nd | 48.9 | Slurry aq. Sb ₂ O ₃ |
| CrSb 1/2 | Cr1Sb2g osl | Nd | 53.1 | Slurry aq. Sb ₂ O ₃ |

Tab. 3.1 Catalysts examined: the first row describes the catalysts composition and the hypothetical Me/Sb atomic ratio, the second row lists the sample I.D., the third row reports the Me/Sb atomic ratio (when available) found by means of (a) elementary AAS-ICP analysis and or (b) SEM-EDX analysis, fourth row reports the specific surface area and the last row describes the synthesis method.

Tab.3.1 compiles the samples prepared and the specific surface area, after thermal treatment in air at 700°C. In the case of the Cr/Sb/O samples, different series of samples were prepared; one series was synthesized with the co-precipitation procedure from ethanolic solution, as reported in the previous works and also employed for the preparation of Sn/V/Sb/O rutile samples (the same procedure was adopted also for the preparation of the Ga/Sb/O samples). A second series also was synthesized with the co-precipitation procedure, but the precipitate was thoroughly washed with water before thermal treatment, an operation aimed at removing the ammonium chloride formed during the co-precipitation step.

Another series was prepared by means of the conventional slurry method, in which Sb is not dissolved in the preparation medium, but indeed is present as a solid. In this procedure, two different raw materials can be used, either Sb oxide (Sb_2O_3 or even Sb_2O_5), or $\text{Sb}(\text{CH}_3\text{COO})_3$. In the former case, Sb oxide is insoluble in the reaction medium, and hence a slurry develops; with Sb acetate, once added to the aqueous solution of the Cr salt, the immediate precipitate of an Sb compound (likely, an Sb oxohydrate) occurs. There are major differences between the various preparation methods, as will be clear after comparison of the characteristics of calcined samples having the same Cr/Sb ratios, but prepared using the different procedures. For example, the osl (slurry method from Sb^{3+} oxide) is hardly reproducible, and samples prepared with exactly the same amount of starting amount and using identical procedures, may finally show quite different features, e.g., a different amount of Sb incorporated in the rutile structure. This may be attributed to the fact that the reproducibility of the solid state reaction occurring in the precipitate between Cr oxohydrate and Sb oxide is negatively affected by the relatively large particle size of the latter compound. Indeed, the same irreproducibility was not observed in the case of the asl method (slurry redox from antimony acetate), probably because the Sb compound that precipitates after dropping the Sb acetate in the aqueous solution is more reactive than Sb oxide, either because of the smaller particle size or because of the higher reactivity of an oxohydrate as compared to the oxide.

In regard to samples prepared with the co-precipitation procedure, the thermal treatment of unwashed precursors (cp method) finally led to samples having greater specific surface area than those prepared by preliminary removal of the salt (cpw method) (Tab.3.1). Since this treatment did not affect so much the crystallinity of calcined samples (that was the same for the two series of Cr/Sb/O samples, as inferred from X-ray diffraction patterns, see below), the effect on surface area was due to a different morphology of samples. It is possible that the decomposition of ammonium chloride, occurring at around 350°C, generates holes and cavities in the particle that finally are responsible for the higher surface area of samples obtained from the untreated precursors. The surface area of Cr/Sb/O samples prepared by means of the slurry procedure (asl) was higher than that of co-precipitated (cpw) samples for Cr/Sb atomic ratio values ranging from 1/1 to 1/1.5, but then became similar for the two series of samples when higher Sb contents were used for catalysts preparation. For what concerns the surface area of Ga/Sb/O samples, Tab.3.1 shows that it was systematically higher than that of Cr/Sb/O catalysts. In this case, the difference was due to the lower crystallinity of Ga/Sb/O samples (see XRD patterns, reported below).

Chemical analysis was used to check the composition of samples; this is particularly important for co-precipitated samples, because the procedure adopted did not lead to the complete precipitation of all metal oxohydrates, and the supernatant solution, still containing dissolved metal cations, was removed by filtration before the thermal treatment of the precipitate. Furthermore, the comparison of ϵ vs pH diagrams highlighted remarkable differences between the metals used, the pH chosen finally representing a compromise aimed at obtaining the concomitant precipitation of corresponding oxohydrates. However, data reported in Tab.3.1 show that the atomic ratio between components, for all samples prepared, was not much different from that one used for the preparation of the starting solution. In the case of samples prepared by the slurry method (asl and osl), there was no need to make chemical analysis of samples, since the precipitation of the solid occurred by solvent evaporation; therefore, the chemical composition of calcined samples was identical of that of the starting solution.

Fig.3.1, Fig.3.2 and Fig.3.3 reports the X-Ray diffraction patterns of Ga1Sbxcp, Cr1Sbxcpw and V1Sbxcp samples. Patterns of Cr1Sbxasl and Cr1Sbxcp (the latter were also reported in a previous work) were quite similar to those of Cr1Sbxcpw, and are been reported for sake of brevity.

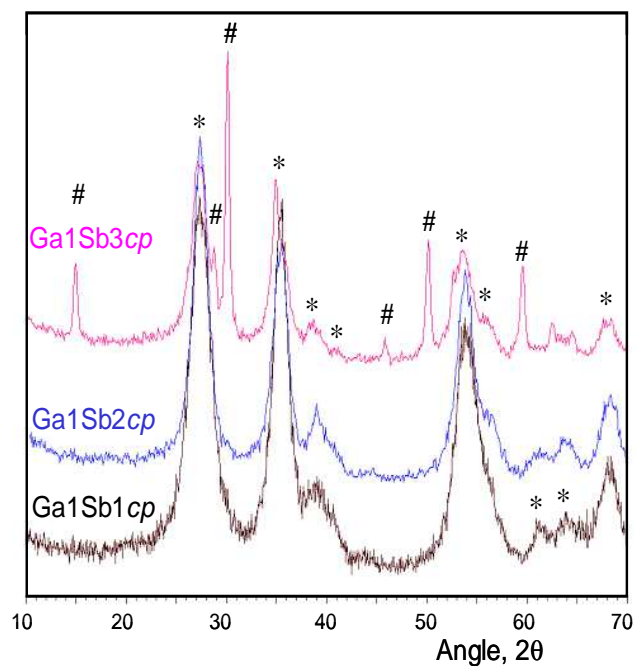


Fig. 3.1 XRD patterns of Ga1Sbxcp. * rutile (JCPDS 81-1219); # Sb₆O₁₃ (71-1091).

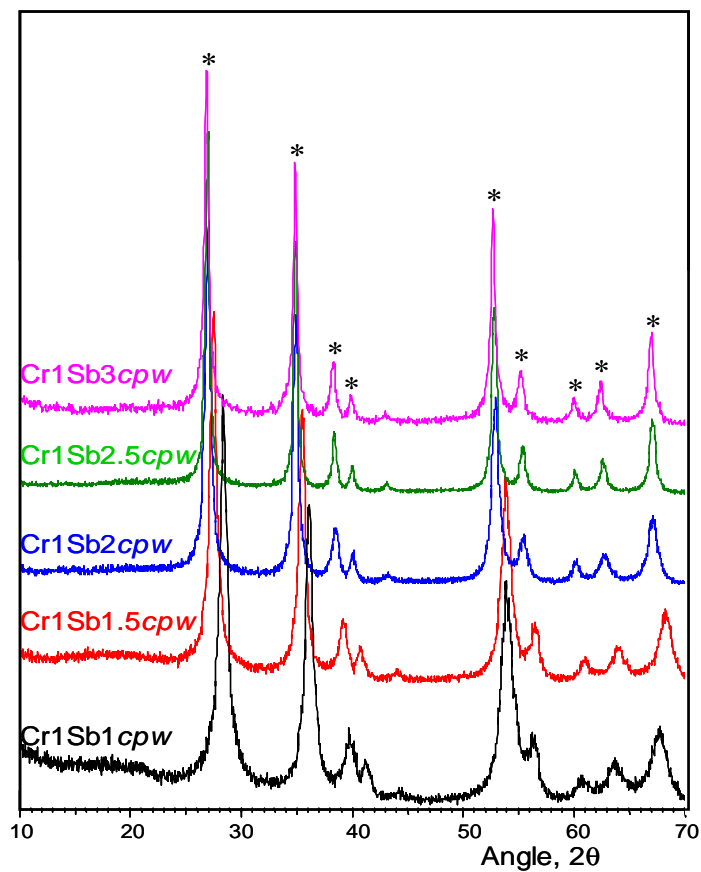


Fig. 3.2 XRD patterns of Cr₁Sb_xcpw. * rutile (JCPDS 81-1219).

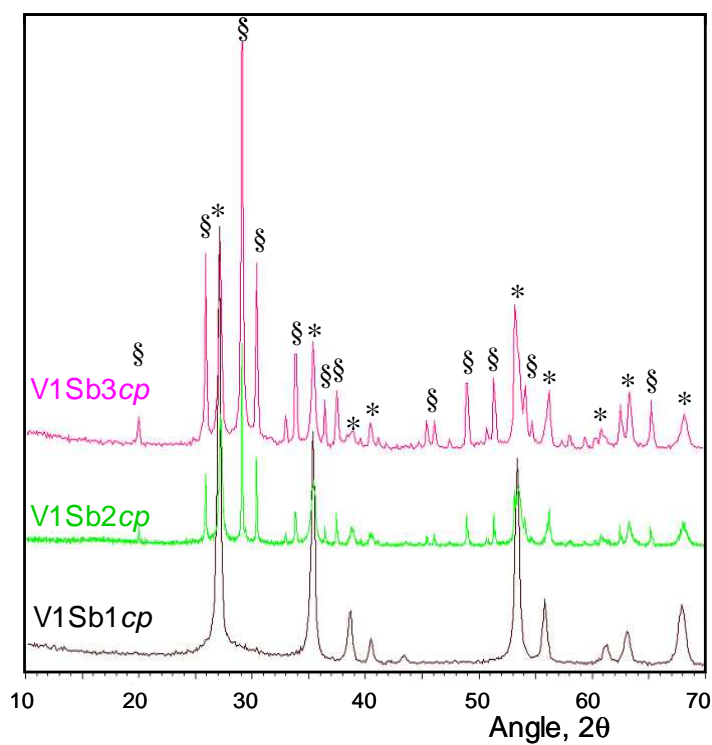


Fig. 3.3 XRD patterns of V₁Sb_xcp. * rutile (JCPDS 81-1219); § Sb₂O₄ (80-0231).

Some major differences between the series of samples are evident:

- The crystallinity of samples was very different; more crystalline samples were V1Sbx (average crystallite size 59 nm), the least crystalline Ga1Sbx (average crystallite size 7 nm). The crystallinity of the Cr1Sbx samples (crystallite size 20 nm) was not much affected by the method of preparation used.
- In XRD patterns of all Cr1Sbx_{cpw} and Cr1Sbx_{cp} samples, the only crystalline compound was rutile CrSbO₄ (JPCDF 35-1288)²⁵, with the exception of sample Cr1Sb3_{cp}, for which crystalline Sb₆O₁₃ also formed, and for the Cr1Sb3_{asl} sample, which contained Cr₂O₃ also (Tab.3.2). Quite different was the situation for Ga1Sbx and V1Sbx samples; in the former case, crystalline Sb₆O₁₃ (JCPDF 71-1091) was present in the sample Ga1Sb3, that however did not form in Ga1Sb2, whereas crystalline Sb₂O₄ formed in both V1Sb2 and V1Sb3 samples. Therefore, rutile V/Sb/O cannot accommodate excess Sb in its structure with respect to the stoichiometric atomic ratio, whereas rutile Cr/Sb/O may host a large excess Sb.
- As mentioned above, the slurry redox method carried out using Sb₂O₃ led to remarkable differences in the characteristics of samples, although all of them were prepared with the same Cr/Sb atomic ratio (1/2), and by means of identical procedure. This is evident from Tables 3.1 and 3.2; sample Cr1Sb2_{nosl}, when prepared several times, gave a surface area that ranged in the interval between 29 and 53 m²/g (Table 1), whereas the amount of Sb₂O₄ oxide (as inferred after Rietveld refinement of the corresponding XRD patterns) decreased and that of rutile correspondingly increased (Tab.3.2). At the same time, the volume of the tetragonal cell also varied remarkably, confirming that the amount of Sb incorporated in the structure was inversely proportional to the amount of extra framework Sb oxide.

| Code | Crystalline phases | Cell volume (\AA^3), c/a |
|-------------|---|-------------------------------------|
| Ga1Sb1cp | Rutile | Nd |
| Ga1Sb2cp | Rutile | Nd |
| Ga1Sb3cp | Rutile + Sb ₆ O ₁₃ | Nd |
| Cr1Sb1cp | Rutile | 64.43, 0.661 |
| Cr1Sb2cp | Rutile | 65.29, 0.658 |
| Cr1Sb3cp | Rutile + Sb ₆ O ₁₃ | 65.52, 0.655 |
| V1Sb1cp | Rutile | Nd |
| V1Sb2cp | Rutile + α -Sb ₂ O ₄ | Nd |
| V1Sb2cp | Rutile + α -Sb ₂ O ₄ | Nd |
| Cr1Sb1cpw | Rutile | 64.03, 0.659 |
| Cr1Sb1.5cpw | Rutile | 64.60, 0.659 |
| Cr1Sb2cpw | Rutile | 65.24, 0.657 |
| Cr1Sb2.5cpw | Rutile | 65.59, 0.656 |
| Cr1Sb3cpw | Rutile | 65.68, 0.655 |
| Cr2Sb1asl | 93% Rutile + 7% Cr ₂ O ₃ | 62.76, |
| Cr1.5Sb1asl | Rutile | Nd |
| Cr1Sb1asl | Rutile | 63.96, 0.663 |
| Cr1Sb1.5asl | Rutile | 64.26, 0.658 |
| Cr1Sb2asl | Rutile | 65.48, 0.653 |
| Cr1Sb2.5asl | Rutile | 65.59, 0.651 |
| Cr1Sb3asl | Rutile + Cr ₂ O ₃ | 65.84, 0.665 |
| Cr1Sb2aosl | 61.8% Rutile + 38.2% Sb ₂ O ₄ | Nd |
| Cr1Sb2bosl | 77.0% Rutile + 23.0% Sb ₂ O ₄ | Nd |
| Cr1Sb2dosl | 81.0% Rutile + 19.0% Sb ₂ O ₄ | 64.62 |
| Cr1Sb2fosl | 89.4% Rutile + 10.6% Sb ₂ O ₄ | Nd |
| Cr1Sb2gosl | 91.3% Rutile + 8.7% Sb ₂ O ₄ | 64.78 |

Tab. 3.2 features inferred from X-ray diffraction patterns of Cr/Sb/O calcined samples

Fig.3.4, 3.5 and 3.6 also reports the crystallographic parameters (Tab 3.2), the volume of the tetragonal cell and the c/a ratio, evaluated by means of the Rietveld refinement. Corresponding values of volume cell for monophasic Cr1Sbxcpw and Cr1Sbxasl samples are also shown in Fig.3.4, in function of the Sb/Cr atomic ratio.

The incorporation of an excess Sb with respect to the stoichiometric composition CrSbO_4 (volume cell 64.31 \AA^3)²⁵] led to an evident expansion of the cell, with a slight decrease of the c/a ratio. This is similar to what experimentally observed for the Fe/Sb/O system, in which an increase of the Sb/Fe ratio leads to an increase of the cell volume of the tetragonal structure, with development of a trirutile like superstructure²⁶. In that case, hosting of an excess Sb^{5+} is compensated for by a reduction of Fe^{3+} to Fe^{2+} ; the limit compound with stoichiometric FeSb_2O_6 is formed for a Sb/Fe atomic ratio of 2, in which Fe is in the divalent oxidation state.

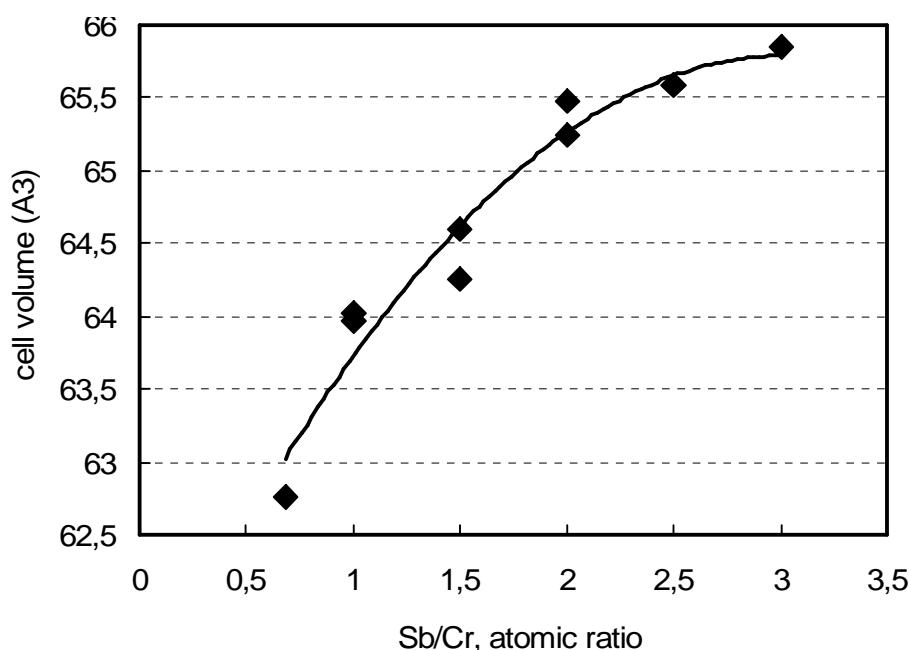


Fig. 3.4 Cell volumes are reported versus the Sb/Cr atomic ratio. A tendency curve is added to clarify the trend.

In the case of our Cr/Sb/O samples, two different hypotheses can be formulated. The first one, by analogy with the proposals of Berry, includes the development of a Sb^{5+} -rich solid solution, with concomitant reduction of Cr^{3+} to Cr^{2+} and development of a trirutile-like cation ordering. The increase in cell volume might thus be due to the presence of the bigger Cr^{2+} cation (0.90 \AA). The second hypothesis involves the development of a compound with stoichiometry $\text{Cr}^{3+}_{1-y}\text{Sb}^{3+}_y\text{Sb}^{5+}\text{O}_4$. In consideration of the ionic radii of the octahedral cations: Cr^{3+} (0.69 \AA), Sb^{3+} (0.76 \AA), Sb^{5+} (0.60 \AA),

an increase in the cell volume with respect to that of CrSbO_4 can be explained by hypothesizing a partial replacement of Cr^{3+} ions with the bigger Sb^{3+} ion.

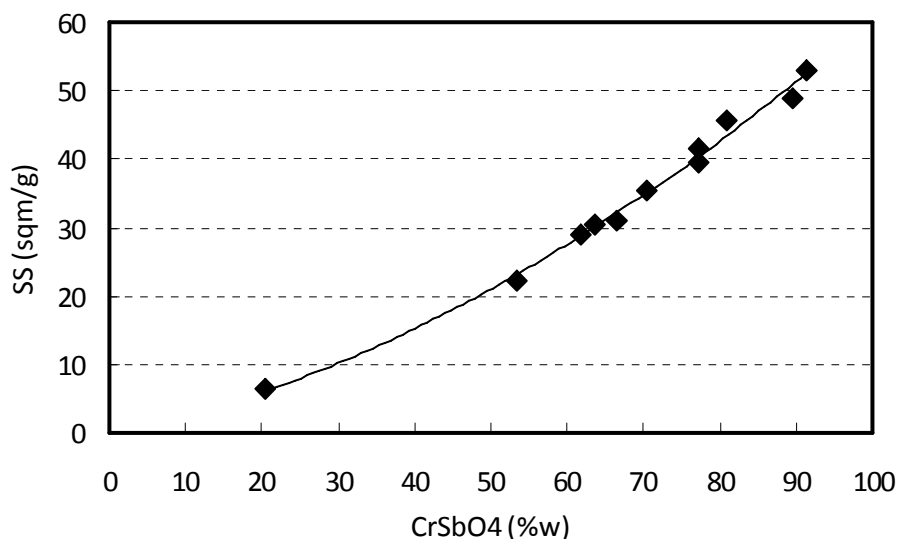


Fig. 3.5 Specific surface area plotted on the relative amount of rutile in the framework.

It is also interesting to note the relationship between the amount of extra framework Sb_2O_4 in $\text{Cr}_1\text{Sb}_2\text{nosl}$ samples and the corresponding value of specific surface area, as well as the relationship between the former parameter and the volume of the tetragonal cell (Fig.3.5 and 3.6, respectively).

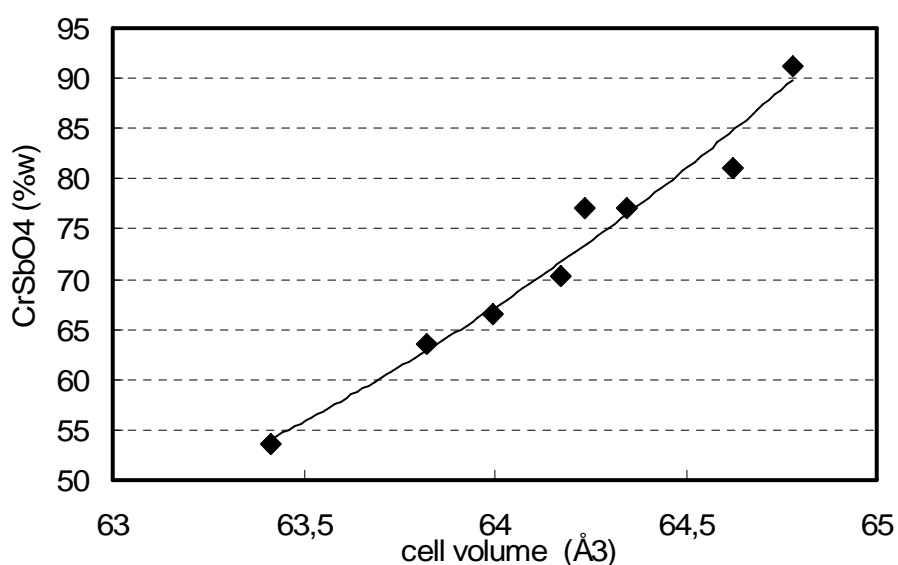


Fig. 3.6 Relative amount of rutile in the structure on the related cell volume.

Samples reported in the Figures are those compiled in Tab.3.2, and many others as well, that were prepared in the attempt to obtain a variable amount of Sb incorporated in the rutile lattice, while keeping the overall Cr/Sb ratio constant. It is evident that an increase of the rutile content in samples leads to an enhancement of the surface area of samples, which is an expected phenomenon because of the intrinsic low surface area of Sb_2O_4 . Moreover, the higher was the amount of Sb incorporated in the rutile lattice (the lower being the amount of extra framework antimony oxide), the greater was the volume of the tetragonal cell of rutile, an observation that agrees with experimental results achieved with samples belonging to samples prepared with the other methods.

Raman spectra of the Cr1Sbxcpw , Ga1Sbxcp , V1Sbxcp and Cr1Sbxasl are shown in Fig.3.7, Fig.3.8, Fig.3.9 and Fig.3.10. Raman bands of TiO_2 rutile are at 143 cm^{-1} (B1g), 235 cm^{-1} (2 phonon process), 448 cm^{-1} (Eg) and 612 cm^{-1} (A1g), whereas SnO_2 rutile shows bands at around 470 , 630 and 770 cm^{-1} , corresponding to the Eg, A1g, and B2g vibration modes, respectively²⁷, which well correspond to bands observed at approximately 470 (or the very weak 560), 670 and 790 cm^{-1} in Ga1Sbxcp samples; an increase of the Sb content leads to a slight shift of the 670 cm^{-1} band towards lower energy, whereas the band at higher energy becomes broader and less defined. However, the position of Raman bands of rutile can be strongly affected by sample crystallinity and surface effects^{28,29}. The band at 470 cm^{-1} , however, can also be attributed to Sb_6O_{13} , and in fact its intensity increases when the Sb content increases also; it becomes the most intense one in sample Ga1Sb3cp , in which crystalline Sb oxide is also present. This sample however also shows a broad band at around 200 cm^{-1} , attributable to $\alpha\text{-Sb}_2\text{O}_4$.

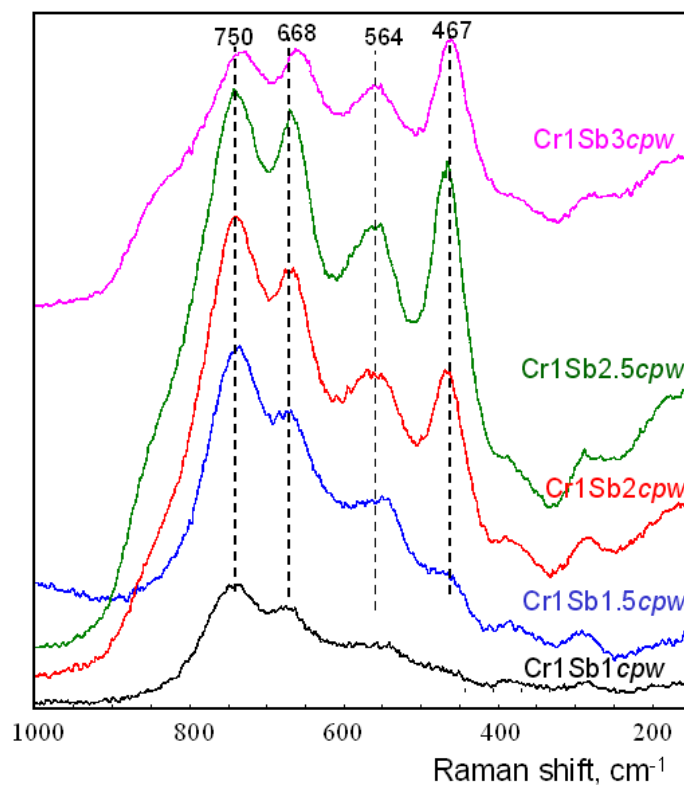


Fig. 3.7 Raman spectra of calcined Cr1Sbxcpw systems.

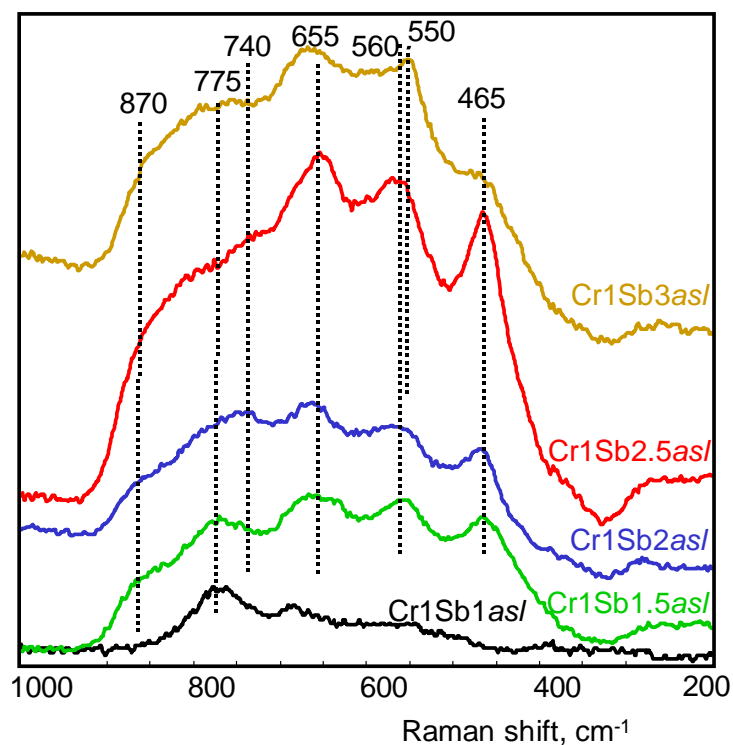


Fig. 3.8 Raman spectra of calcined Cr1Sbxasl systems.

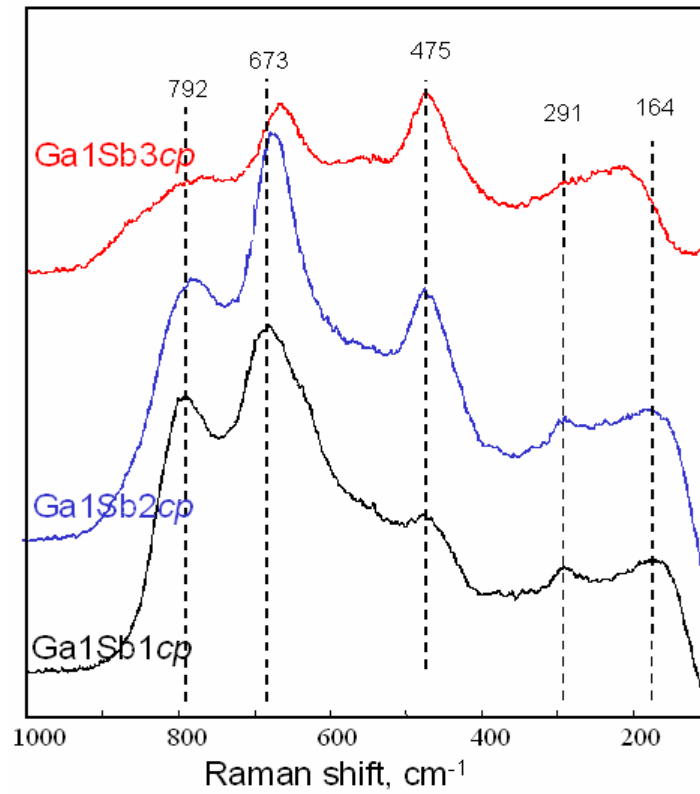


Fig. 3.9 Raman spectra of calcined Ga₁Sb_xcp systems.

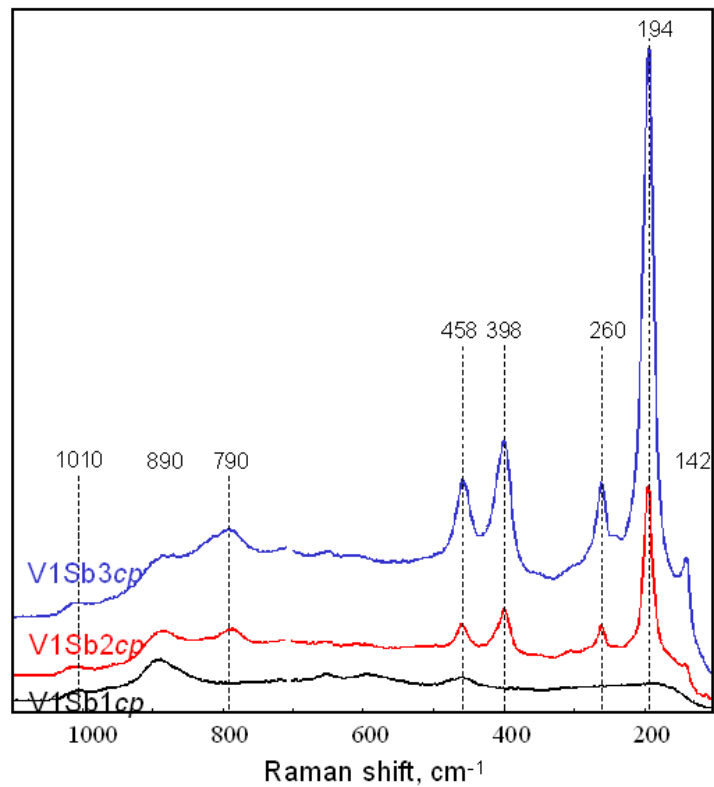


Fig. 3.10 Raman spectra of calcined V₁Sb_xcpw systems.

Spectra of Cr1Sbx cpw samples have analogies with those of Ga1Sbx cp catalysts, and differences as well. Main rutile bands are at approx 750, 670, 565 and 467 cm^{-1} ; also in this case, the latter band might be attributable to Sb_6O_{13} , a compound that however is not observed in any X-ray diffraction pattern of the well-crystallized Cr1Sbx samples. It is worth noting that a part from a better resolution, hinting for a better crystallinity of the rutile compound (a phenomenon also observed in XRD patterns), and for the development of a shoulder at around 850 cm^{-1} , an increase of the Sb content does not lead to any major modification of Raman spectra. A broad weak band at about 200 cm^{-1} , that can correspond either to the main band of α - Sb_2O_4 (200 cm^{-1}) or the main band of β - Sb_2O_4 (212 cm^{-1}) shows a slight increase. Unluckily secondary bands useful to recognize the phase, are placed in uncollected area of the spectra (62 cm^{-1} and 79 cm^{-1}) or are too weak to be observed, 30% and 25% of the main band intensity, at 403 cm^{-1} and 405 cm^{-1} (data referred to α - Sb_2O_4 or β - Sb_2O_4 , respectively).

Raman spectra of samples Cr1Sbx asl show some major differences if compared with spectra of Cr1Sbx cpw samples. Specifically, the band at approx 750 cm^{-1} is shifted towards higher energy in Cr1Sb1 cpw ; then, an increase of the Sb amount leads to weakening of the intensity for this band, at the same time components at both higher (at about 860 cm^{-1}) and lower (at about 740 cm^{-1}) energy becoming progressively more intense. Finally, in Sb-richer samples a broad band, probably consisting of the three different components, dominates the spectrum in the 700-900 cm^{-1} spectral region. The band at 465 cm^{-1} is again attributable to Sb_6O_{13} ; remarkably, this band is substantially absent in the Cr1Sb1 cpw sample, it is well evident in Sb-richer samples, but it almost disappears in the Cr1Sb3 cpw sample. Worth noting, the XRD pattern of this latter sample highlighted for the unexpected formation of Cr_2O_3 ; even in the Raman spectrum, a band at 550-555 cm^{-1} corresponds to the most intense band of Cr_2O_3 .

In literature, the high-energy band is attributed to the development of cationic vacancies in the rutile structure, and is specifically related to vibrations of Me-O bond involving coordinatively unsaturated O atoms. Therefore, Raman spectra indicate that major variations in the rutile structure because of excess Sb incorporation are obtained

with the slurry-redox procedure. In this case, the starting Sb compound is Sb(III)acetate, whereas in the co-precipitation procedure SbV pentachloride is used. With the latter procedure, the development of the rutile mixed oxide and the scarce amount of defects hints for the incorporation of excess Sb in the form of both Sb^{3+} and Sb^{5+} , thus with formation of a stoichiometric solid solution of the type $\text{CrSb}_{1-x}^{\text{III}}\text{Sb}_x^{\text{V}}\text{O}_{4+4x}$. The size of the trivalent cations explains the expansion of the tetragonal cell experimentally observed; the driving force for the reduction of Sb^{5+} to Sb^{3+} is the formation of the stable rutile compound, and is accounted for by the fact that the Sb_2O_5 self-reduces to Sb_2O_4 (a mixed-valence $\text{Sb}^{3+}/\text{Sb}^{5+}$ compound) at around 800°C . The same expansion of the tetragonal cell is observed with the more defective samples obtained by the slurry-redox method, that also suggests either the incorporation of Sb^{3+} cation, or the formation of Cr^{2+} ; in this case, the presence of Sb^{3+} is quite expected, because of the starting compound used for the preparation of samples. We note that the formation of a non-stoichiometric structure may derive from various factors: (i) excess Sb is incorporated mainly as Sb^{5+} , that would lead to the reduction of part of Cr^{3+} to Cr^{2+} : $\text{Cr}_{1-x}^{\text{III}}\text{Cr}_x^{\text{II}}\text{Sb}_{1+x}^{\text{V}}\text{O}_{4+2x}$, up to the limit trirutile-like CrSb_2O_6 for a Sb/Cr atomic ratio of 2; (ii) Sb is incorporated mainly as Sb^{3+} , that if taking the place of Sb^{5+} would lead to the development a corresponding amount of anionic vacancies, $\text{CrSb}_{1-x}\text{Sb}_x^{\text{III}}\text{O}_{4-x}$ (this structure however might probably host a limited amount of Sb^{3+}); (iii) excess Sb is incorporated as Sb^{3+} , that would either lead again to the reduction of Cr^{3+} to Cr^{2+} : $\text{Cr}_{1-3x}^{\text{III}}\text{Cr}_{3x}^{\text{II}}\text{Sb}_x^{\text{V}}\text{Sb}_x^{\text{III}}\text{O}_4$ (also in this case only a limited amount of excess Sb might be incorporated), or to the formation of cationic vacancies, or to the incorporation of excess O^{2-} , for example in the interstitial positions ($\text{CrSb}_x^{\text{V}}\text{Sb}_{1-x}^{\text{III}}\text{O}_{4+3/2x}$). However, the question arises how much Sb could be incorporated in all of these cases, while at the same time maintaining the (defective) rutile structure. One relevant experimental result is the behaviour shown by sample *Cr1Sb3cpw*; in this case, the presence of segregated Cr oxide and of rutile only, with no Sb oxide (as inferred from both XRD pattern and Raman spectrum) suggests that Sb in excess may finally take wholly the place of trivalent Cr in the rutile structure; the segregation of Cr might occur as a consequence of its reduction to Cr^{2+} , whose size is too big to fit

within the rutile mixed oxide for a large amount of it; the reduced Cr would then be oxidized to Cr_2O_3 during the thermal treatment in air.

In Fig.3.11 are shown Raman spectra of samples Cr1Sb2xosl in which the cations relative amount still much the same ($\text{Sb/Cr} = 2$), but low reproducibility of the synthesis method leads to differences in the rutile to antimony oxides ratio. Rietveld data extrapolated on XRD diffractograms are collected in Tab.3.2: Cr1Sb2aosl 61.8% rutile, Cr1Sb2bosl 77.0% rutile, Cr1Sb2dosl 81.0% rutile, Cr1Sb2fosl 89.4% rutile and Cr1Sb2gosl 91.3% rutile.

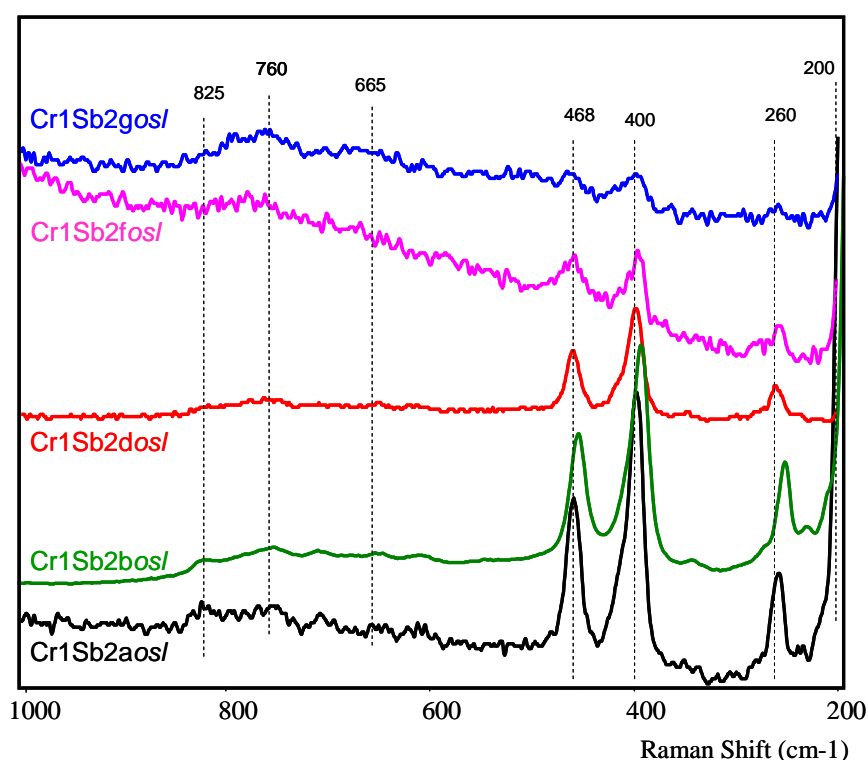


Fig. 3.11 Raman spectra of calcined Cr1Sb2xosl systems. The rutile amount in the structure increases along with y-axis:

Bands at 760 and 665 cm^{-1} are associated to rutile structure; weakness and broadness may be due to low crystallinity of the phase, as already treated previously. Other bands associated to Sb_6O_{13} (468cm^{-1}) and to Sb_2O_4 (200 and 400cm^{-1}) are present, along with a band at 460cm^{-1} , present also in vanadium antimonate spectra, is due to the presence of Sb_2O_3 . In this case the presence of the trioxide is explained by the use of its in the catalysts preparation. All the bands correlated to the antimony

oxides decrease along with the increase of rutile percentage, obviously because the remainder to 100% is Sb_2O_4 (detected by XRD analysis).

Fig.3.12 plots the Sb/Cr surface ratio as determined by XPS, in function of the Sb/Cr preparation ratio, for samples Cr1Sbxasl . The surface ratio was close to the preparation one for Cr1Sb1sl , but then increased exponentially when the Sb/Cr preparation ratio was increased, showing a considerable surface enrichment of Sb. The latter was mainly present as Sb^{5+} , but an increase of the Sb content led to an increase of the relative amount of Sb^{3+} . This effect might be attributed to the formation of pentavalent Sb oxide dispersed over the surface of rutile in samples having more Sb than the amount required for the stoichiometric formation of the rutile. However, we would like to note that Raman spectroscopy did not provide any evidence for the formation of free Sb_2O_5 ; the band at Raman shift 465 cm^{-1} might be attributed to Sb_6O_{13} (containing 66.5% Sb^{5+} and 33.5% Sb^{3+}), but we would like to note that the relative intensity of this band did not increase remarkably when the Sb content was increased, and that the relative amount of Sb^{3+} (as inferred from XPS) was much less than the 33%, and moreover it did increase when the amount of Sb was increased, that is not the expected effect if excess Sb were segregated at the rutile surface in the form of Sb_6O_{13} . Finally, it is evident that in sample Cr1Sb2.5sl , that should contain the greater amount of free antimony oxide, there are no experimental evidences neither from Raman spectrum nor from XRD pattern of the presence of such compound. Therefore, we propose here that the Raman band observed at 465 cm^{-1} indeed is attributable to Sb-O-Sb vibration for excess Sb incorporated in the rutile structure, and that the considerable surface enrichment of Sb is attributable to the fact that excess Sb accumulates towards the surface zone of rutile crystallites.

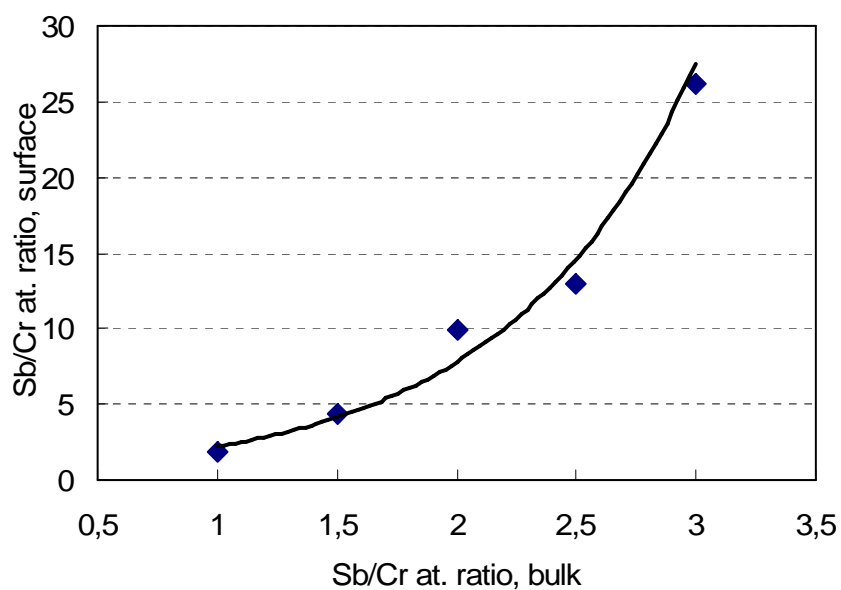


Fig. 3.12 Surface ratio calculated by XPS analysis plotted on theoretical atomic ratio

More accurate data on antimony surface enrichment are showed in Fig.3.13, Fig.3.14 and Fig.3.15, in which sputtering XPS analysis of Cr1Sb1cpw, Cr1Sb2cpw and Cr1Sb2asl are illustrated. The estimated sputtering speed is 6 nm/min and collected results are reported as atomic percentage concentration.

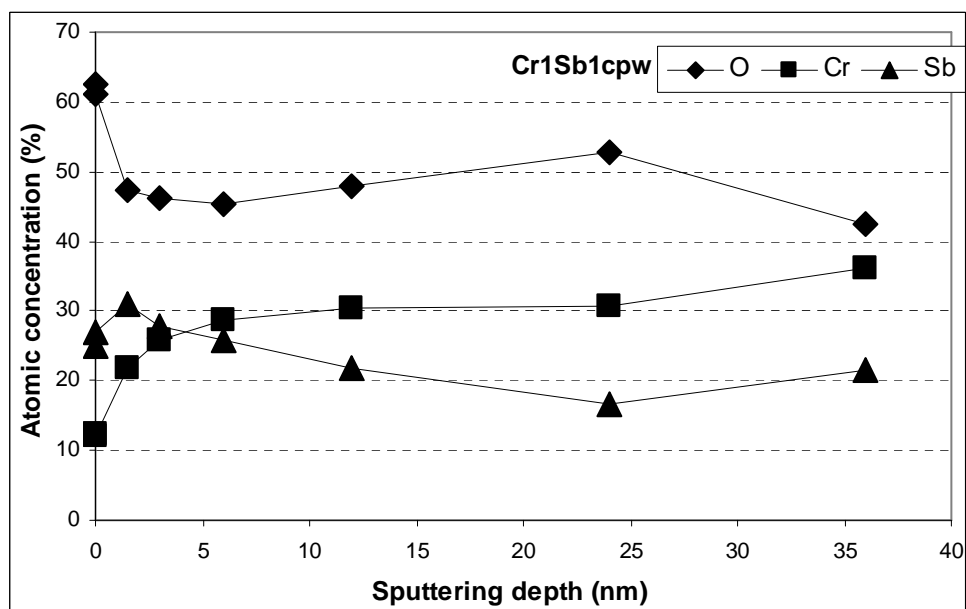


Fig. 3.13 Atomic concentrations of oxygen, antimony and chromium in Cr1Sb1cpw sample plotted on sputtering depth.

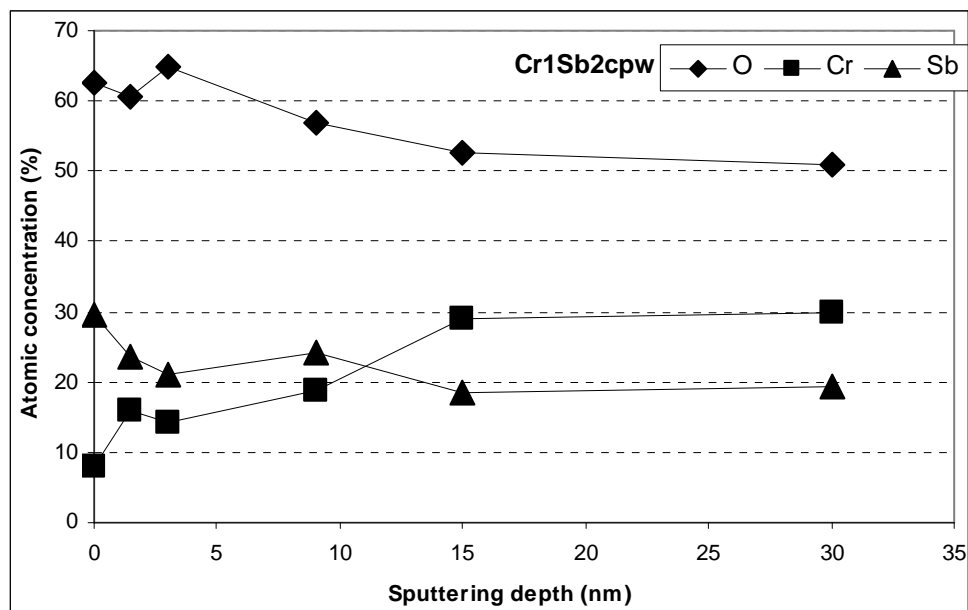


Fig. 3.14 Atomic concentrations of oxygen, antimony and chromium in Cr1Sb2cpw sample plotted on sputtering depth.

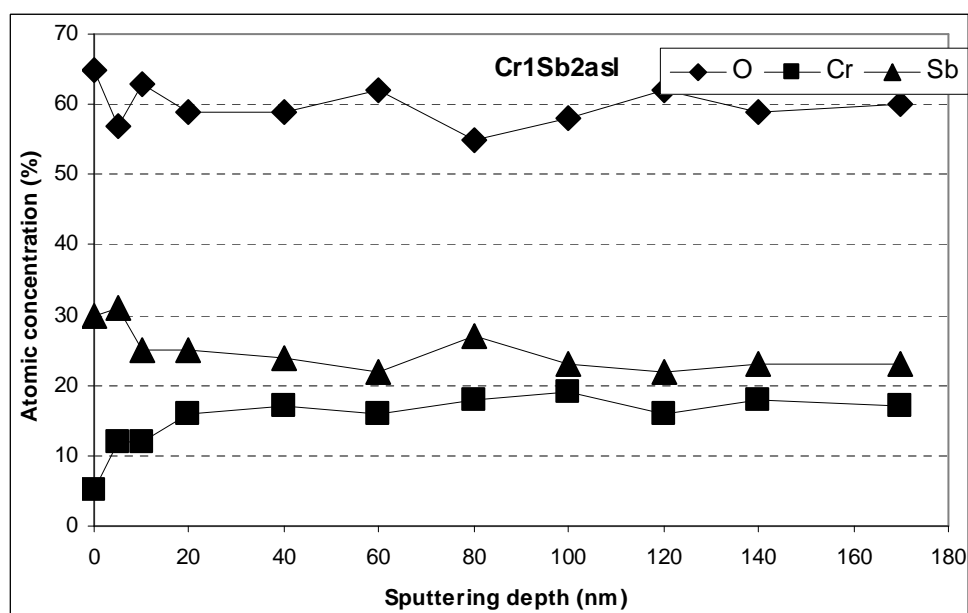


Fig. 3.15 Atomic concentrations of oxygen, antimony and chromium in Cr1Sb2asl sample plotted on sputtering depth.

Each sample shows surface antimony enrichment along with chromium decrease; the contemporaneous surface oxygen enrichment means that the antimony in the surface is mainly present as pentavalent cation, so that oxygen surplus is needed to maintain electro neutrality (the Sb^{5+} substitutes the Cr^{3+}). However, some antimony

may be present as trivalent cation, in order to form surface domes similar to Sb_2O_4 or Sb_6O_{13} , which are the structures commonly detected on rutile surface.

Catalysts prepared with the same method (Cr1Sb1cpw and Cr1Sb2cpw) show a similar trend, but in the sample with Sb/Cr ratio equal to 2 the amount of oxygen is generally higher to compensate the great charge due to the excess of Sb^{5+} . In both samples, the Cr amount in bulk is higher than the Sb one, despite of the excess of antimony in catalyst Cr1Sb2cpw . This effect may be explained with the following mechanism: during its formation, the structure starts from a situation of homogeneity, in which the cations are randomly dispersed in the lattice. The antimony surface enrichments, induced by energy lowering, draw Sb^{5+} and Sb^{3+} from the bulk to the surface while Cr^{3+} is pushed inside, in a cations exchange mechanism.

Actually, the oxygen trend slope is clearly higher in the equimolar sample; it allows us to state that in samples with Sb/Cr ratio equal to 2, it is favoured the movement of the trivalent antimony (in exchange mechanism with trivalent chromium) in order to limit the oxygen displacement and save energy.

It is also evident that even in the case of the equiatomic compound ($\text{Sb/Cr} = 1$), for which there is no accumulation of Sb oxide at the rutile surface", there are considerable intracrystalline gradients of the two elements. In other word, it is no longer possible to talk about random distribution of the two elements inside the rutile lattice, but of the preferential segregation of Sb towards the external/surface part of rutile crystallites (with predominance of Sb-O-Sb bonds), and of preferential segregation of Cr in the more internal part of rutile crystallites. The possible predominance of Cr-O-Cr bonds might also explain why sometimes we recorded the preferential segregation of chromia, during recording of Raman spectra with high-energy laser (spectra not reported)

3.2 Catalytic results

3.2.1 *Cr1Sbxcpw* - Propene ammoxidation

Ammoxidation of propene is carried out in a quartz reactor at the following temperatures: 410, 420, 430, 440, 460°C. Feed composition is approximately propene 7%, oxygen 17% and ammonia 10%. A total flow of about 45mL/min crosses 1mL of catalyst placed in the isotherm part of a tubular oven so that the contact time is about 1,3s.

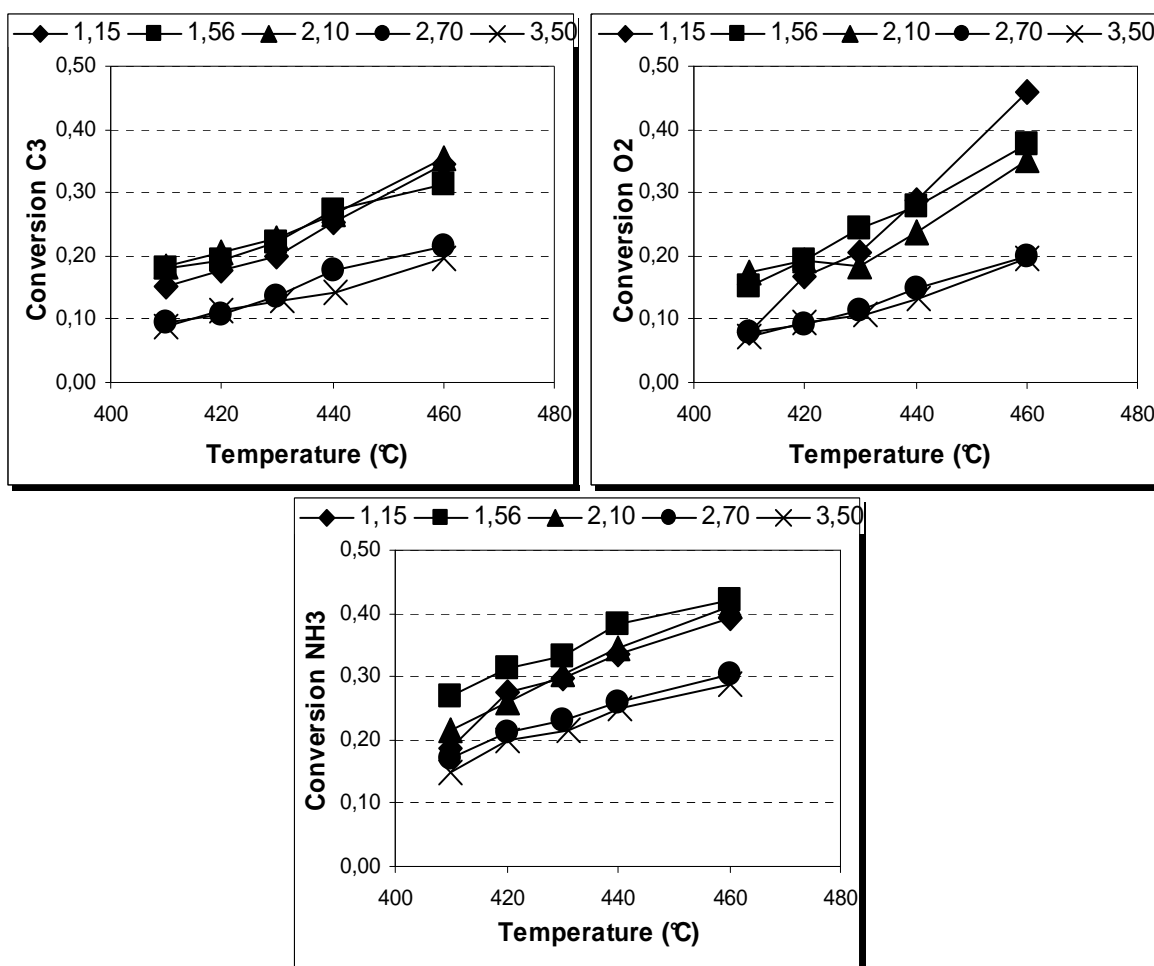


Fig. 3.16 Conversion of propene (top left), oxygen (top right) and ammonia (bottom) on catalysts *Cr1Sb1cpw* (Sb/Cr 1.15), *Cr1Sb1.5cpw* (Sb/Cr 1.56), *Cr1Sb2cpw* (Sb/Cr 2.10), *Cr1Sb2.51cpw* (Sb/Cr 2.70) and *Cr1Sb3cpw* (Sb/Cr 3.50)

Conversions of propene, oxygen and ammonia, as showed in Fig.3.16, arise along with temperature and never overstep 50%. In each reagent, the activity rises with the

increases of the antimony content. Samples with Sb/Cr ratio higher than 2,0 show a lower conversion of reagents, with a grater effect on oxygen. The other samples (Sb/Cr = 1.15, 1.56 and 2.10) show similar values in every picture, so that it is difficult to observe a trend in conversion properties along with Sb/Cr ratio.

In Fig.3.17, performances on ACN production are shown. The catalysts less active in conversion of the hydrocarbon exhibit the best efficiency in ACN formation. In samples with low Sb/Cr ratio (1,15 and 1.56), the selectivity drops linearly with the conversion increase. In catalysts with Sb/Cr ratio upper to 2, the selectivity trend is with maximum; in Cr1Sb2.5cpw and Cr1Sb3cpw samples the selectivity is much the same in all the conversion range (70 – 75%). This way ACN yield increases linearly with the conversion rise in high Sb samples (double in 50°C temperature gap, 12-22% in Sb/Cr=2,10 ca. 7-15% in Sb/Cr in 2.70 and 3.50) and it is much the same in others (ca. 13%).

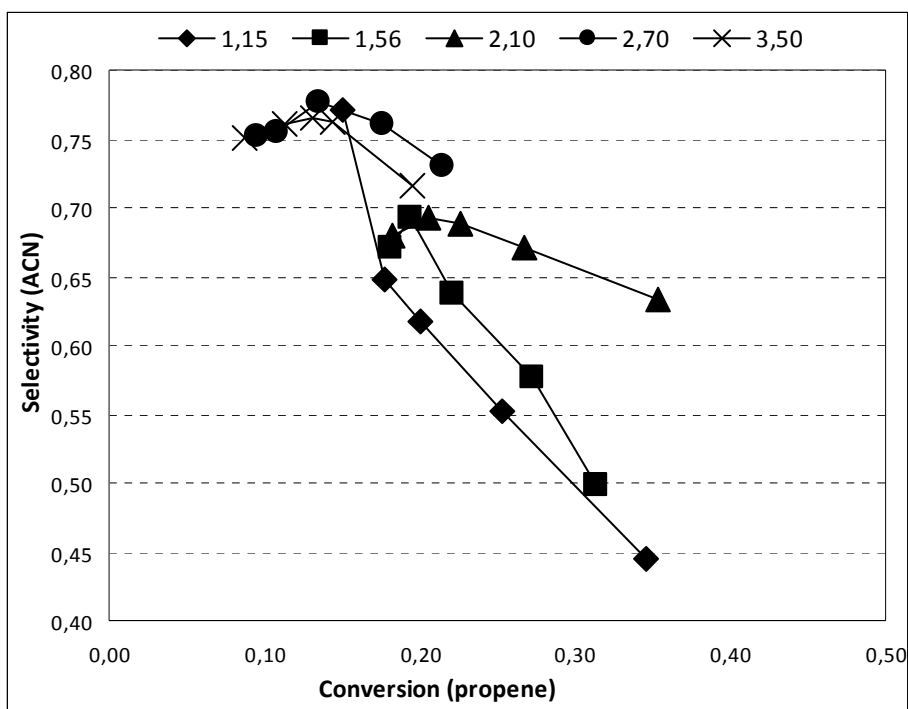


Fig. 3.17 Selectivity in ACN plotted on conversion of propene for catalysts Cr1Sb1cpw (Sb/Cr 1.15), Cr1Sb1.5cpw (Sb/Cr 1.56), Cr1Sb2cpw (Sb/Cr 2.10), Cr1Sb2.51cpw (Sb/Cr 2.70) and Cr1Sb3cpw (Sb/Cr 3.50). Scale on y-axis is in the range of 40-80% to evidence the difference.

In Fig.3.18 are shown selectivities in Carbon oxides (CO_2 , CO), Hydrogen cyanide (HCN), Acrolein (ACR), Acetonitrile (AcCN) and ACN of catalysts Cr1Sb1cpw (Sb/Cr 1.15), Cr1Sb2cpw (Sb/Cr 2.10) and Cr1Sb3cpw (Sb/Cr 3.5). Sample Cr1Sb1.5cpw (Sb/Cr 1.56) is omitted because it is in between the first two, while Cr1Sb2.5cpw (Sb/Cr 2.7) is left out because it is equal to the latter sample.

Looking at the general trends of the products selectivity, it is clear that at low temperature the catalysts behave similarly. Increasing the amount of antimony in the structure, at 410°C , selectivity in ACN arises from ca. 60% to ca. 80% while CO_2 , HCN and AcCN are the main coproducts. CO and ACR are not produced (less than 2% in selectivity). Upon 430°C , differences in reactivity are pointed out; the temperature favours the products of total oxidation, CO_2 , CO and HCN, which have much the same values and consequently the production of ACN is pulled down. Numerically, the arise in carbon dioxide corresponds to the drop of ACN. The oxidation properties given to the solid systems by chromium are clear at high temperatures, especially considering the higher conversion of propene. The mechanism on which lays this behaviour may be explained with the site isolation theory; antimony works as a chromium thinner and sets up the oxidation power of the system.

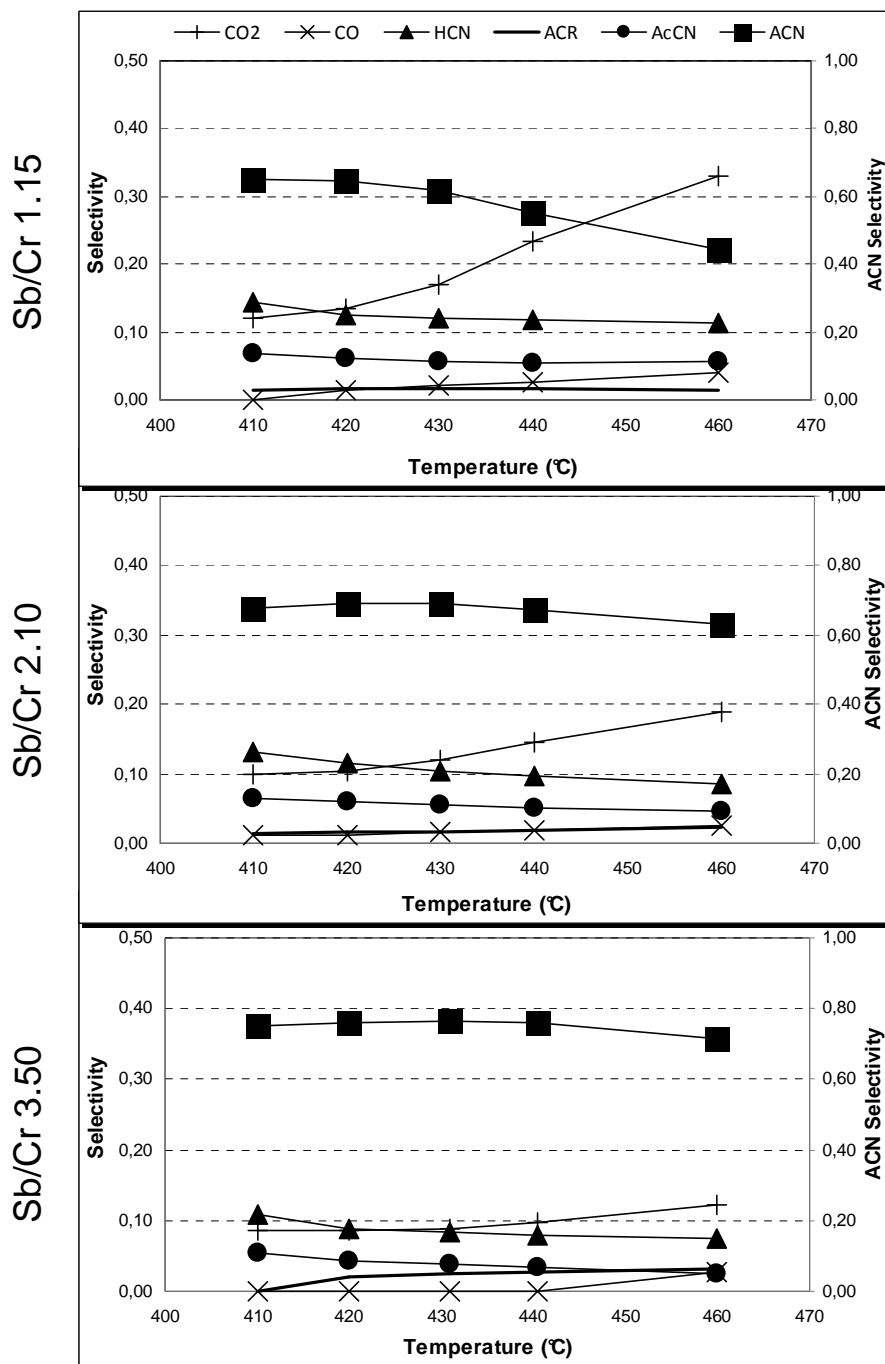


Fig. 3.18 Selectivities in CO₂, CO, HCN, ACR, AcCN (left y-axis) and in ACN (right y-axis), for catalysts with Sb/Cr ratio 1.15 (up), 2.10 (middle) and 3.50 (bottom).

3.2.2 Cr1Sbxcpw - Propane ammoxidation

Ammoxidation of propane is carried out in a quartz reactor, at the following temperatures: 420, 450, 480, 510, 540°C. Feed composition is approximately propane 7%, oxygen 17% and ammonia 10%. A total flow of about 45mL/min crosses 1mL of catalyst placed in the isotherm part of a tubular oven so that the contact time is about 1,3s.

Propane ammoxidation, compared to propene, shows a lower catalysts activity, so that it is necessary to perform the reaction at higher temperatures in order to reach a considerable conversion of the hydrocarbon. However, the activity is very low, in fact in propene conversions at 410 – 460°C are 10 – 35%, while in propane conversions at 420 – 540°C are 0 – 20%.

In Fig.3.19 conversion and selectivity data are shown: conversion of the alkane rises linearly with temperature, but it never oversteps 20%. An increase in the temperature upon 540°C is unproductive because of the increase of selectivity in over-oxidation products with the consequent decrease in high value products (ACN, AcCN and Propene).

As in propene ammoxidation, activity is higher in samples with low antimony amount, so it is possible to state that higher relative amount of chromium boosts the alkane activation and the related oxidative dehydrogenation.

Selectivity in carbon oxides, not reported, is double compared to the one in alkene reaction (20-50%), because of the higher temperatures needed to activate the alkane. Selectivity in ACN does not differ much in this set, but the trend followed in activation is clear (better performance with low antimony in structure); an increase in Sb/Cr ratio leads to an increase in propene formation.

The highest Sb sample is the most selective in propene, so it is presumable that high amounts of alkene are well converted to ACN by the most selective catalyst in propene ammoxidation; especially if we accept the theory of propene intermediate in propane ammoxidation.

The data in Fig.3.19 show the opposite situation: catalysts more active in ACN formation from alkene are selective in propene, but not efficient in conversion to

ACN. This means that the ACN formation does not occur via propene desorption, but directly on adsorbed dehydrogenated/activated propane.

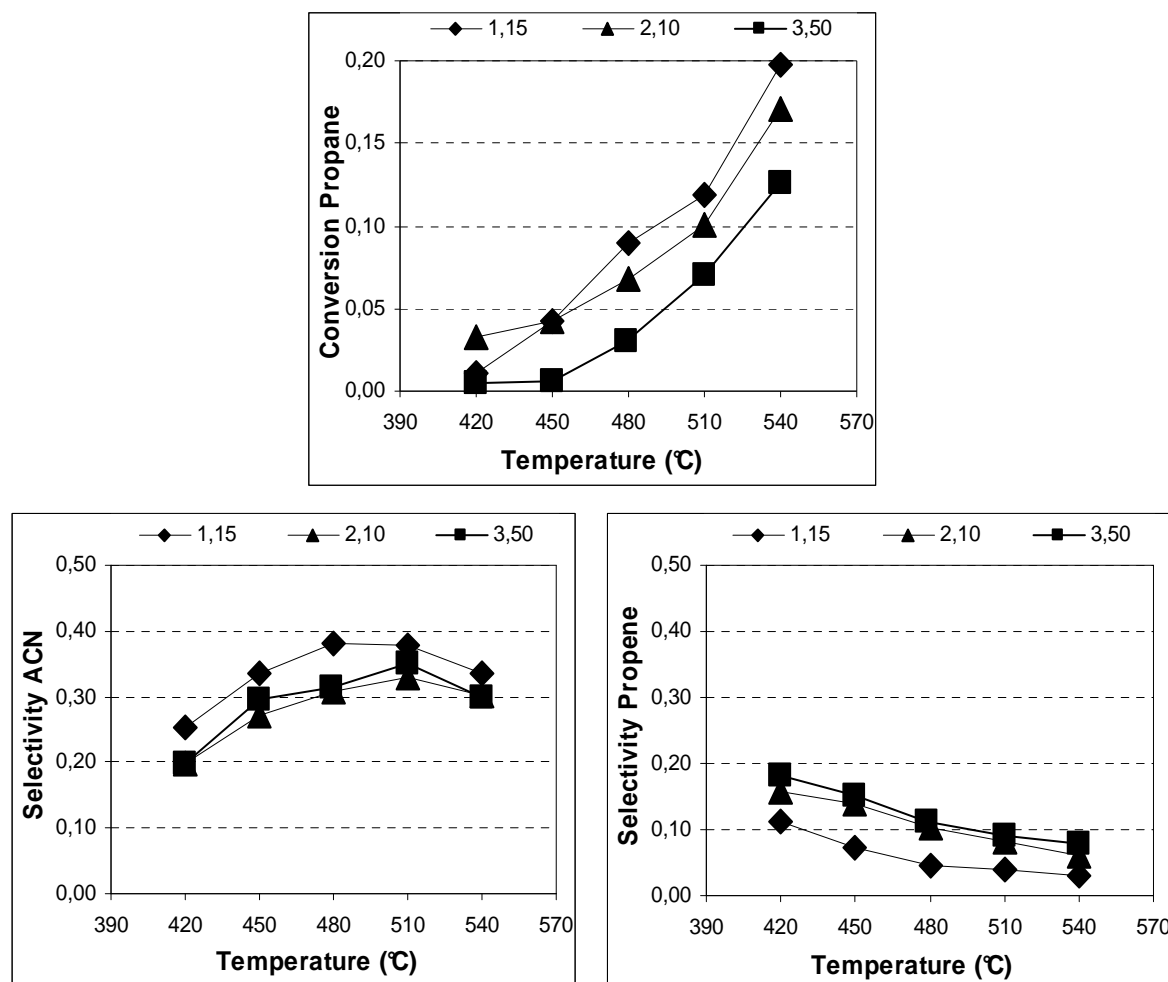


Fig. 3.19 Conversion of propene and selectivity in ACN and propene in alkane ammoxidation tested on samples Cr1Sb1cpw (Sb/Cr 1.15), Cr1Sb2cpw (Sb/Cr 2.10) and Cr1Sb3cpw (Sb/Cr 3.50).

Propane undergoes activation and dehydrogenation operated by Cr^{3+} . The dehydrogenation continues to form allylic intermediate, which is subjected to nitrogen insertion. The H-abstraction, needed to the allylic complex formation, is made by a trivalent cation.

Equimolar catalyst consists of Cr^{3+} and Sb^{5+} while catalysts with higher amount of antimony consist of Cr^{3+} , Sb^{3+} and Sb^{5+} . In conclusion, the activated hydrocarbon placed on a Cr^{3+} may undergo to oxidation on Sb^{3+} or Cr^{3+} ; it seems that Cr^{3+} is more

active than Sb^{3+} in allyl-formation starting from the activated propane (adsorbed propene): Cr-O-Cr group is necessary so antimony excess does not increase selectivity like in propene ammoxidation.

Selectivity in HCN from propane and from propene is much the same in samples Sb/Cr 2.10 and 3.50, while it is double in alkane if compared to alkene in equimolar catalyst. It means that probably the ammoxidation does not occur exclusively via adsorbed intermediate, but mainly via propene desorption. The mechanism is competitive and the first is more efficient in nitriles formation (also AcCN follows this trend).

3.2.3 Ga1Sbxcp – Propene ammoxidation

Ammoxidation of propene is carried out in a quartz reactor at the following temperatures: 410, 420, 430, 440, 460°C. Feed composition is approximately propene 7%, oxygen 17% and ammonia 10%. A total flow of about 45mL/min crosses 1mL of catalyst placed in the isotherm part of a tubular oven so that the contact time is about 1,3s.

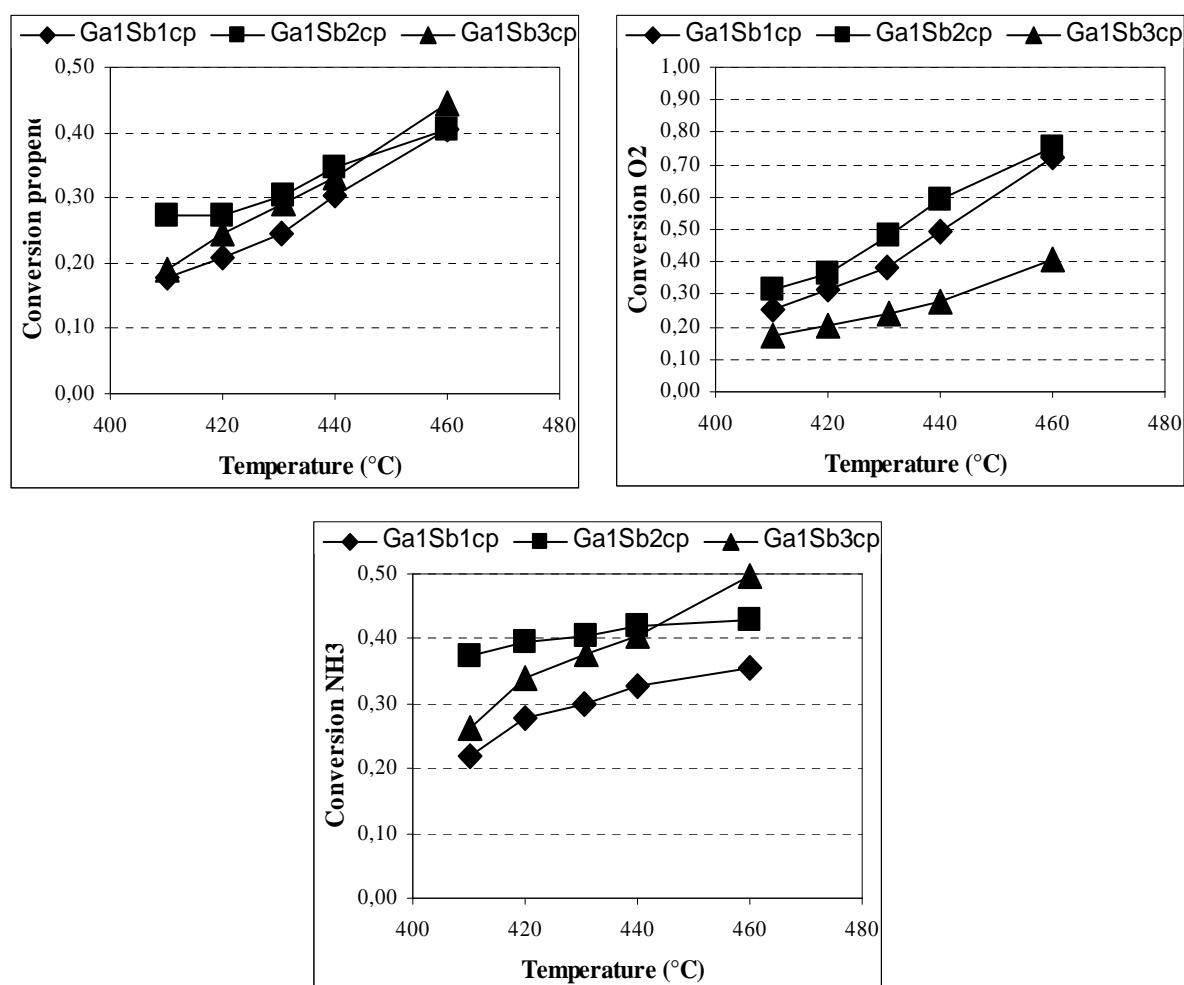


Fig. 3.20 Conversion of propene (top left), oxygen (top right) and ammonia (bottom) in Ga1Sbxcp samples.

In Fig.3.20, conversions of propene, oxygen and ammonia are shown. The activation properties of the catalysts on hydrocarbon do not differ very much; the values recorded at different temperatures diverge of about 5%. The increase of Sb amount (from 1 to 3 times the amount of Ga) leads to halve the oxygen consumption

and to double the ammonia one. It means that Ga is very operative in oxygen activation and that the site isolation made by antimony is indeed necessary to slow down the oxidation. In the same way, Ga/Sb ratio affects the ammonia activation: an excess of antimony leads to better performances.

As shown in Fig.3.21, the excessive oxygen activation on Ga1Sb1 leads to high carbon oxides production, mainly dioxide, near to 80%. At the same time, very low consumption of oxygen showed by Ga1Sb3 does not mean a low productivity (propene conversion is almost the same), but a good performance in ACN (ca. 80%). Secondary products are HCN (5-15%) and AcCN (ca.5%). Negligible amounts of acrolein are detected.

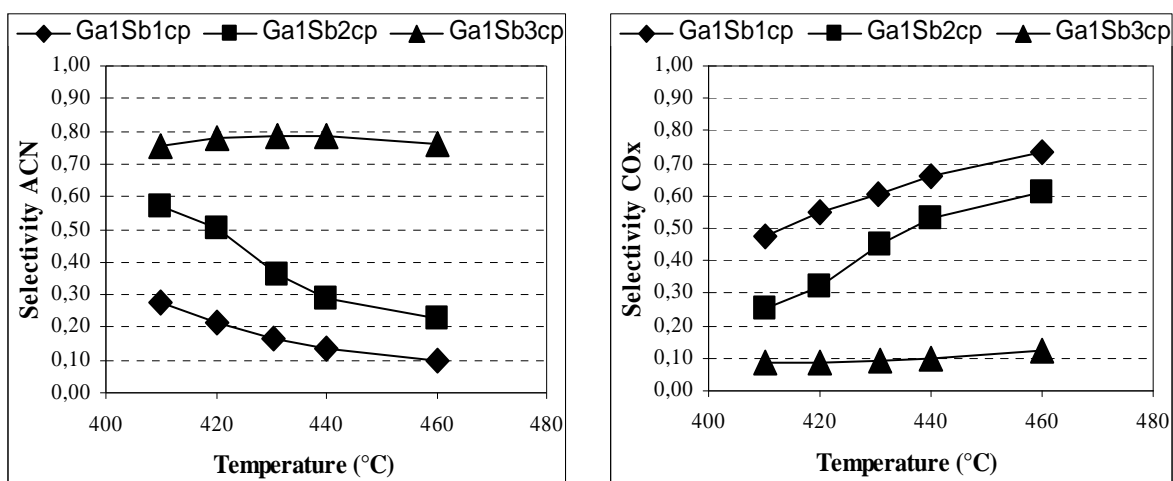


Fig. 3.21 Selectivity in ACN (left) and CO_x (right) along with reaction temperature of Ga1Sb_xcp samples.

3.2.4 Ga1Sbxcp – Propane ammoxidation

Ammoxidation of propane is carried out in a quartz reactor, at the temperatures in the 400 – 500°C range. Feed composition is approximately propane 20%, Oxygen 20% and ammonia 10%. A total flow of about 45mL/min crosses 1mL of catalyst placed in the isotherm part of a tubular oven so that the contact time is about 1,3s.

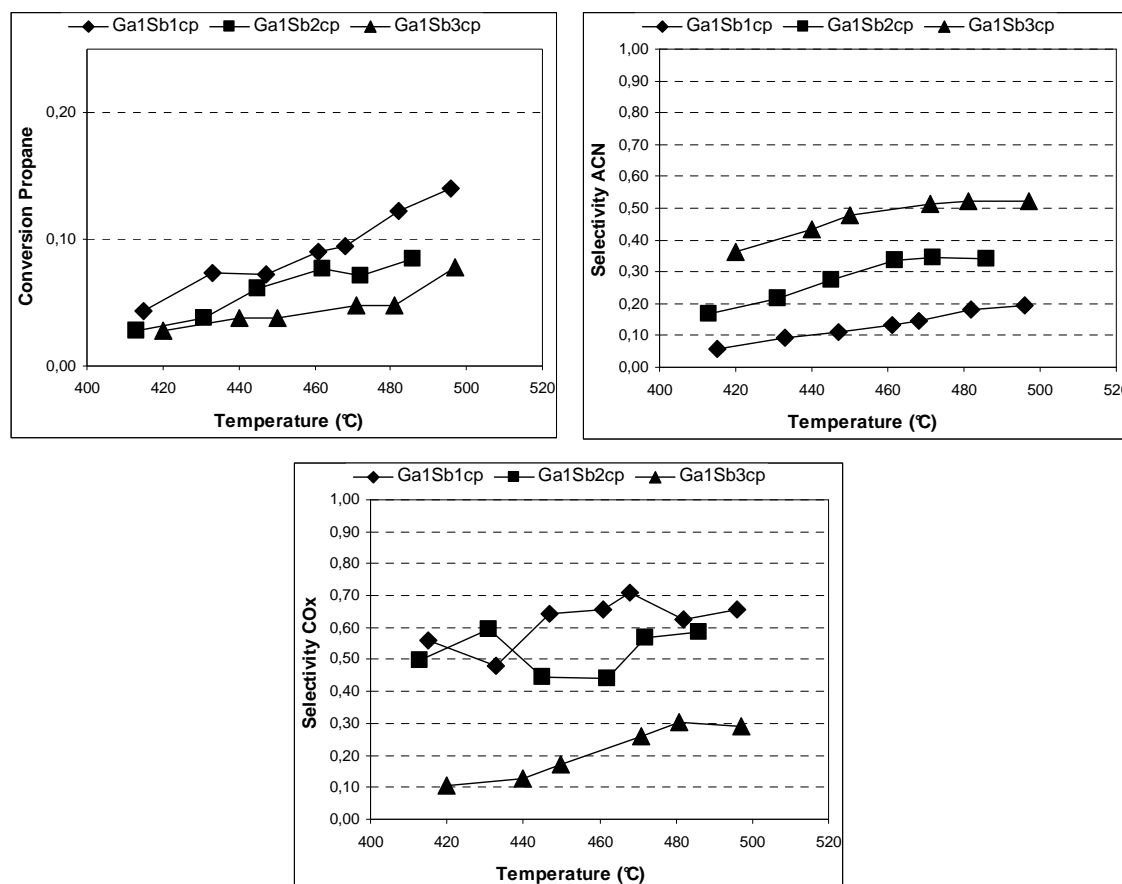


Fig. 3.22 Conversion of propane (top left) selectivity in ACN (top right) and selectivity in COx (bottom) in Ga1Sbxcp samples.

As shown in Fig.3.22, in gallium antimonate, an increase in the antimony amount leads to a decrease in the hydrocarbon activity. The conversion of propane never oversteps 15% and Ga1Sb3 sample is double than the Ga1Sb1 one in all range temperatures. In the same way, oxygen conversion is higher at low Ga/Sb ratio. The strong oxygen consumption leads to high carbon oxides production and causes a worsening in ACN yield. The selectivity in ACN shows a trend with maximum, placed around 490°C, which reaches values around 50% in Ga1Sb3cp, 35% in Ga1Sb2cp and

20% in Ga1Sb1cp; upon 490°C overoxidation prevails on ammoxidation while below 490°C HCN is a bit favoured and gains about 10% on ACN (5 – 20%). Selectivity in propene holds under 10% in every sample and remainder to 100% are practically only carbon oxides.

3.2.5 Cr1Sbxasl – propene ammoxidation

Ammoxidation of propene is carried out in a quartz reactor, at the following temperatures: 410, 420, 430, 440, 460°C. Feed composition is approximately propene 7%, oxygen 17% and ammonia 10%. A total flow of about 45mL/min crosses 1mL of catalyst placed in the isotherm part of a tubular oven so that the contact time is about 1,3s.

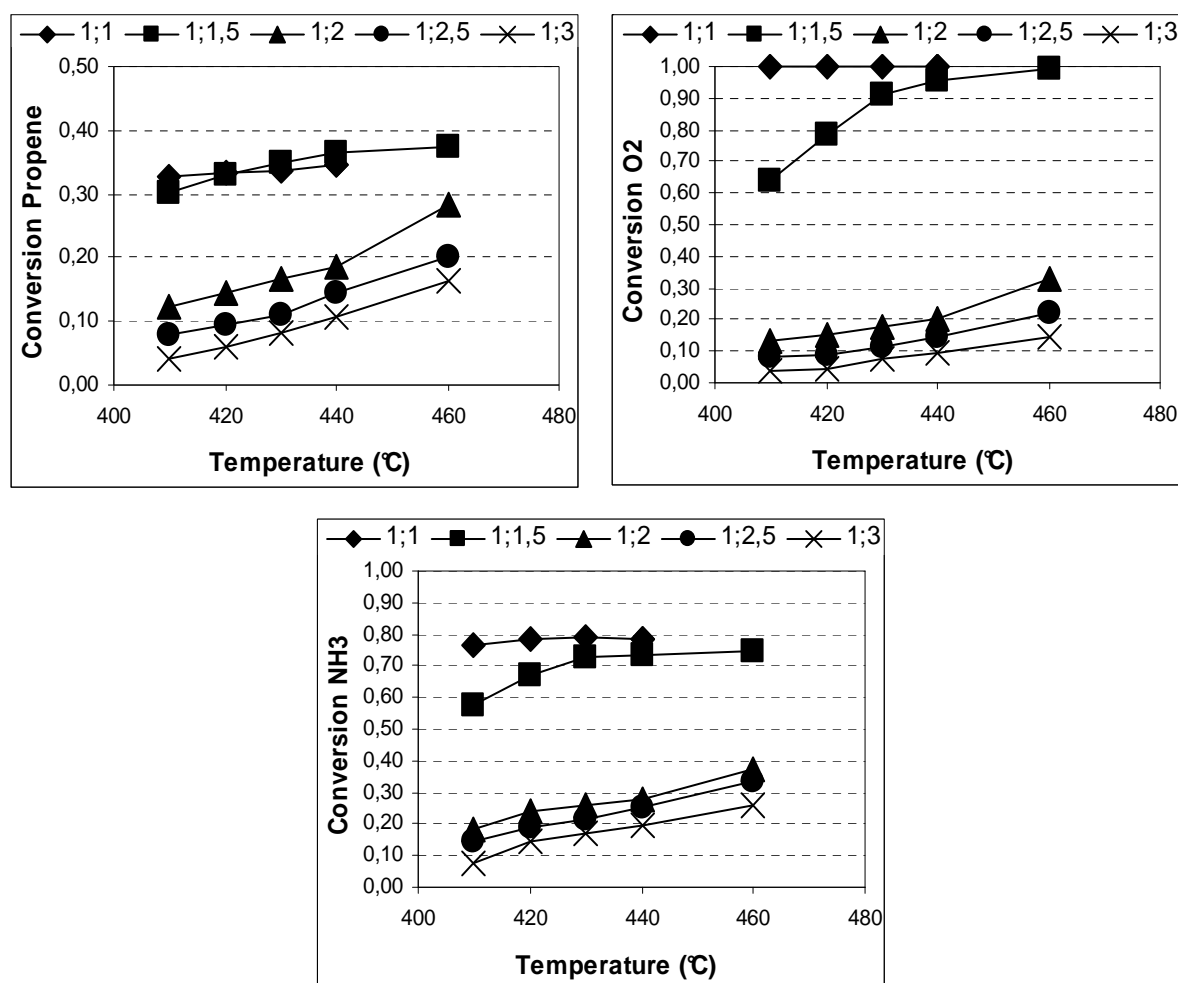


Fig. 3.23 Conversion of propene (top left), oxygen (top right) and ammonia (bottom) of Cr1Sbxasl sample.

In Fig.3.23 conversion of propene, oxygen and ammonia are shown. Conversions of reagents rise as well as temperature increasing in each sample, except for catalysts with Sb/Cr ratio equal to 3, in which complete oxygen conversion is reached at low temperature and further consumption of hydrocarbon and ammonia can not proceed. The reason can be ascribed to the presence of Cr₂O₃ (a strong oxidation catalyst).

As already seen in other samples, conversion performances increase linearly with the Cr/Sb ratio with a clear gap between samples near stoichiometry (Sb/Cr = 1 or 1,5) and samples in clear excess of antimony.

In Fig.3.24, selectivities in ACN and conversions are reported. It is clear the low performances of catalysts with low antimony amount, in which selectivity deficit to 100% is CO (ca. 10%) and CO₂. Samples with high ACN selectivity (Sb/Cr 1, 1.5 and 2) produce also HCN (ca. 10%), CO (less than 10%) and CO₂; negligible amount of ACR and AcCN are detected. Good selectivity is reached at conversions lower than 30%, but conversions higher than 50% are not allowed because of the oxygen depletion.

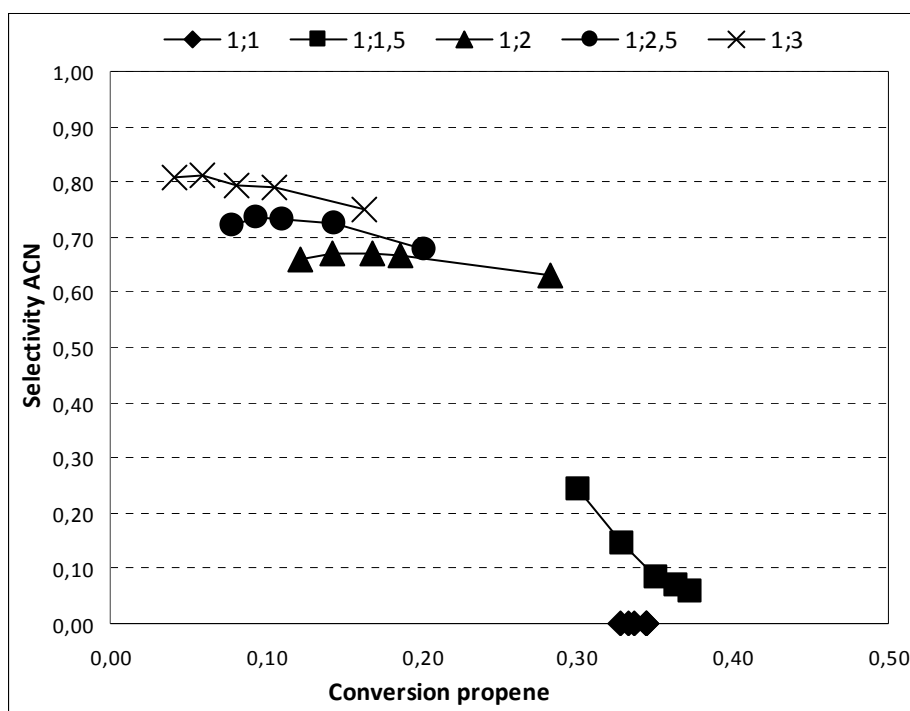


Fig. 3.24 Performances in propene conversion and ACN selectivity of Cr₁Sb_xas_l.

3.2.6 *Cr1Sb2xosl* – propene ammoxidation

Ammoxidation of propene is carried out in a quartz reactor, at the following temperatures: 410, 420, 430, 440, 460°C. Feed composition is approximately propene 7%, oxygen 17% and ammonia 10%. A total flow of about 45mL/min crosses 1mL of catalyst placed in the isotherm part of a tubular oven so that the contact time is about 1,3s.

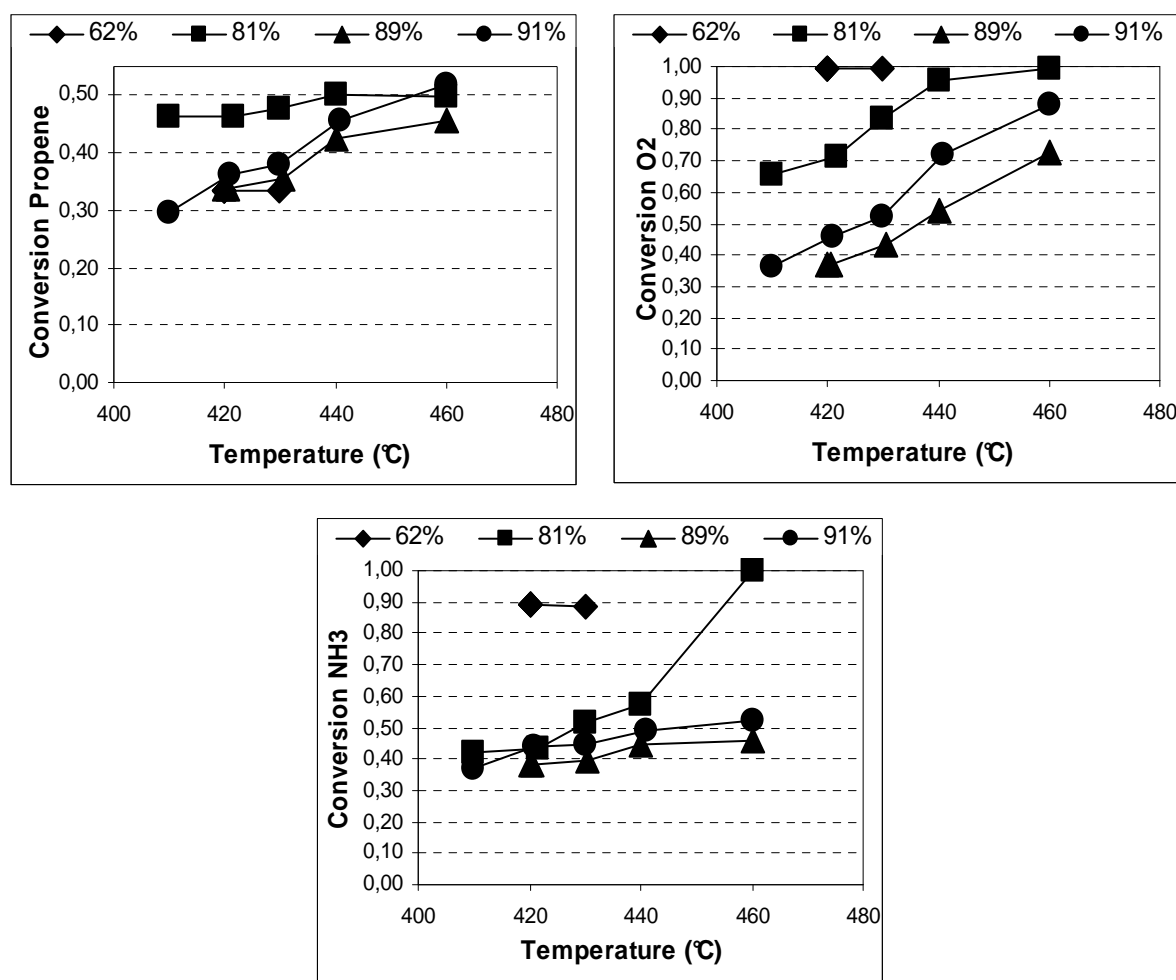


Fig. 3.25 Conversion of Propene (top left), oxygen (top right) and ammonia (bottom) of *Cr1Sb2aosl* (62% rutile) , *Cr1Sb2dosl* (81% rutile), *Cr1Sb2fosl* (89% rutile), *Cr1Sb2gosl* (91% rutile).

Samples are showed in Fig.3.25 and labelled by rutile amount, as detected by XRD analysis, expressed in percentage units. Sample *Cr1Sb2aosl*, containing 62% of rutile and 38% of Sb_2O_4 is quite an inefficient catalyst in propane ammoxidation, in so far it

is very active in oxygen conversion and very selective in carbon oxides (Fig.3.25). This sample reaches a propene conversion of about 32% and can not go beyond because of the lack of oxygen (completely converted) . Sample *Cr1Sb2dosl* is the more active in propene conversion and it is also very efficient in oxygen activation; in Fig.3.26 selectivities in ACN and carbon oxides are reported and the tendency of this catalyst to burn the hydrocarbon to CO_x , especially CO_2 , is very clear.

Samples with the higher amount of rutile in the structure (*Cr1Sb2fosl* and *Cr1Sb2gosl*) have shown similar conversion performances and the catalyst with 89% of rutile gives the best performance in ACN selectivity. This set of catalysts shows a trend with maximum and allows claiming that an excess of Sb_2O_4 effectively leads to a better performance in ACN synthesis. However, a large amount of antimony oxides makes the system unselective in nitriles formation.

In all these samples the selectivity in HCN is surprisingly low, as in AcCN and ACR.

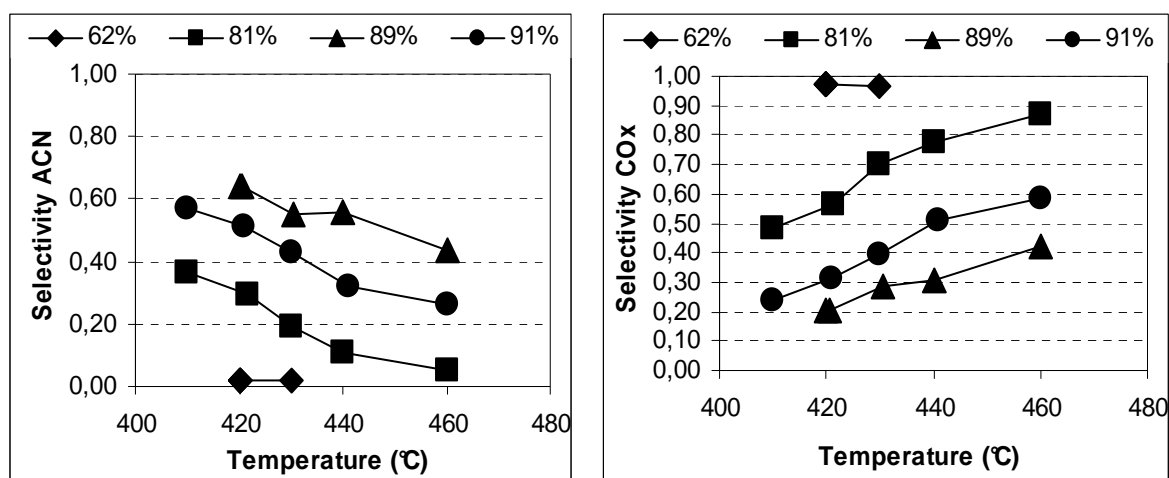


Fig. 3.26 Selectivity in ACN and carbon oxides of *Cr1Sb2aosl* (62% rutile) , *Cr1Sb2dosl* (81% rutile), *Cr1Sb2fosl* (89% rutile), *Cr1Sb2gosl* (91% rutile).

3.3 Catalysts comparison

As already seen above, in propene ammoxidation gallium antimonate reaches higher conversion than chromium antimonate (10% higher in propene and ammonia and 20% higher in oxygen). In fig.3.27 selectivities in ACN and CO_x data for Cr₁Sb_xcp and Ga₁Sb_xcp catalysts are compared. Low antimony systems show big differences, mainly due to the relevance of the trivalent cation properties: chromium and gallium are added to the structure as oxidant compounds and, when their amount is high, this character is very pronounced. Ga is a strong oxidant, more than Cr, and this is clearly visible in CO_x selectivity. Along with the increase in the antimony amount, Ga needs more dilution than Cr in order to constraint oxidation features. High antimony systems show very similar performances, so X₁Sb₃cp catalyst reaches the same selectivities in ACN and in CO_x. This reflects the importance of the structure and the role of antimony in nitrogen insertion.

An increase of the amount of antimony, starting from the equimolar structure of a catalyst, leads to better performances in ACN selectivity, hence lower Carbon oxides formation. Sb/X = 3 is the ratio limit at which CO_x selectivity stops decreasing and reaches the unbreakable limit of 10%.

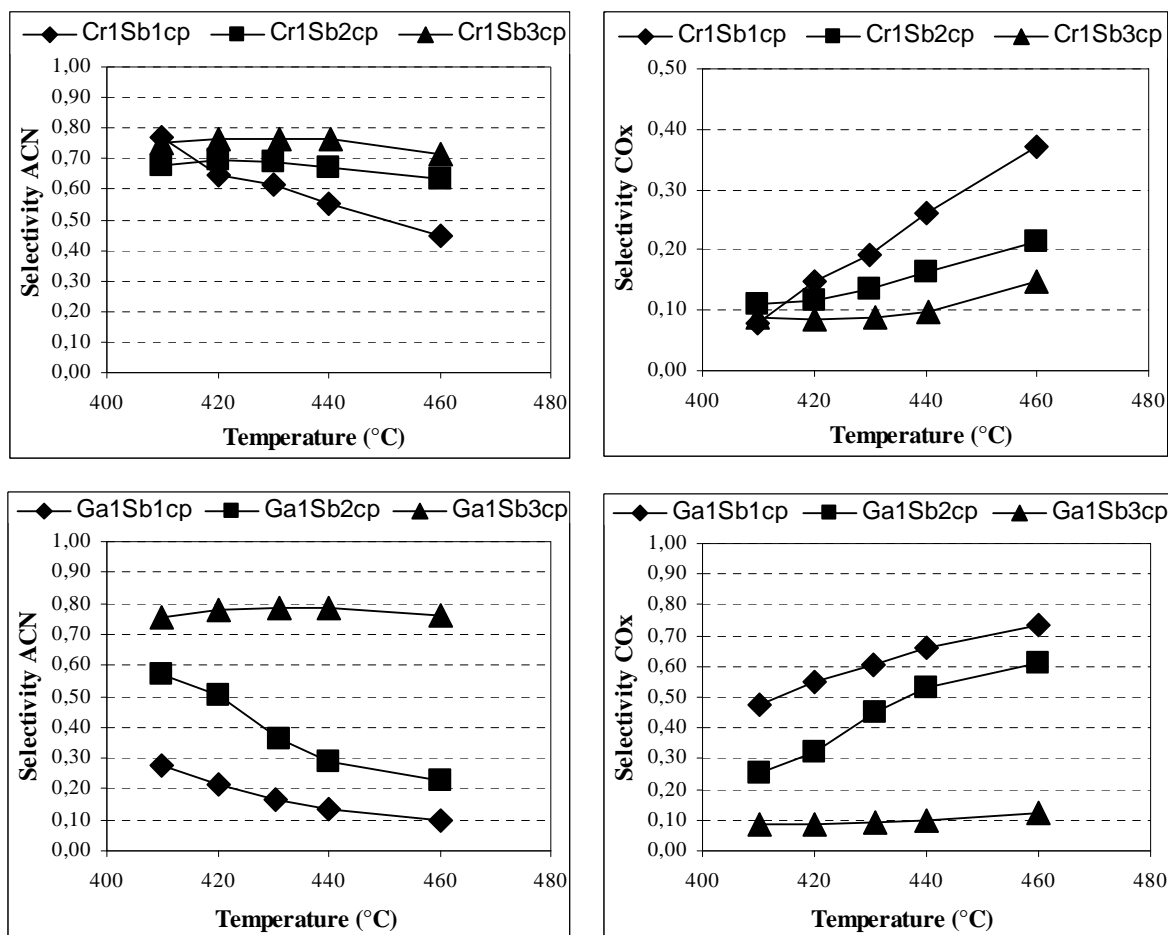


Fig. 3.27 Selectivity data of Cr1Sbxcpw catalysts (top) and Ga1Sbxcp catalysts (bottom)

In Fig.3.28 are shown the data of chromium and gallium antimonates catalysts along with the most popular Vanadium antimonate, with molar ratio equal to 1/1, 1/2 and 1/3. Vanadium antimonate tests have been performed at the following conditions: O₂ 20%, NH₃ 9,5%, propane 25,5% and temperature from 350°C to 500°C. Data are sorted primary in the hosted cations and secondary in the antimony amount. Conversions at 420°C and 480°C are represented with thick black lines and the best selectivities in ACN (always attained around 480°C) are shown with black balls.

Propane conversions in Ga1SbX and Cr1Sbx are almost the same, about half the V1Sbx ones. In the same cationic class of samples, activity falls along with antimony increase, especially at high temperatures, and it seems that heat works better on catalysts with great oxidant cation amount.

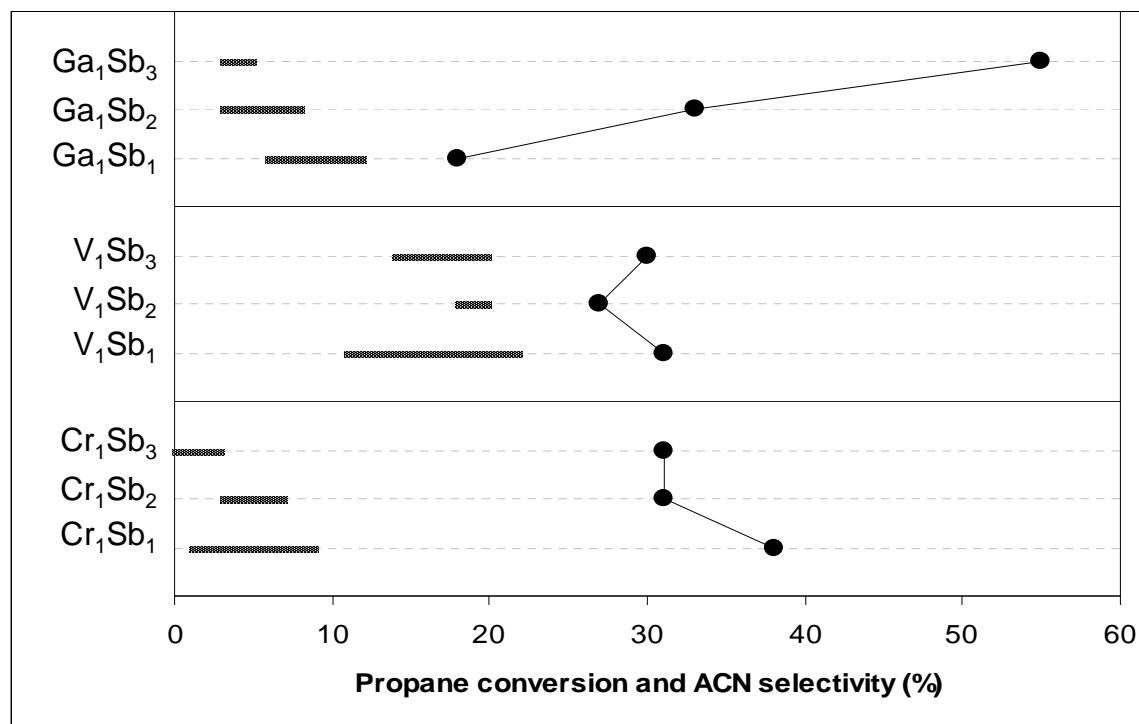


Fig. 3.28 Performances of chromium, gallium and vanadium antimonate sorted by hosted cation. In each group of catalysts antimony amount increases from 1 to 3 along with y-axis. Conversions of propane at 420°C and 480°C are showed with thick black lines and the best selectivities in ACN reached in the whole temperature range are represented with black balls linked by thin lines.

The best selectivity (55%) is reached in Ga₁Sb₃ sample, while the other catalysts are around 30%. Focusing on the cationic groups in Cr and V systems there are not many differences in performances as the antimony amount changes, while in Ga₁Sb_x sample the antimony variance leads to an increase of 3 times in ACN selectivity (from ca. 20 to ca.60%).

As shown in Tab.3.3, reagents conversion arises along with the temperature increase. Generally speaking, a decrease of antimony in the structure leads to a higher conversion of oxygen and hydrocarbon; this observation can not be applied to the vanadium samples because of the particular conditions created by the whole or quasi-whole oxygen consumption. The ammonia conversion does not show many differences.

Some values require paying particular attention:

- The remarkable change in ACN selectivity, observed in Fig.3.21 in gallium group, is linked with the high selectivity in CO_x of the equimolar sample, noticed also at low temperatures. Moreover, the oxygen conversion is quite lower than the vanadium catalysts one. Ga in large excess is very effective in oxygen activation and, even though the hydrocarbon activated is not much, yield in carbon oxides is high. The oxidation mechanism removes the substrate from ammoxidation, so that ACN production is low. The site isolation operated by antimony reduces the oxidation tendency and increases the selectivity in nitrogenated molecules. This effect is clear comparing the data collected at 420°C are because, while selectivity in Cr and V systems ACN is much the same, in Ga systems it is higher.
- The fact that Ga samples show low selectivity in propene at low temperature is a further indication that the oxygen activated leads to overoxidation of activated alkane.
- Poor oxygen concentration on V1Sb3 environment, due to its high conversion, makes the Carbon oxides production unfavoured, as it is particularly evident in CO_x selectivity.

| | | Cr1Sb1 | Cr1Sb3 | V1Sb1 | V1Sb3 | Ga1Sb1 | Ga1Sb3 | |
|-------------|-------------------------------|--------|--------|-------|-------|--------|--------|----|
| Conversion | C ₃ H ₈ | 420°C | 1 | 1 | 11 | 14 | 6 | 3 |
| | | 480°C | 9 | 3 | 22 | 20 | 12 | 5 |
| | O ₂ | 420°C | 6 | 1 | 40 | 67 | 23 | 6 |
| | | 480°C | 20 | 10 | 90 | 100 | 60 | 23 |
| | NH ₃ | 420°C | 10 | 8 | 43 | 52 | 14 | 12 |
| | | 480°C | 31 | 23 | 60 | 58 | 20 | 27 |
| Selectivity | ACN | 420°C | 25 | 20 | 25 | 25 | 5 | 38 |
| | | 480°C | 38 | 31 | 31 | 30 | 18 | 55 |
| | C ₃ H ₆ | 420°C | 11 | 18 | 15 | 10 | 6 | 8 |
| | | 480°C | 5 | 11 | 10 | 8 | 6 | 8 |
| | CO _x | 420°C | 14 | 39 | 30 | 21 | 50 | 10 |
| | | 480°C | 39 | 42 | 46 | 15 | 60 | 30 |
| | HCN | 420°C | 28 | 15 | 18 | 38 | 8 | 10 |
| | | 480°C | 16 | 11 | 11 | 46 | 7 | 14 |

Tab. 3.3 Performances of Chromium, Gallium and Vanadium antimonates are reported: conversions of propane, oxygen and ammonia along with selectivities in Acrylonitrile, propene, carbon oxides and hydrocyanic acid in catalysts with equimolars and large excess of antimony.

To make it simpler the analysis of data, only samples with cation to antimony ratio equal to 1 and 3 have been showed in Tab.3.3. Observing all the catalytic data on propane which we have at our disposal, along with characterizations described in chap.3.1.1, it is possible to notice that:

- Cr systems are structurally and catalytically coherent because samples are monophasic and catalytic properties change linearly in the whole Sb/Cr ratio range. The antimony increase leads to:
 - Decrease in activity.
 - Increase in Carbon oxides.
 - Similarity or slight decrease in N-containing products.
- Ga systems show bad structural properties, in fact rutile crystals is small and, upon $Sb/Ga = 2$, antimony can not be incorporated and forms Sb_6O_{13} domes. Data clearly show some changes passing from monophasic (Ga1Sb1 and Ga1Sb2) to biphasic (Ga1Sb3) lattice:
 - Carbon oxides halves (Ga1Sb1-Ga1Sb2-Ga1Sb3 = CO_x selectivity 50-55-10 at 420°C and 60-59-30 at 480°C).
 - ACN selectivity increases from 3 to 8 times (Ga1Sb1-Ga1Sb2-Ga1Sb3 = ACN selectivity 50-55-10% at 420°C and 18-33-55% at 480°C).
- V systems exhibit very high crystallinity, but they do not accept excess of antimony, in fact Sb_2O_4 is clearly visible and well crystallized starting from V1Sb2. Catalytic changes visibly happen:
 - Carbon oxides decrease considerably (V1Sb1-V1Sb2-V1Sb3 = CO_x selectivity 30-20-21% at 420°C and 46-10-15% at 480°C).
 - HCN increase more than double (V1Sb1-V1Sb2-V1Sb3 = HCN selectivity 18-43-38% at 420°C and 11-56-46% at 480°C).

- Oxygen conversion rises along with the antimony increase while the other reagents decrease everywhere but in VSb systems.
- The decrease in CO_x selectivity noticed along with Sb₂O₄ and Sb₆O₁₃, may be seen from another point of view: monophasic rutile leads to Carbon oxides formation. In particular, as shown in Tab.3.4, rutile leads to a higher CO₂ formation compared to CO:

| | Cr1Sb1 | Cr1Sb2 | Cr1Sb3 | V1Sb1 | V1Sb2 | V1Sb3 | Ga1Sb1 | Ga1Sb2 | Ga1Sb3 |
|---------------------|--------|--------|--------|--------|--|--|--------|--------|---|
| Phases | Rutile | Rutile | Rutile | Rutile | Rutile α-Sb ₂ O ₄ | Rutile α-Sb ₂ O ₄ | Rutile | Rutile | Rutile Sb ₆ O ₁₃ |
| CO _x | 39 | 43 | 42 | 46 | 10 | 15 | 60 | 59 | 30 |
| CO ₂ /CO | 10 | 10 | 6 | 3 | 3,5 | 3 | 14 | 18 | 5 |

Tab. 3.4 Carbon oxides selectivities and oxide/monoxide ratio related to the phases observed by means of XRD in Cr, V and Ga coprecipitated catalysts. All data refer to propane ammoxidation at 480°C.

To sum up:

- Sb₂O₄ comparison is related to higher HCN formation and higher O₂ consumption
- Sb₆O₁₃ comparison is related to higher ACN formation
- Rutile structure XSbO₄ is related to higher carbon oxides formation, especially CO₂.

3.4 Starting materials

As described in the previous chapters, different synthesis methods and different starting materials are used in order to obtain rutile-type structure. In particular, CrSbO_4 structure may be obtained starting from Sb(III) and Sb(V).

In order to check the influence of the starting materials on the final characteristics, catalysts have been synthesized by means of the coprecipitation method starting from SbCl_3 and SbCl_5 as antimony source; catalytic properties are tested in propane (Fig.3.1) and propene ammoxidation. No differences were pointed out, so that it is possible to state that the starting materials do not affect the rutile formation, as supported by Raman spectra.

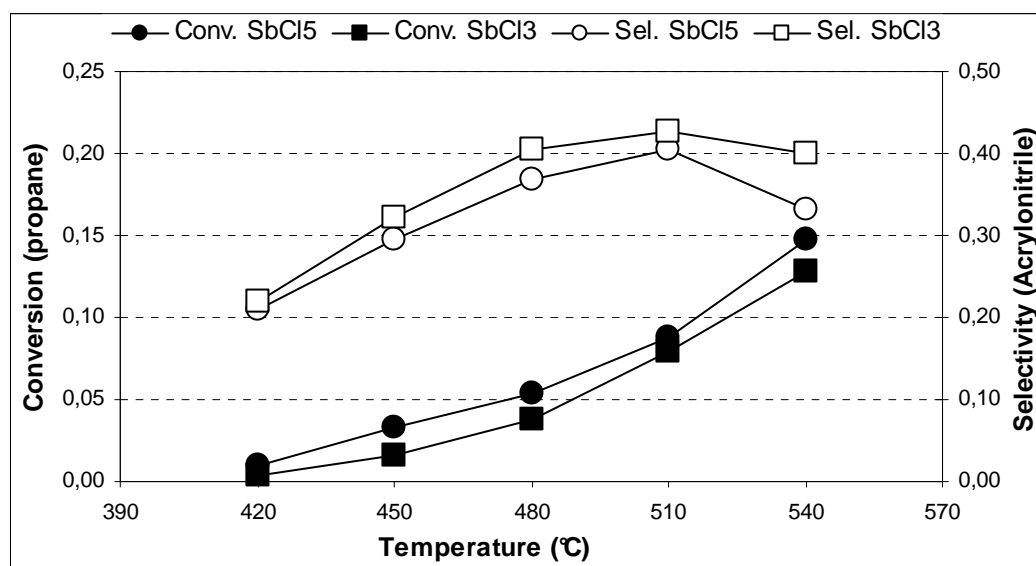


Fig. 3.29 Conversion of propane and selectivity in acrylonitrile of catalysts AF04 (circle) and AF05 (square), made respectively starting from SbCl_5 and SbCl_3 with the same antimony and chromium amount ($\text{Sb/Cr} = 2,70$).

Other antimony sources have been tested with the coprecipitation method and no evidence of differences in catalytic performances has been carried out.

4 CONCLUSIONS

The production of acrylonitrile is one of the most important reactions in the petrochemical manufacture and it is also so prolific that little developments in the processes and in the catalysts lead to big economical aftermath.

Nowadays acrylonitrile is produced with very good efficiency starting from propene, but one of the bigger issue is the development of systems which are able to convert propane selectively.

Rutile-type catalysts are effective systems in the ammoxidation of alkane and alkene to the relative nitrile but, except for vanadium antimonates, structural studies about these systems are not extensive. Vanadium is a very active component in hydrocarbon activation and it is useful to allow a good alkane conversion, but it yields too many carbon oxides. Chromium and gallium are elements with oxidant features, less active than vanadium which are able to form rutile-type structures with antimony.

Different preparation methods of rutile structures are present in literature and different raw materials may be used with this aim; each synthesis gives to the solid system different properties and the obtained catalysts behave differently into the reaction mechanism. One of the main catalyst features is the number and the kind of the formed phases along with rutile-type structures, especially if an excess of antimony is introduced in the system.

In this work we have studied chromium and gallium antimonate obtained with coprecipitation method starting from antimony chlorides and slurry method starting from antimony oxide and antimony acetate. The hosted cations are added as soluble salt in each case.

By means of chemical and physical analyses we found out that:

- Each Cation leads to the formation of rutile crystallites with different dimensions, hence different phase qualities.
- Each cation behaves differently with an excess of antimony and leads to the segregation of different antimony oxides.

- The method of preparation as well as the raw materials used lead to the formation of different solid systems, mainly as far as the quality of the crystals is concerned. This is probably due to the intimate contact within the reactants in the catalysts syntheses.
- Solid state reaction is not a suitable method of preparation for chromium antimonates, contrary to vanadium systems.
- The insertion of an excess of antimony leads to:
 - The formation of a monophasic sample in chromium antimonates (which points out that the lattice is very elastic).
 - The segregation of Sb_6O_{13} in gallium antimonates (very active in ACN selectivity).
 - The segregation of Sb_2O_4 in vanadium antimonates, also at a very low excess of antimony (very active on carbon oxides and hydrocyanic acid yields)
- Bulk and surface compositions are not equal in each cation/Sb ratio. Surface enrichments in antimony let us understand that the segregation of antimony oxides in the surface of the catalysts is due to the tendency of antimony to form Sb–O–Sb bonds.

All the catalysts synthesized have been tested in propane and propene ammoxidation and they proved themselves to be active and selective in formation of acrylonitrile. In propene ammoxidation, an excess of antimony in Cr and Ga systems is needed to limit the oxidant features of the hosted cations. Selectivities of about 80% have been reached along with conversions up to 50%. In propane ammoxidation the activation of the alkane is the limiting step, so that conversions never overstep 20%; nevertheless, selectivities of about 40% are reached along with high production of carbon oxides due to the high temperature needed in alkane transformation.

From the catalysts comparison it is clear that an excess of antimony oxides on the surface allows reaching better performances and gallium antimonate with a Ga/Sb

composition of 1/3 is the best catalyst in each ammoxidation reaction. The presence of a small amount of Sb_6O_{13} is preferable to the presence of the antimony tetroxide.

The formation of a good rutile crystal lattice does not lead to having better performances: the rutile structure is needed to operate good site isolation on the oxidant compound (which activates the substrate) and it allows, at the same time, the presence of Sb-O-Sb species (active in N-insertion). These features prescind from the phases, so that monophasic chromium antimonates are active systems and do not differ much from gallium antimonates; the monophasic lattice simply does not allow big domes of Sb-O-Sb sites.

Data point out that probably the mechanism of propane ammoxidation occurs in adsorbed conditions and that a whole propene molecule desorbed from the systems and readsorbed to perform a “propane ammoxidation” is not so commonly found.

5 BIBLIOGRAPHY

1. Styrene-Acrylonitrile (SAN) Resins :: Chemical Economics Handbook :: SRI Consulting. a <<http://www.sriconsulting.com/CEH/Public/Reports/580.6000/>>
2. Acrylonitrile-butadiene-styrene (ABS) CAS No: 9003-56-9. a <<http://www.icis.com/v2/chemicals/9071028/acrylonitrile-butadiene-styrene-copolymer.html>>
3. Nylon - Wikipedia. a <<http://it.wikipedia.org/wiki/Nylon>>
4. Acrylonitrile production process. a <http://portal.acs.org/portal/acs/corg/content?_nfpb=true&_pageLabel=PP_ARTICLEMAIN&node_id=924&content_id=WPCP_007593&use_sec=true&sec_url_var=region1&__uuid=60f2dbc4-d94d-4fa0-87a0-7ce8dbe648c6>
5. ICSC:NITL0092 International Chemical Safety Cards (WHO/IPCS/ILO) | CDC/NIOSH. a <<http://www.cdc.gov/niosh/ipcsnitl/nitl0092.html>>
6. Safety (MSDS) data for acrylonitrile. a <<http://msds.chem.ox.ac.uk/AC/acrylonitrile.html>>
7. Langvardt, P.W. Acrylonitrile. *Ulmann* **A1**, 177 - 183
8. Cavani, F., Centi, G. & Marion, P. Catalytic ammoxidation of hydrocarbons on mixed oxides. *Metal oxide catalysis* **2**, 771 - 818 (2009).
9. Albonetti, S. Ammonossidazione del propano ad acrilonitrile su catalizzatori a base di ossidi misti a struttura rutilo. (1995).
10. Grasselli, R.K. Ammoxidation. **Selective oxidation**, 2302 - 2327
11. Ammoxidation. 177 - 201
12. Sokolovskii, V.D. Mechanism of Selective Paraffin Ammoxidation. *Catal. Rev. - Sci. Eng.* **37**, 425 - 459 (1995).
13. Moro-Oka, Y. & Ueda, W. Partial Oxidation an Ammoxidation of Propane: Catalysts and Process. 223 - 245
14. Centi, G., Marchi, F. & Peratoner, S. Surface chemistry of V-Sb-Oxide in relation to the mechanism of acrylonitrile syntesis from propane pt.I Chemisorption and transformation of possible intermediates. *J. Chem. Soc., Faraday Trans.* **92**, 5141 - 5149 (1996).

15. Shannon, R. Revised Effective Ionic Radii and Systematic Studies of Interatomic Distances in Halides and Chalcogenides. *Acta Crystallographica* **A32**, 751 - 767 (1976).
16. Berry, F.J. & Brett, M.E. Vanadium Antimonate. *J. Chem. Soc. Dalton Trans.* (1983).
17. Filipek, E., Kurzawa, M. & Dabrowska, G. Initial studies on the oxide system Cr₂O₃-Sb₂O₄. *J. Therm. Anal. and Cal.* **60**, 167-171 (2000).
18. Bruckner, A. & Zanthoff, H. The structure of catalytically active vanadium sites in V-Sb oxides: an EPR study of asynthesized and tungsten promoted working catalysts. *Colloids and surfaces A* **158**, 107 - 113 (1999).
19. Cavani, F., Ligi, S., Masetti, S. & Trifirò, F. SbVO₄: the chemistry of preparation. *Preparation of catalysis VII* 377 - 383 (1998).
20. Centi, G. & Mazzoli, P. Structure-activity relationship in Sb-V-oxide catalysts for the direct synthesis of acrylonitrile from propane. *Catalysis Today* **28**, 351 - 362 (1996).
21. Antimony compounds. *Kirk-Othmer Encyclopedia of chemical technology*
22. Golunski, S.E. & Jackson, D. Antimony oxide: a guide to phase change during catalyst preparation. *Applied Catalysis* **48**, 123 - 135 (1989).
23. Cody, C.A., Di Carlo, L. & Darlington, R.K. Vibrational and thermal study of antimony oxide. *Inorg. Chem.* **18**, 1572 - 1576 (1979).
24. Blanchard, G., Burattin, P., Cavani, F., Masetti, S. & Trifirò, F. WO Patent 97/23,287 A1. (1997).
25. Amador, J. & Rasines, I.J. *Appl. Cryst.* **14**, 248 (1981).
26. Berry, F.J., Holden, J.G. & Loretto, M.H. Iron Antimonate. *J. Chem. Soc. Dalton Trans.* 1727 - 1731 (1987).
27. Geng, B., Zhang, L. & Zuo, J. *Chem. Phys. Lett.* **376**, 103 - 107 (2003).
28. Swamy, V., Muddle, B. & Dai, Q. *Appl. Phys. Lett.* **89**, (2006).
29. Ocana, M., Fornes, V., Garcia Ramos, J. & Serna, C.J. *Solid State Chem.* **75**, 364 - 372 (1988).

6 ACKNOWLEDGEMENTS

As far as the achieved results are concerned, the PhD experience has been very important and it allowed me to acquire a great deal of consciousness about the scientific approach to data, organization and research. This learning experience has been possible thanks to Prof. Fabrizio Cavani and Dr. Guido Petrini who helped me during my work with their experience and passion, who shared with me different outlooks and gave me useful advice . . . and reproaches of course. In the same way Nicola Ballarini partially followed my project, sharing with me his knowledge about ammoxidation and giving me important technical advice.

I would like to thank Sud Chemie Catalysts Italia for the economical support.

The department of Industrial Chemistry is such a good place to perform research in catalysis that I'm really proud to be a little part of it. A little part of its passion. I would like to acknowledge all the professors and all the people who crossed my room and helped me to increase my knowledge, my experience and my doubts. Beautiful people.

I think that the academic advance is linked to the personal advance, so it has to do with all the people inside and outside the University. It is important, then, to thank all my friends and my family who have filled my time and my mind outside the lab.

Last but not least, I would like to thank the most important person of my life. My wife Francesca who gave me two beautiful children and supported me during the PhD years. She represents all I've got, and if it is not enough, she provided to check my English in the thesis. She read all the pages, word by word, to find out the errors. Well, she now hates Chemistry for sure (at last more than before) and I still keep on missing the "s" in verbs and in plurals. An incredible work.